RENSSELAER POLYTECHNIC INSTITUTE

KNOWLEDGE AND THOROUGHNESS

1824

Rensselaer Polytechnic Institute

Troy, New York

R.P.I. Technical Report MP-39

A Progress Report for
July 1, 1973 to December 31, 1973

ANALYSIS AND DESIGN OF A CAPSULE LANDING SYSTEM AND SURFACE VEHICLE CONTROL SYSTEM FOR MARS EXPLORATION

National Aeronautics and Space Administration

Grant NGL 33-018-091

Submitted by the Special Projects Committee

D.K. Frederick
P.K. Lashmet
W.R. Moyer
G.N. Sandor
C.N. Shen
E.J. Smith
S.W. Yerazunis

School of Engineering
Rensselaer Polytechnic Institute

ABSTRACT

Problems related to the design, construction and evaluation of a mobile planetary vehicle and its control intended for an unmanned exploration of Mars have been under study. Broad problem areas receiving attention include: vehicle configuration, dynamics, control, systems and propulsion; systems analysis; terrain sensing and modeling and path selection; and chemical analysis of samples.

The following tasks have been under active study: design and construction of a 0.5 scale dynamic vehicle, mathematical modeling of vehicle dynamics, experimental 0.4 scale vehicle dynamics measurements and interpretation, vehicle electro-mechanical control systems, remote control systems, collapsibility and deployment concepts and hardware, design, construction and evaluation of a wheel with increased lateral stiffnes, system design optimization, design of an on-board computer, design and construction of a laser range finder, measurement of reflectivity of terrain surfaces, obstacle perception by edge detection, terrain modeling based on gradients, laser scan systems, path selection system simulation and evaluation, gas chromatograph system concepts, experimental chromatograph separation measurements and chromatograph model improvement and evaluation.

These tasks are defined in detail and the progress which has been achieved during the period July 1, 1973 and December 31, 1973 is summarized. Projections of work to June 30, 1974 are included.

TABLE OF CONTENTS

		Page
INTRODUCTION		1
DEFINITION OF TASKS		1
A.	Vehicle Configuration, Control, Dynamics, Systems and Propulsion	1
B.	General Systems Analys	2
C.	Surface Navigation and Path Control	2
D.	Chemical Analysis of Specimens	2
SUMMARY OF RESULTS		2
DETAILED SUMMARIES OF PROGRESS		7
A.	Vehicle Configuration, Control, Dynamics, Systems and Propulsion	8
A.1.	Vehicle Structure and Dynamics	8
A.1.a.	Experimental and Analytical Studies of Vehicle Dynamics	8
A.1.b.	Detailed Design of Structural Components	13
A.1.c.	Design of Deployment Hardware	15
A.1.d.	Motor Drive and Mechanical Transmission Details	18
A.2.	Development of Launch Configuration and Deployment Procedure	21
A.3.	Wheel Design and Testing	21
A.3.a.	Wheel Tester and Grouser Design	21
A.3.b.	Wheel Analysis	21
A.3.c.	Detailed Design and Wheel Construction	24
A.4.	Radio Control	24
A.4.a.	On-board Electrical Controls	24
A.4.b.	Radio Link	27
A.4.c.	Remote Control Station and Transmitter Design	29
B.	General Systems Analysis	29
B.1.	System Modeling and Design Optimization	29
B.2.	On-Board Computer Design	30
C.	Surface Navigation and Path Control	32
C.1.	Terrain and Obstacle Sensors	32

C.1.a. Construction of a Laser Range Finder..... 32
C.1.b. Surface Reflectivity, Laser Power Requirements and Receiver Selection..... 38

C.2. Obstacle Detection, Terrain Modeling and Scanning Systems..... 48

C.2.a. Recognition of Three-dimensional Obstacles by an Edge Detection Scheme..... 48
C.2.b. Parameter Estimation for Terrain Modeling from Gradient Data..... 61
C.2.c. Scanning Scheme for a Laser Rangefinder..... 67

C.3. Path Selection System Simulation and Evaluation... 73

C.3.a. Development of Standard Test Terrains and Evaluation Procedures..... 74
C.3.b. Early Cornell System Evaluation..... 82

D. Chemical Analysis of Specimens..... 93

D.1. Chromatograph System Characteristics..... 93

D.2. Chromatograph Simulation Development..... 99

D.2.a. Multicomponent Chromatography..... 99
D.2.b. Chromatograph Model Improvement..... 101

REFERENCES..... 111

Analysis and Design of a Capsule Landing System and Surface Vehicle Control System for Mars Exploration

I. Introduction

Current national goals in space exploration include a detailed study and examination of the planet Mars. The effectiveness of Mars exploration missions would be enhanced according to the extent to which the investigative devices which are landed are mobile, to the range of their mobility, and to the ability to control their motion. In order to achieve basic mission objectives, and beyond that, to maximize the return on the commitment of resources to the mission, formidable technical problems must be resolved. The major factor contributing to these problems is the round trip communications time delay between martian and earth control stations which varies from a minimum of about 9 minutes to a maximum of 25 minutes. This time delay imposes stringent requirements on the vehicle, on its control and communication systems and on those systems included on board to make the scientific measurements, in terms of their ability to function autonomously. These systems must be able to operate with a high degree of reliability and must be capable of calling for earth control under appropriate circumstances.

A number of important problems originating with these factors and relating directly the basic mission objectives of an unmanned exploration of Mars have been and are currently being investigated by a faculty-student project team at Rensselaer Polytechnic Institute with the support of NASA Grant NGL-33-018-091.

This progress report describes the tasks which have been undertaken and documents the progress which has been achieved in the interval July 1, 1973 to December 31, 1973.

II. Definition of Tasks

The delay time in round trip communication between Mars and Earth gives rise to unique problems relevant to martian and/or other planetary explorations. All phases of the mission from landing the capsule in the neighborhood of a desired position to the systematic traversing of the surface and the attendant detection, measurement, and analytical operations must be consummated with a minimum of control and instruction by earth based units. The delay time requires that on board systems capable of making rational decisions be developed and that suitable precautions be taken against potential catastrophic failures. Four major task areas, which are in turn divided into appropriate sub-tasks, have been defined and are described below.

A. Vehicle Configuration, Control, Dynamics, Systems and Propulsion
The objective of this task is the design of a roving vehicle for the exploration of Mars. This design includes the aspects of vehicle configuration, collapsibility for launch configuration, deployment, dynamics, motion and attitude control, obstacle negotiation capability, and performance evaluation. The efforts of this task are made within the context of the mission definition and delivery system constraints. The ultimate goal is the development of a vehicle capable of operating within the constraints of the Mars mission, but flexible in design, to insure reliability

with respect to the unknowns of Mars, and to accommodate the alterations in the mission as a result of information gathered during the exploration.

B. General Systems Analysis. One major objective of this task is to develop a framework within which decisions in design involving conflicting requirements can be made rationally and in the context of the whole system and mission. Relationships between alternative mission profiles and specifications and weight, energy and space allocation and management will be sought.

The second major objective is to develop the software and hardware design specifications for the on-board computer of a Mars roving vehicle.

C. Surface Navigation and Path Control. Once the capsule is landed and the roving vehicle is in an operational state, it is necessary that the vehicle can be directed to proceed under remote control from the landing site to specified positions on the martian surface. This task is concerned with the problems of terrain sensing, obstacle detection, terrain modeling, path selection and navigation between the initial and terminal sites when major terrain features precluding direct paths are to be anticipated. On board decision making capability must be designed to minimize earth control responsibility except in the most adverse circumstances.

D. Chemical Analysis of Specimens. A major objective of martian surface exploration will be to obtain chemical, biochemical or biological information. Many experiments proposed for the mission require a general duty, gas chromotgraph-mass spectrometer for chemical analysis. The objective of this task is to generate fundamental data and concepts required to optimize this chemical analysis system.

III. Summary of Results

Task A. Vehicle Configuration, Control, Dynamics, Systems and Propulsion

This broad task has been subdivided into the following subtasks: experimental and analytical studies of vehicle dynamics; detailed design of structural components; design of deployment hardware; motor drive and mechanical transmission details; development of launch configuration and deployment procedure; wheel tester and grouser design; wheel analysis; detailed wheel design and construction; on-board controls for steering, motor drive for levelizing, deployment and emergency maneuvers; radio link for remote operation; and remote control station and transmitter design.

A.1. Vehicle Structure and Dynamics

A.1.a. Experimental and Analytical Studies of Vehicle Dynamics

Physical characteristics such as spring constants, damping constants and moments of inertia of the 0.4 scale vehicle model were measured experimentally. A three dimensional,

three degree-of-freedom mathematical model was developed and its predictions were compared with the dynamic behavior of the model. Satisfactory agreement was observed indicating that the mathematical model can be used as a design tool to obtain desired dynamic characteristics. Extensions of the mathematical model have been identified. No further work is planned pending construction of the 0.5 dynamic vehicle.

A.1.b. Detailed Design of Structural Components for the 0.5 Scale Model

Half-scale model dimensions have been established and the designs of the front steering gear box, payload box and front axle have been completed. Design of the front and rear struts, torsion bar assembly and motor drive system is proceeding.

A.1.c. Design of Deployment Hardware

The conceptual design of the deployment devices is complete and final detail design is proceeding. Bench testing of these components is planned prior to incorporation into the overall vehicle structure.

A.1.d. Motor Drive and Mechanical Transmission Details

Motors have been selected and procured. Conceptual design of the gear train has been established and is being analyzed.

A.2. Development of Launch Configuration and Deployment Procedure

The basic launch configuration has been modified from last year's concept in order to simplify the deployment procedure. The new configuration remains consistent with all Viking capsule constraints and yields a satisfactory center of gravity location.

A.3. Wheel Design and Testing

A.3.a. Wheel Tester and Grouser Design

No work beyond that reported in the preceding progress report has been undertaken. Further work will be undertaken after construction of the new 0.5 scale wheel.

A.3.b. Wheel Analysis

A modified wheel design has been developed to increase the lateral stiffness of the wheel on the basis of several hoop designs which were constructed and tested during this past period.

A.3.c. Detail Design and Wheel Construction

An improved detail design of a wheel with increased lateral stiffness has been obtained and construction of such wheels for installation on the 0.5 scale model is underway.

A.4. Radio Control

A.4.a. On-Board Electrical Controls

A system for controlling the motors with digital input has been conceived. The system which involves digital/analog converters and analog feedback at the motors is currently under construction and test.

A.4.b. Radio Link

Frequency shift key encoding is used with walkie-talkies to provide a 100 bit/sec radio link to the vehicle. The entire system has been tested on the bench and is currently under construction.

A.4.c. Remote Control Station and Transmitter Design

Construction is underway on the remote control package which will interface with the vehicle either by the radio link or via an umbilical for bench testing. This device will permit open loop, manual control of the 0.5 scale model.

Task B. General Systems Analysis

B.1. System-Modeling and Design Optimization

Optimal designs have been developed for three major alternative models, i.e. four-wheeled vehicle with either direct earth link or an orbiter-earth link and a six-wheeled vehicle with direct earth link. The method by which to obtain optimal design for these and other cases has been developed in general terms. Methods for determining the sensitivity of the optimal designs to perturbation of design parameters have also been developed. This task is now complete and a technical report is scheduled for issuance in February of 1974.

B.2. On-Board Computer Design

Previous work in this area involved the use of a statistical approach using queuing theory and random variables to study the average behavior of the computer-vehicle system. This study identified a higher level problem in design of an on-board computer, namely the need to define computer design specifications both in regard to software and hardware prior to the computer design process. The present task is aimed at defining the software and hardware specifications for an on-board computer. It is assumed that all control and scheduling decisions will be provided autonomously. The goal will be to synthesize a design that will meet the lowest realizable specification bound. Ultimately, volume, weight, cost, power requirements and heat generation will have to be optimized to meet mission requirements. Alternative hardware and software configurations will have to be considered and trade-offs evaluated.

Task C. Surface Navigation and Path Control

This task deals with problems of terrain sensing, terrain modeling, obstacle detection, path selection algorithms and evaluation of path selection systems. Active tasks are: design and construction of a laser range finder, measurement of bidirectional reflectance ratios, three dimensional obstacle recognition, terrain parameter estimation from gradient data, laser range finder scanning systems and path selection system evaluation.

C.1. Laser Range Finding

C.1.a. Construction of a Laser Range Finder

Following a thorough search of the literature, a design for a laser range finder with the potential of achieving a 5 cm accuracy has been formulated. Most of the required parts have been obtained and construction has been started.

C.1.b. Surface Reflectivity, Laser Power Requirements and Receiver Selection

Primary emphasis has been directed to determining the experimental measurements which will be necessary to specify laser power and receiver requirements for an effective scanning system. A test apparatus for making the measurements has been designed and is under construction. Experimental procedures and data processing methods have been developed.

C.2. Obstacle Classification and Detection and Terrain Modeling

C.2.a. Obstacle Identification by an Edge Detection System

An algorithm which can be used to "outline" an obstacle and therefore lead to its detection has been developed and applied to the case of a hemispherical boulder. A second algorithm existing in the literature has also been used. Both algorithms were evaluated with perfect sensor range data and with sensors involving range error. Both algorithms are found to be effective provided that the proper threshold values are used. The results are encouraging and future work to determine minimum information requirements for effective boulder identification is underway.

C.2.b. Parameter Estimating for Terrain Modeling from Gradient Data

A two-step terrain modeling procedure has been developed. The first step involves the use of four discrete data points whose heights and locations are provided by an appropriate range sensor. These four points are fitted by least mean square methods to a plane forming a section of known height, location and gradient. Four such sections are then fitted in a second step by a third degree, two-dimensional polynomial. An error analysis of this modeling method has been completed and a computer program to apply the method is in the process of completion.

C.2.c. Scanning Scheme for a Laser Rangefinder

A study of alternative scanner schemes, i.e. the pattern of data points to be sought by the increments of pointing angles as determined by a hardware system, was initiated. The goal was to establish uniform elevation and azimuthal angle increments which would provide sensor data of sufficient quality to define the terrain adequately. Unfortunately, reliable gradient data require relatively large data spacing whereas large data spacings increase the probability of missing an obstacle. Since data spacing is a function of range as well as incremental angles, constant angle increments lead to small data spacings at close range and therefore large gradient errors whereas they lead to large data spacing at long range and an increased probability of missing obstacles. Future work will be aimed at resolving these conflicting objectives.

C.3. Path Selection System Simulation and Evaluation

C.3.a. Development of Standard Test Terrains and Evaluation Procedures

A path selection system evaluation test procedure has been developed. The procedure investigates the obstacle avoidance ability of a path selection system by simulating its performance on a sequence of test terrains with and without random effects. The test procedure begins with simple single obstacle encounters in a series of increasingly difficult circumstances, i.e. flat terrains, rolling terrains, rolling inclines, etc., and ends with complex multi-obstacle tests. The simulation code has been improved in many details and computer time requirements have been reduced.

C.3.b. Evaluation of an Early Cornell Path Selection System

An early and preliminary Cornell path selection system proposed several years ago was evaluated using the simulation to determine the strengths and weaknesses not only of the proposed system but also of the simulation and evaluation program. The Cornell method which has the strong advantage of hardware and computational simplicity was found to be able to contend reasonably well with clearly defined obstacles but had some difficulties dealing with rolling terrains especially when random effects such as bouncing of the vehicle because of rubble are included. A number of recommendations for modifying the Cornell system have been proposed and will be investigated.

Task D. Chemical Analysis of Specimens

This task is concerned with developing fundamental concepts which will be required to optimize a gas chromatograph - mass spectrometer chemical analysis system. Topics receiving active effort include analysis of chromatograph characteristics, multicomponent chromatography, and chromatograph model improvement.

D.1. Chromatograph System Characteristics

These studies are intended to provide chromatograph design

techniques and guides using simulation models currently under development. Current efforts involve the definition of resolution or degree of separation obtained in a specific system under particular operating conditions. A systematic study of the effect of system parameters upon resolution using simulation will provide a quantitative understanding of chromatograph behavior and design guides. Resolution as often defined in the literature and based on moment analysis was shown to represent inadequately separations in multicomponent systems because the definition was insensitive to chemical composition. A definition based on each component's contribution to the area under a chromatograph peak is under investigation and shows promise. Verification by simulation for several conditions used in the experimental program will be undertaken, to be followed by a more systematic analysis of design parameter effects.

D.2. Chromatograph Simulation Development

D.2.a. Multicomponent Chromatography

Modifications to the chromatographic test facility resulted in sharper input pulses for liquid samples and full scale chromatogram recordings which reduced relative reading errors by a factor of 3 or 4 in some cases. To supplement pentane-heptane data on the porous Chromosorb-102 column, which deviated appreciably from linear superposition predictions, additional experiments were conducted on two nonporous columns. A Carbowax-1500 column failed to separate the two chemicals because values of the thermodynamic parameter mR_0 were too similar. A DES column separated the two components and superposition of pure component data was an excellent representation of the binary data. Furthermore, pure component data were well represented by the simple equilibrium adsorption model. Future work includes porosity determinations for the columns and review of mechanisms possibly responsible for deviations from linear superposition in multicomponent systems.

D.2.b. Chromatograph Model Improvement

A recently released technical report documented a more complete chromatograph model which included intraparticle as well as interparticle transport effects and finite rates of adsorption. Mathematical complexity precluded analytical solutions, so numerical techniques were investigated. Orthogonal collocation was applied to two simplified versions of the model which were solved analytically. Comparison between the exact and numerical solutions was then possible. Space discretizations using seven and fifteen elements have represented responses for the simple models well. Corresponding accuracy by conventional finite difference methods would require at least an order-of-magnitude increase in the number of space elements. The complete model is currently being coded for machine computation.

IV. Detailed Summaries of Progress

Task A. Vehicle Configuration, Control, Dynamics, Systems and Propulsion

The objective of this task is to design and construct an operational half-size demonstration model of a Mars roving vehicle to verify proposed concepts for:

1. Collapsibility
2. Deployment
3. Controllability of propulsion and maneuvering
4. Obstacle negotiation capability
5. Payload carrying capability
6. Operation by radio control

Towards the accomplishment of this objective, the vehicle design task has been organized into several subtasks. While these subtasks are intimately related and there is a good deal of interaction between the team members working on them, each will be described separately under the following headings:

Task A.1. Vehicle Structure

- A.1.a. Experimental and Analysical Studies of Vehicle Dynamics
- A.1.b. Detailed design of structural components
- A.1.c. Design of deployment hardware
- A.1.d. Motor drive and mechanical transmission details

Task A.2. Development of Launch Configuration and Deployment Procedure

Task A.3. Wheel Design and Testing

- A.3.a. Wheel tester and grouser design
- A.3.b. Wheel analysis
- A.3.c. Detail design and wheel construction

Task A.4. Radio Control

- A.4.a. On-board electrical/electronic controls for steering, motor drives for levelizing, deployment and emergency maneuvers
- A.4.b. Radio link for remote operation
- A.4.c. Remote control station and transmitter design

A.1. Vehicle Structure - P. Marino, D. Kern, M. Miecznikowsik, J. Harrison, C. Deno and G. Scapellati
Faculty Advisor: Prof. G. N. Sandor

A.1.a. Experimental and Analytical Studies of Vehicle Dynamics

Subtask Objective. To determine the dynamic response of the .4 size model and develop a mathematical tool for the dynamic optimization of the forthcoming half-size model and eventually the full-size prototype vehicle.

Progress Summary. Physical characteristics, such as spring constants, damping constants and moments of inertia of the .4 size vehicle model were measured experimentally. A three-dimensional, three-degree-of-freedom mathematical

model was developed, programmed for digital computation and its predictions compared with the dynamic behavior of the model. Satisfactory agreement was found, thus indicating that the mathematical model can be used as a design tool. Further extensions of the mathematical model to include more degrees of freedom have been outlined.

Discussion. The dynamic analysis of the MRV was approached by two methods:

1. mathematical modeling
2. physical testing

Initially the equations of motion of a three-dimensional, three-degree-of-freedom (roll, pitch, vertical displacement) model were established. Then, the measurement of the physical characteristics of the 0.4 MRV model and dynamic tests were conducted. Finally, a comparison of actual response with the mathematically predicted response was made. The result showed the mathematical model to be a basic design tool from which gross vehicle motions may be predicted. It also may be expanded to develop a more sophisticated mathematical model. Figure 1 shows the schematic model. The wheels have been replaced by springs and dashpots. This is the schematic from which the mathematical model was developed.

For simplicity, three degrees of freedom were considered. Vertical displacement was an obvious choice since the MRV bouncing across Martian terrain will be carrying a scientific payload. Because of the "dragster" design of the RPI-MRV, the vehicle center of gravity was located near the rear wheel base far from the center of suspension. A natural pitching motion was therefore introduced by the vehicle design. As a result, the mathematical model also includes pitch motion. Finally the movement of the MRV over rocks and potholes easily introduced a rolling motion. Therefore, with the three degrees of freedom chosen to be vertical displacement, roll, and pitch rotation, the development of the equations of motion proceeded.

In order to simplify the equations of motion, the MRV was considered to be a two-mass system: a rolling (sprung) mass, and a non-rolling (unsprung) or fixed mass. Additionally,if a moving coordinate system, x'y'z' fixed to the vehicle was adopted, the inertial terms in the equations of motion would become much easier to determine. Therefore, the coordinate system of Figure 2 was used. The xyz axis system was fixed to the unsprung portion of the vehicle.

To determine the external forces and moments, the vehicle model assumed two sets of virtual displacements:

1. roll with vertical displacement, Fig. 3
2. pitch with vertical displacement, Fig. 4

The resulting equations are a set of second-order linear differential equations to be solved simultaneously. A digital computer program titled, DYNAMO (from DYNAmic MOdels) was used to solve these equations.

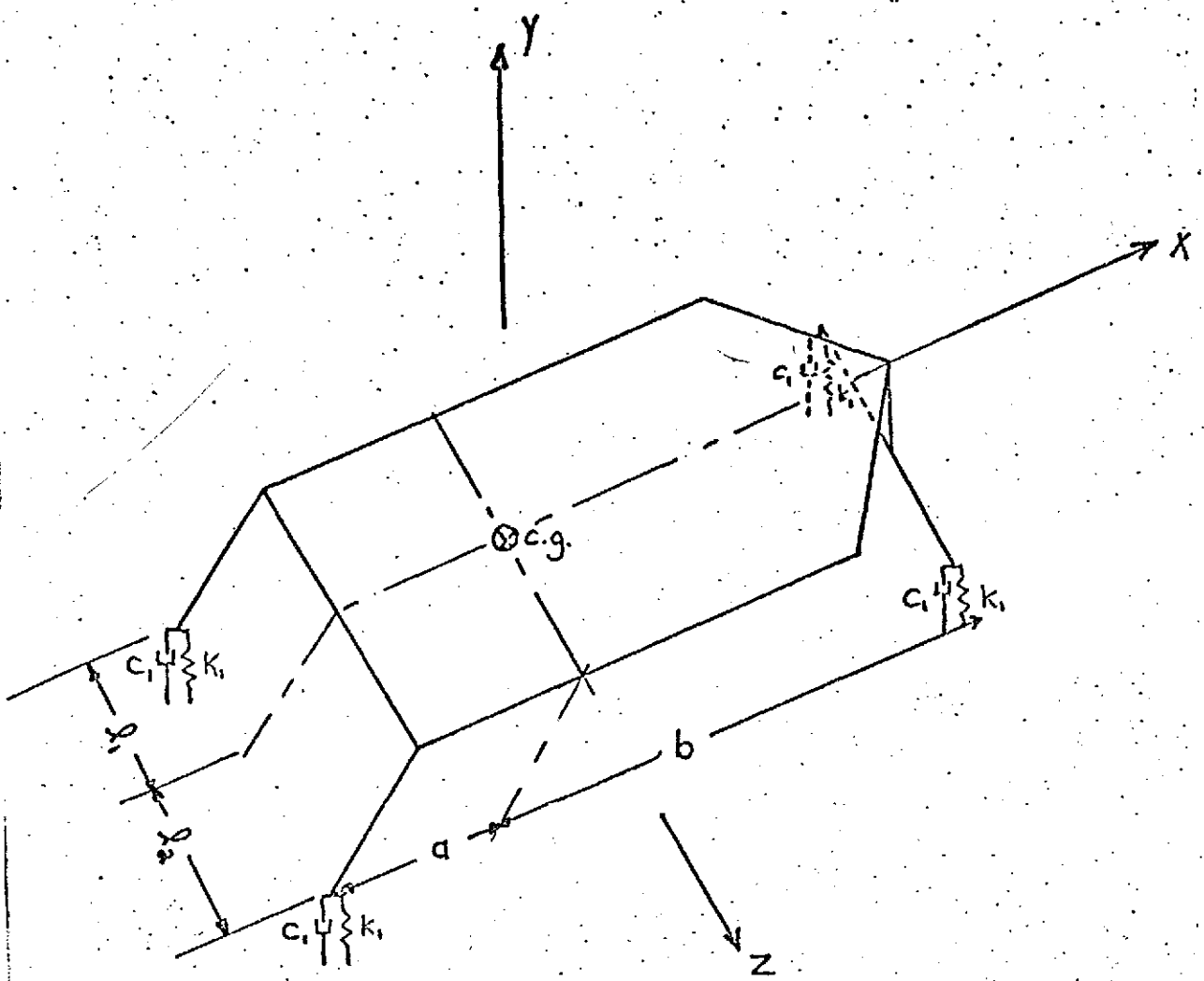

FIGURE 1

RPI-MRV Schematic Model

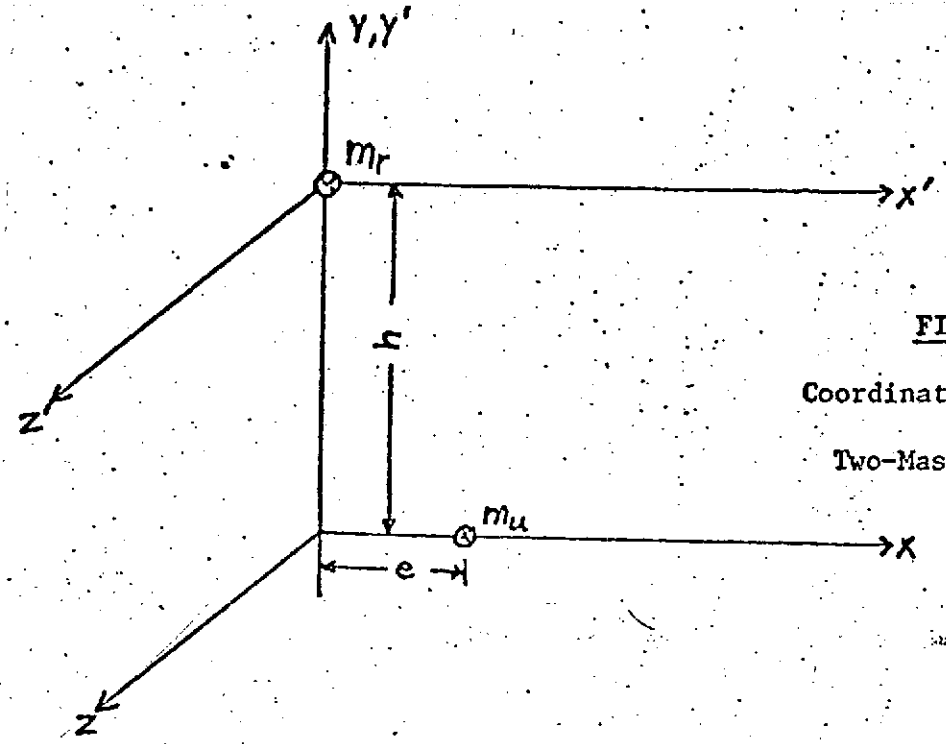

FIGURE 2

Coordinate System of

Two-Mass Vehicle

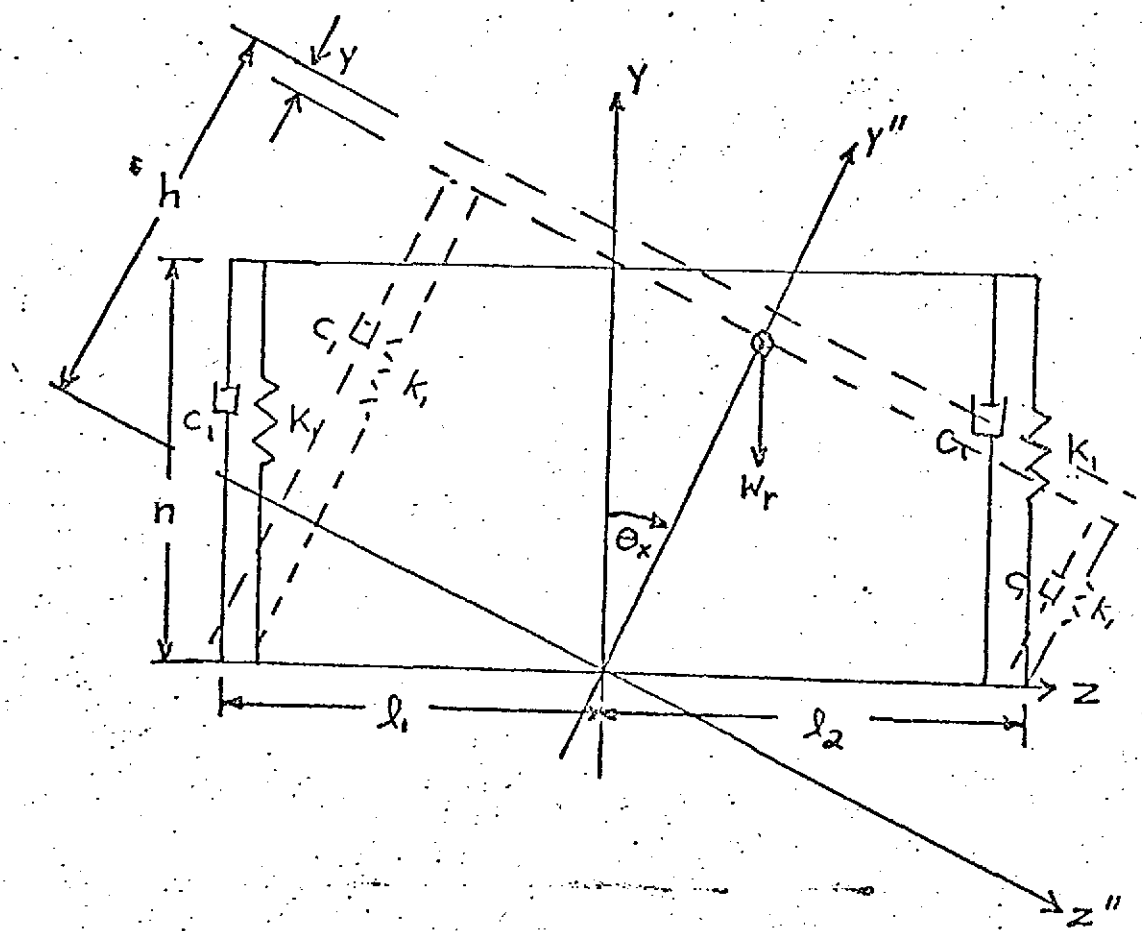

FIGURE 3

Roll (θ_x) with Vertical Displacement (y)

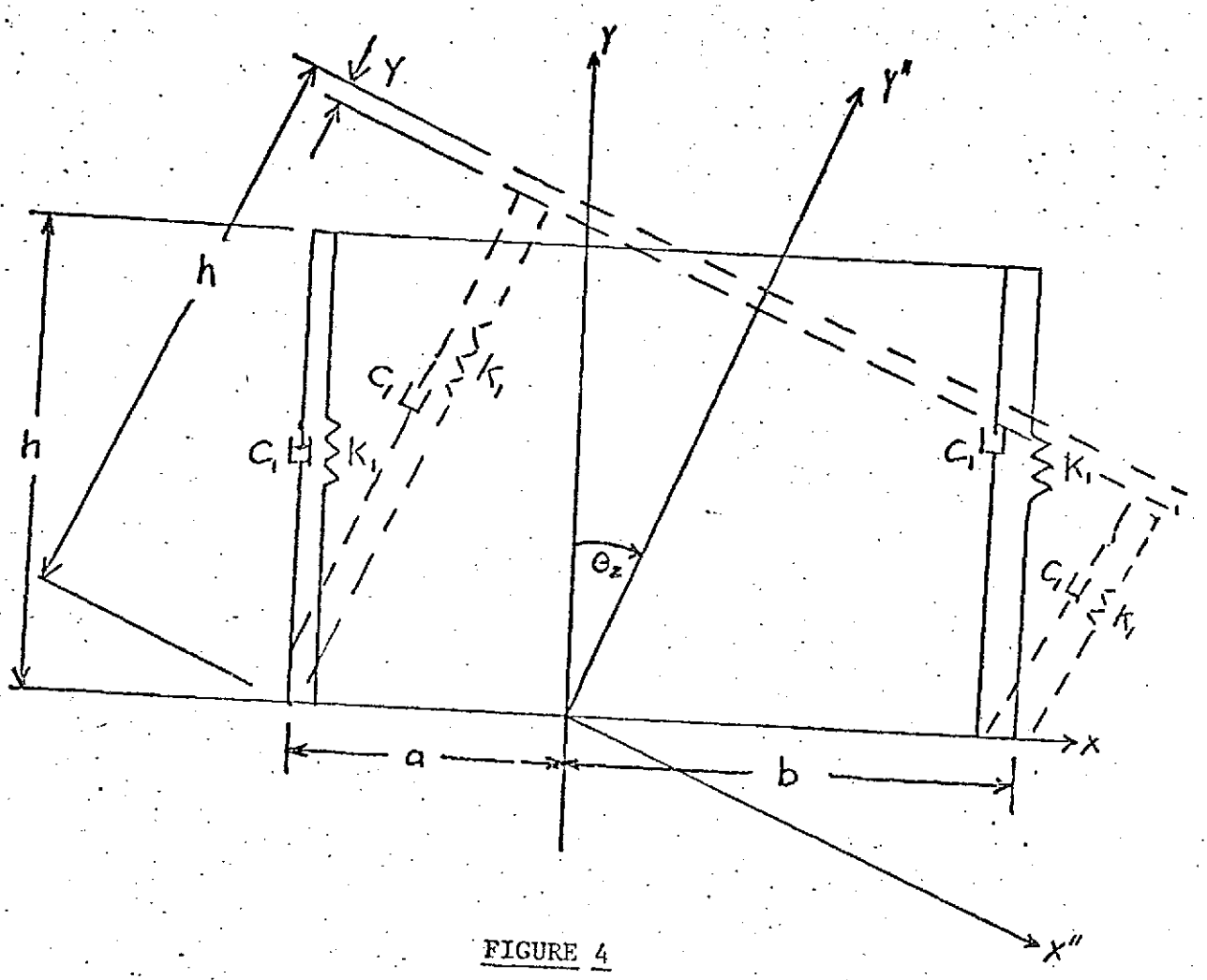

FIGURE 4

Pitch (θ_z) with Vertical Displacement (y)

Various terrain conditions may be simulated on the mathematical model. A step input to the vehicle c.g. was simulated by assuming an initial condition on the vertical displacement. An initial condition on pitch displacement simulates a step either to the front or rear wheel pair as would be encountered by the vehicle's front wheels hitting a sudden difference in elevation. Similarly an initial condition on roll displacement simulates a step to either the right or left side wheel pair. A washboard terrain effect can be modeled by equating the left side of the first equation of motion to a sinusoidal forcing function of desired frequency and amplitude. The c.g. response to various terrains may be simulated by equating the left side of the corresponding equation of motion to the appropriate function.

The mathematical model may be easily extended

1. to include a spring and damper to be located in the connection of the frame to the front axle, or

2. to consider wheels of different elastic properties.

No further work is contemplated at this time until the 0.5 scale model becomes operational. A technical report summarizing this study is to be issued in February 1974.

A.1.b. Detailed Design of Structural Components

Objective. Design and construction of the individual parts of the model are to be completed early enough for assembly and testing of the vehicle by early May, 1974.

Progress Summary. The full scale vehicle dimensions, and thus the half-scale model dimensions, have been firmly established. Designs of the front steering gear box, the payload box, and the front axle have been completed. Design is progressing on the back and front struts, the torsion bar assembly, and motor drive system.

Front steering gear box (Fig. 5). This component must turn the front axle through the proper steering angles and, in the emergency maneuver (flip over of the vehicle), pivot the front axle 180° about the front struts. These two functions are accomplished by two self-locking worm gear pairs at right angles to each other. One worm gear pair governs the steering angle and the other controls the angle between the front axle pivot and the vehicle's front struts. Being self-locking, this design requires no brakes or other locking devices, and at the same time provides large gear reductions across each gear set.

Payload box. This component holds the scientific package, torsion bar assembly, batteries, etc. It is also a main structural member of the vehicle frame. It consists of an aluminum

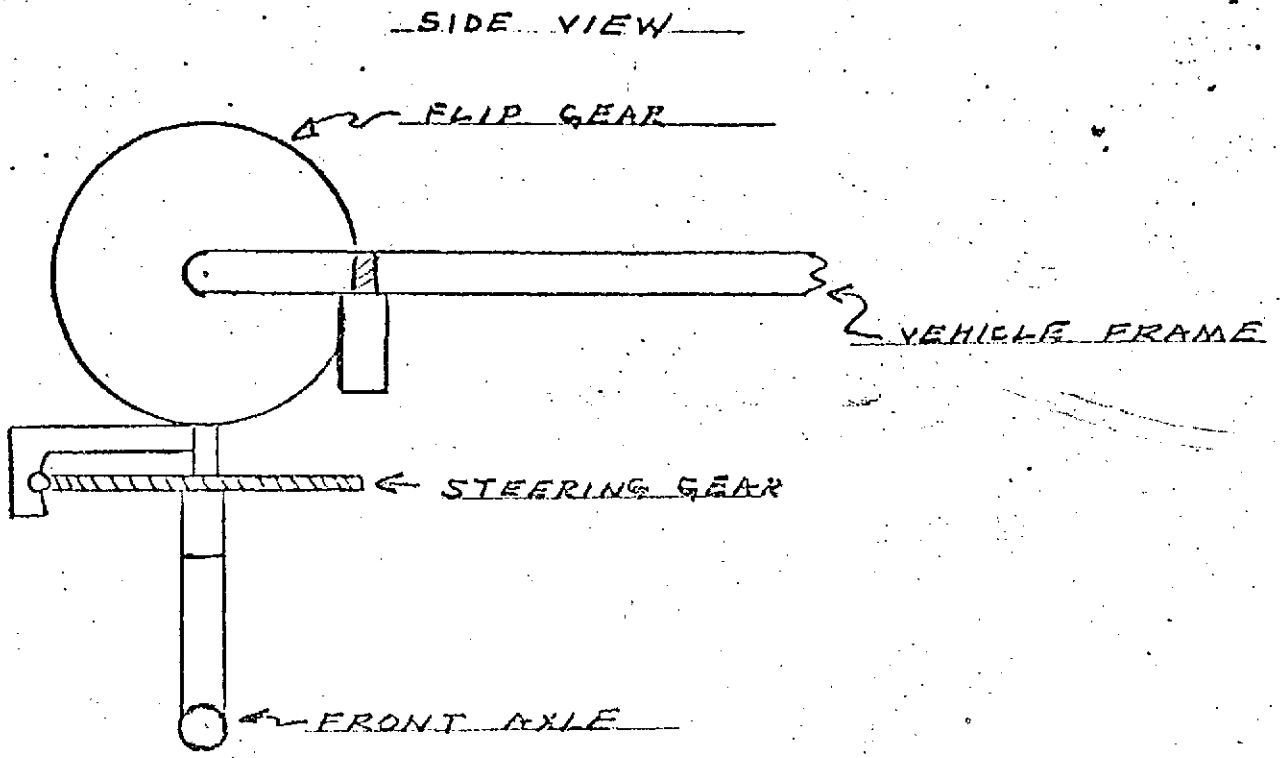

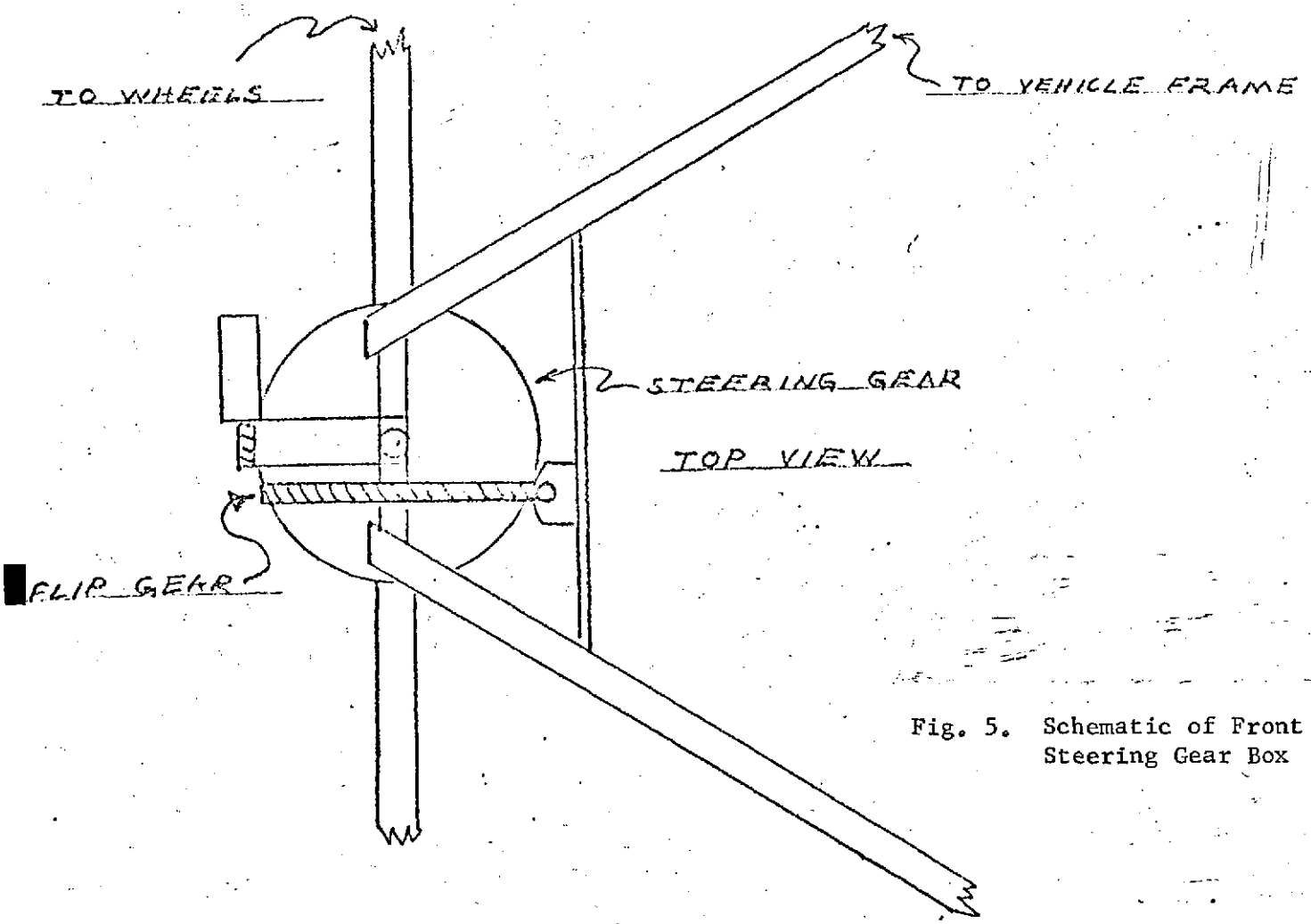

Fig. 5. Schematic of Front Steering Gear Box

angle box frame with a 1/8" thick plexiglass skin. This construction allows visual inspection of contents and mechanisms inside the payload box while the vehicle is being demonstrated.

Schedule:

All parts to be designed by	2/28/74
Construction and assembly to be completed by	5/10/74
Initial mechanical testing of 0.5 size model to be completed by	6/30/74

A.1.c. Design of Deployment Hardware

Objective. To finalize the design of hardware components which will enable the 0.5 scale model vehicle to deploy. The design of these components is based on the results of Task A.2., "Development of Launch Configuration and Deployment Procedure."

Progress Summary. The conceptual design of deployment devices is complete. Finalized detail design and bench testing of hardware is to be done before embodiment into the overall vehicle structure.

Discussion. The deployment system consists of four subassemblies. These are:

- the front axle flip-over mechanism,
- the torsion bar assembly,
- the front strut hinge and locking mechanisms, and
- the rear strut unfolding and locking mechanisms

The front axle flip-over mechanism has been finalized (Fig. 5). It consists of a motor driving the front axle via a worm-gear pair.

The torsion bar assembly, Fig. 6, which controls vehicle height and payload attitude, and also takes part in deployment, is complete in its preliminary design. Motors and gears have been selected, but some detailed design has yet to be completed.

The basic design of the front hinge and locking device, Fig. 7, is complete. This mechanism will be constructed and bench-tested before it is incorporated into the overall design.

The rear strut unfolding mechanism is dependent upon the drive motor configuration. Therefore, the latter will have to be completed before the rear struts are designed.

No major problems are foreseen in any of these areas.

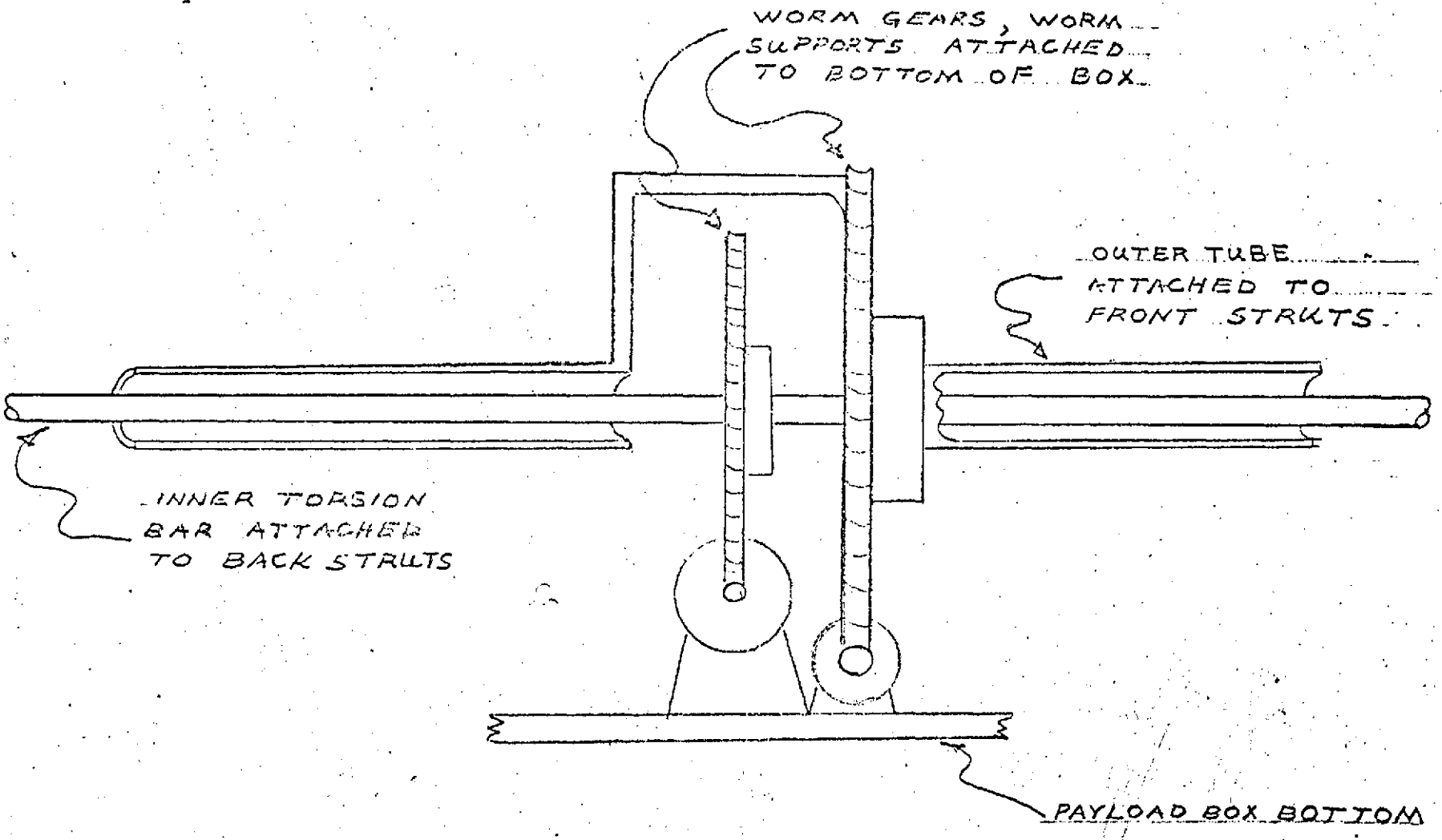

Fig. 6. Torsion Bar Schematic

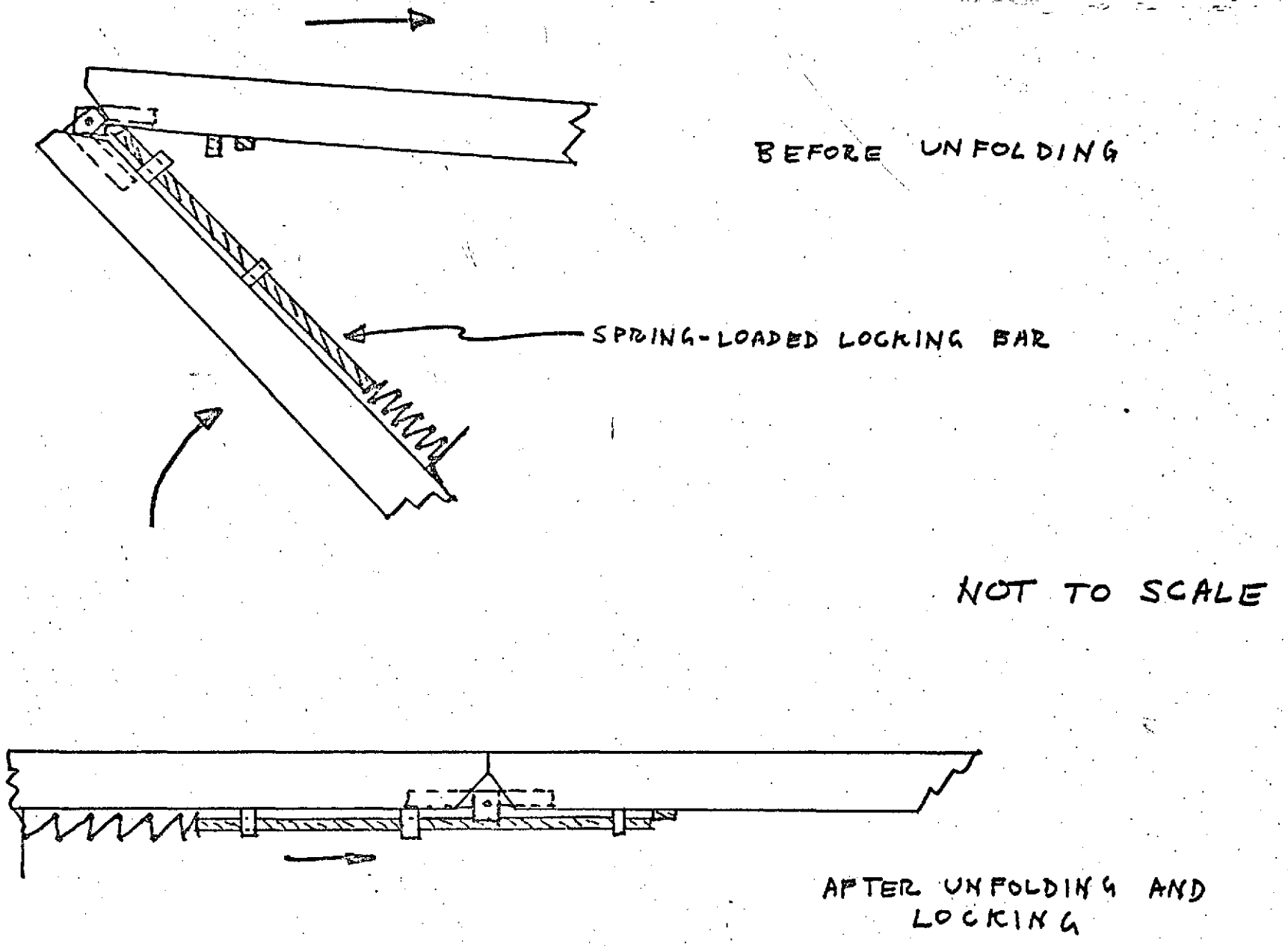

Fig. 7. Locking Mechanism for Front Strut Deployment Hardware

Schedule:

Detailed design of all parts should be completed by mid-February with fabrication of all parts completed in early May.

A.1.d. Motor Drive and Mechanical Transmission Details

Objective: To design the most advantageous main drive motor and gear system for the half-scale model considering both physical and economic constraints.

Progress Summary. Motors have been selected and procured. Conceptual design of the gear train, Fig. 8 and 9, has been established and is now being analyzed.

Progress (detailed discussion). Based on tests and analysis of the previous 0.4 scale model, power and torque requirements were established for the half-scale model. With a selected design speed of approximately 1 mph the power required from each back wheel drive motor was set at 1/8 hp.

The market place was then searched for available motors. It was quickly established that torque motor types could not be used because of both their cost and their relatively high weight. It was also found that most other motors that would meet specifications would have to be made to order. This meant high price and long delivery delays.

A solution was found in some government surplus aircraft control motors. These motors could be obtained in a reasonable time and for a reasonable price. They will serve our purpose with only slight modification.

Because the speed of the motors is 7500 rpm and the speed of the wheel at 1 mph is approximately 20 rpm, a gear train is necessary with a ratio of between 300 and 400. This is in the conceptual stage, Fig. 8. It is thought to obtain the desired gear ratio from two sets of gears, a primary set of spur gears and a secondary set of worm and wheel. The design and analysis of the gear assembly is in progress.

Major Problems. The only problem that might occur is a space conflict between the frame and gear assemblies. This will probably slow down the final design and result in trade off in both gear assembly and strut design.

Schedule:

Design to be completed by	2/28/74
Construction and assembly to be completed by	5/10/74
Initial mechanical testing to be completed by	6/30/74

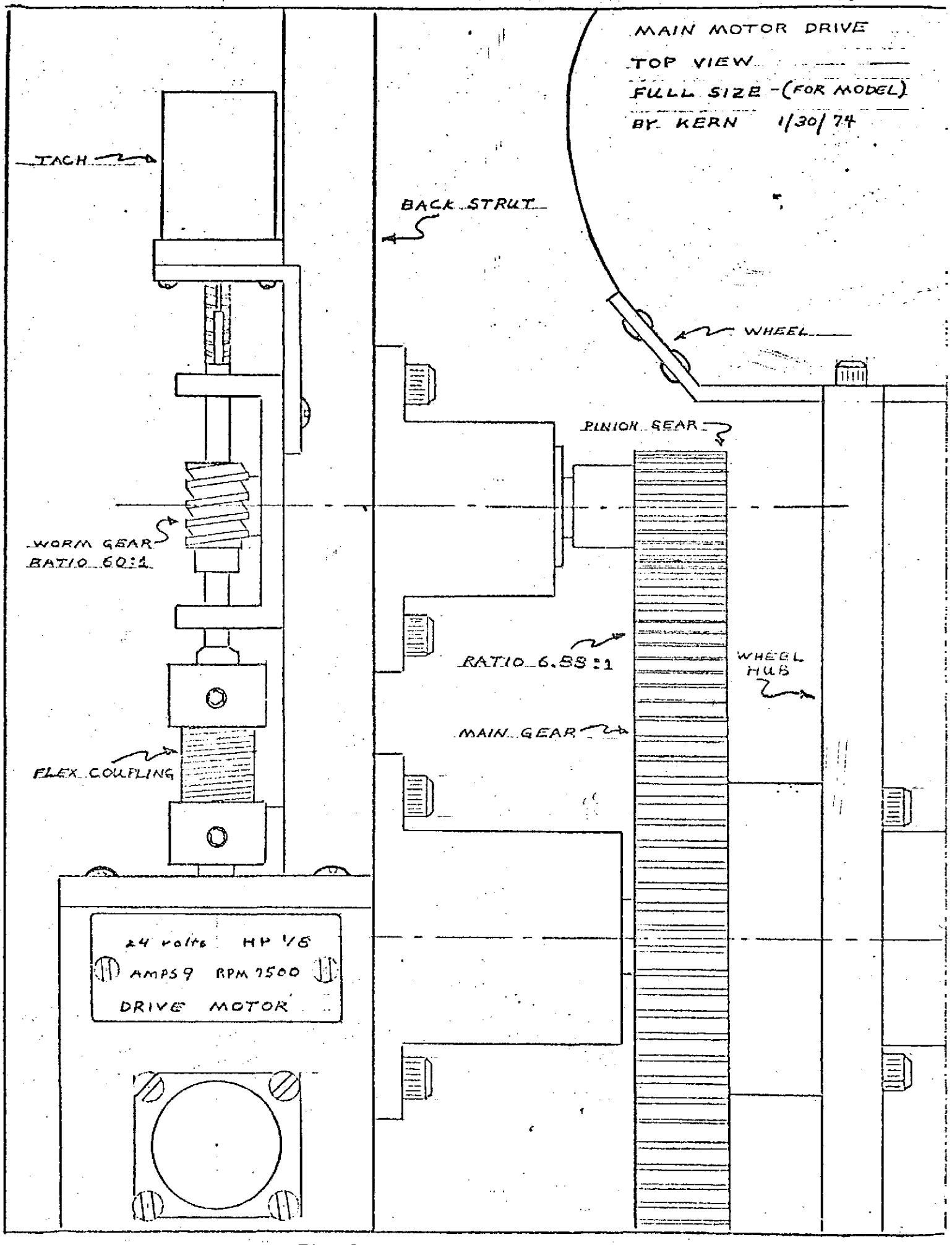

Fig. 8. Top View of Drive System

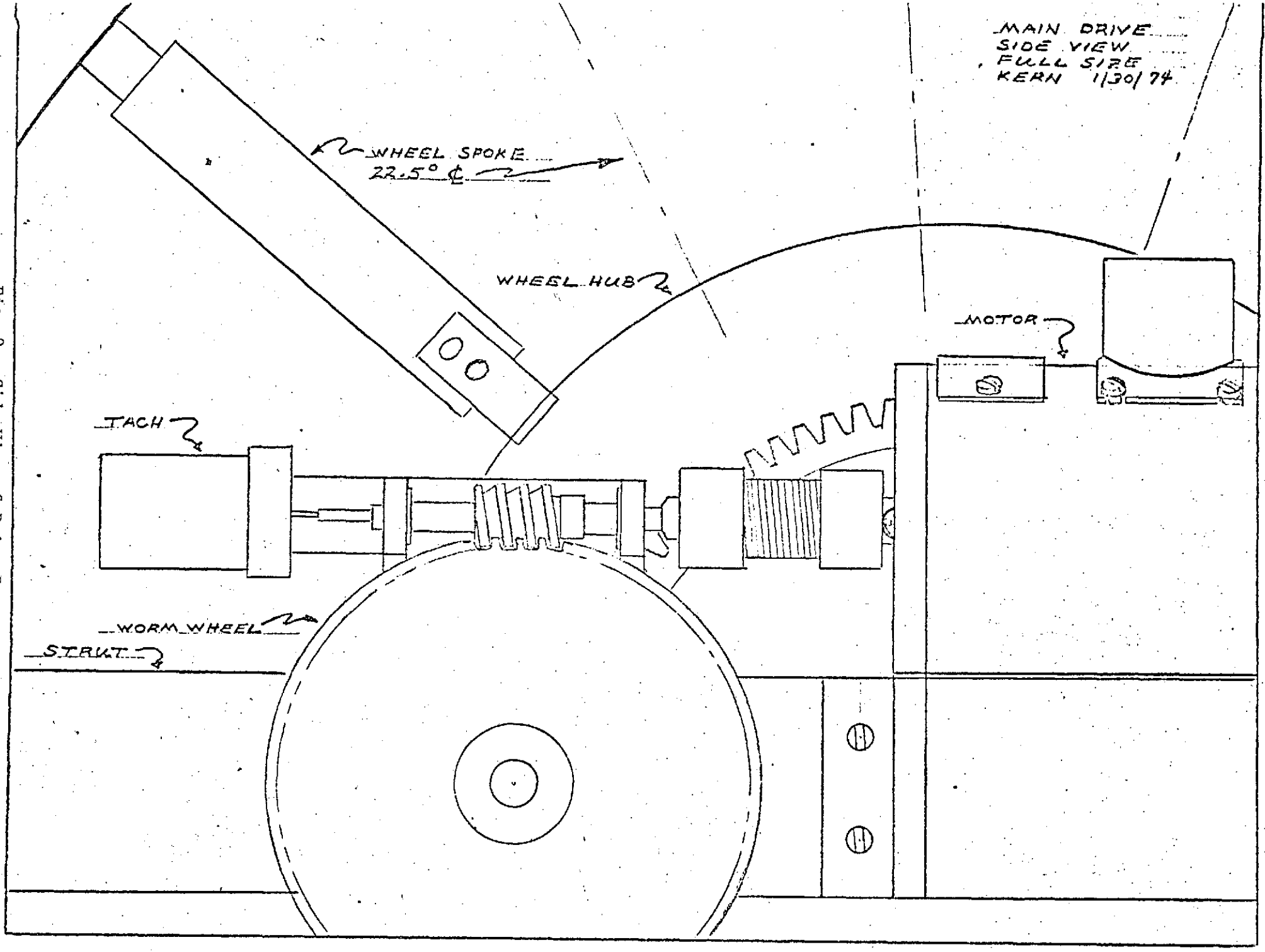

Fig. 9. Side View of Drive System

A.2. Development of Launch Configuration and Deployment Procedure - P. Marino
Faculty Advisor: Prof. G. N. Sandor

Objective. To devise a launch configuration with Viking Aeroshell limitations which would allow simple and reliable deployment.

Progress Summary. The basic launch configuration has been changed since last year's design so as to simplify the deployment procedure. This configuration is consistent with all Viking capsule constraints and yields a satisfactory center of gravity location, Figs. 10 and 11.

Discussion. Last year's launch configuration required some type of device to lift the front section of the vehicle in order to put the Rover into its operational mode. Investigation showed this to be a source of difficulty because of the large torques required and space and weight restrictions. With this in mind, a new launch configuration was devised which enables the motors and gearing associated with the torsion-bar assembly in the payload to double as the source of power for deploying the front section of the vehicle. This seems, at this time, to be an excellent solution to a potential problem.

Accordingly, the deployment procedure has been changed in that the deployment of front and rear sections must occur simultaneously. This is because the rear sections will be deployed via disposable cables which are actuated by the unfolding of the front section.

Possible problems may be encountered in the unfolding of the rear struts due to interference with the motor and gear train but this will not be determined until the drive design is complete. Little work remains to be done in this area as the configuration seems acceptable. The remaining work falls into the deployment hardware subtask A.1.c. discussed earlier.

A.3. Wheel Design and Testing - D. Kern, J. Harrison, C. Deno and G. Scapellati
Faculty Advisor - Prof. G. N. Sandor

A.3.a. Wheel Tester and Grouser Design

Objective. To determine the optimum grouser design for use on the RPI MRV.

Progress Summary. Several grouser designs have been tested on the wheel testing machine. One design has shown to be superior to the others. No work has been done in this area pending construction of the 0.5 size wheels.

A.3.b. Wheel Analysis

Objectives. To analyze the various possible wheel hoop configurations and select the optimum design for the RPI MRV.

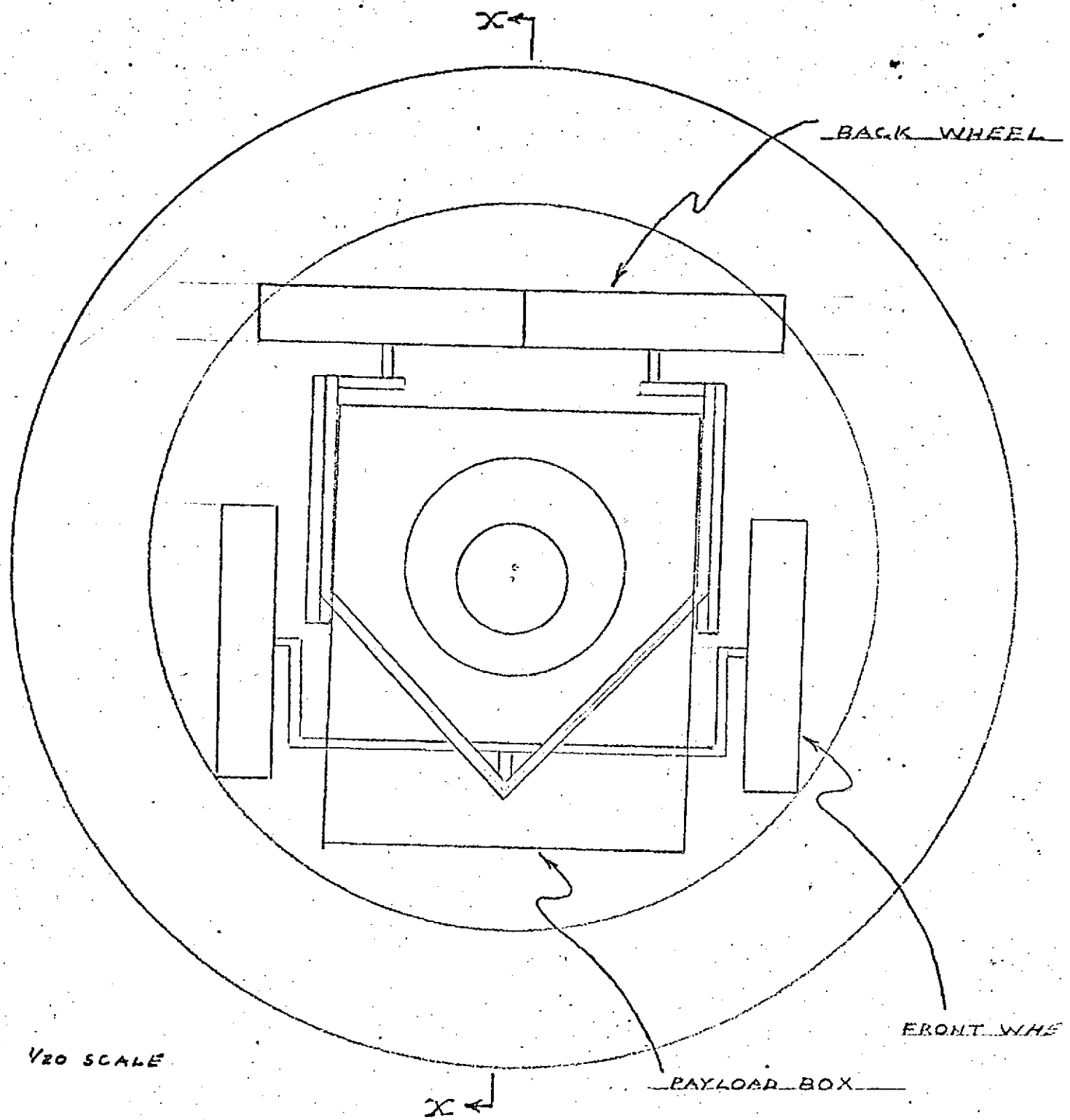

Fig. 10. Folded Vehicle in Capsule - Top View

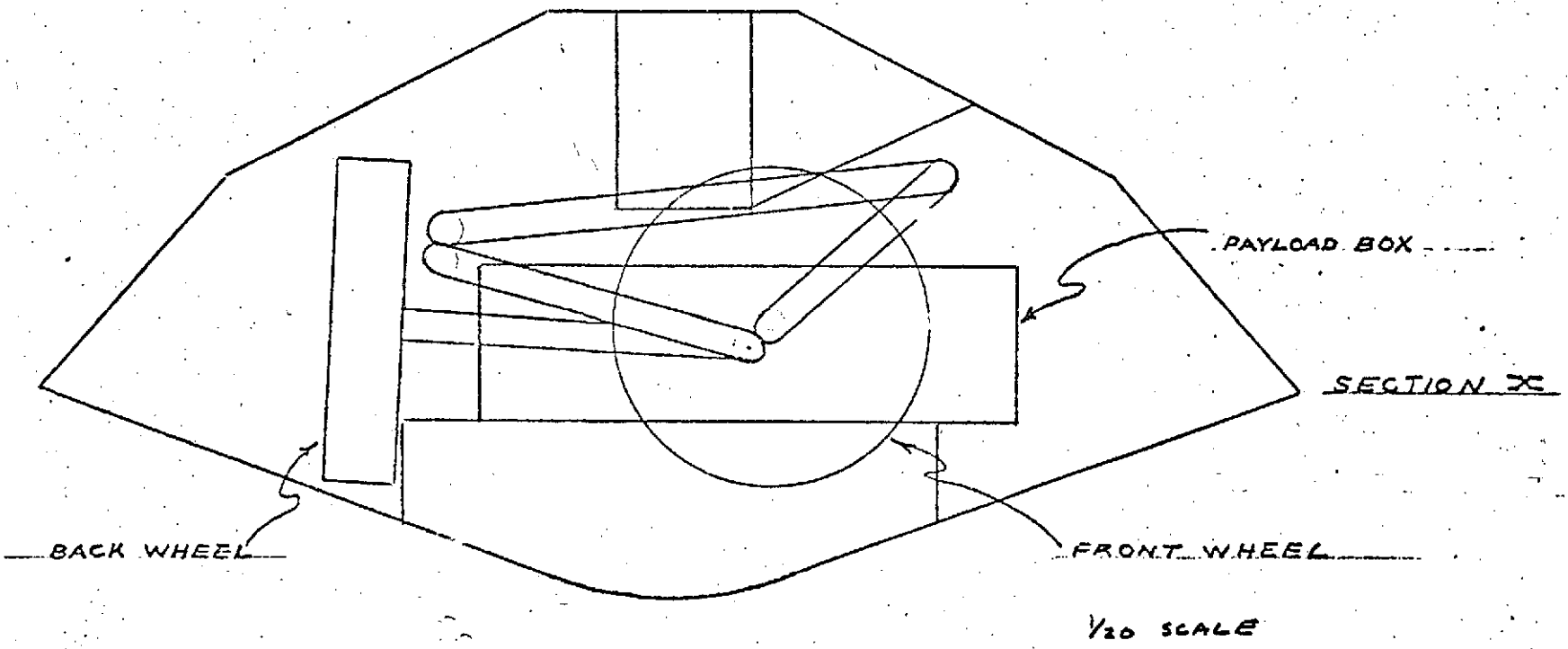

Fig. 11. Folded Vehicle in Capsule

Progress Summary. A wheel design has been chosen which appears superior to last year's wheel.

Discussion. Last year's circular hoop-spoke design proved to lack sufficient lateral stiffness. During this past summer several hoop designs were constructed and analyzed. The best design with respect to lateral stiffness was chosen and is being used on the wheel at this time, Fig. 12.

No problems are seen to exist at this time. Future work involves completion of an actual wheel and complete testing of the design. This is planned for the spring term.

A.3.c. Detailed Design and Wheel Construction

Objective. Wheels of the new improved design will be provided for the half-scale model in time for assembly.

Progress Summary. An improved design for the toroidal metal wheel has been developed and construction is underway.

Discussion. The previous design for the MRV wheels had a problem in lateral stability in that the wheels could not resist side loads of any great magnitude. To solve this problem the hoop-spokes were stiffened near the hub and their shape altered from the former circular configuration to a pear-shaped curve, Fig. 12.

The detailed mechanical configuration of hub and bearings has been established. A method of construction of the wheel hubs was found to save aluminum and reduce costs, heliarc welded bearing supports in the wheel web save many hours of machining. In addition to these points, it was decided to make the rear wheels stiffer than the front wheels by increasing the thickness of the metal involved rather than configuration or the number of spokes. Rubber mounts were selected and procured to serve as hinges between spokes and outer rim.

Schedule.

Construction to be completed by	5/10/74
Testing on vehicle through	6/30/74

A.4. Radio Control - J. Cooley, F. Gorton, D. Perly, L. Heyl, L. Bradshaw, T. Geir, K. Fell
Faculty Advisor: Prof. G. N. Sandor, Prof. W. Moyer

A.4.a. On-board Electrical Controls

Objective. Control of on-board motors for steering, speed, payload, and emergency maneuver.

Progress Summary. A scheme for controlling the motors with digital information has been developed, Fig. 13. It involves digital/analog (D/A) converters and analog feedback at the

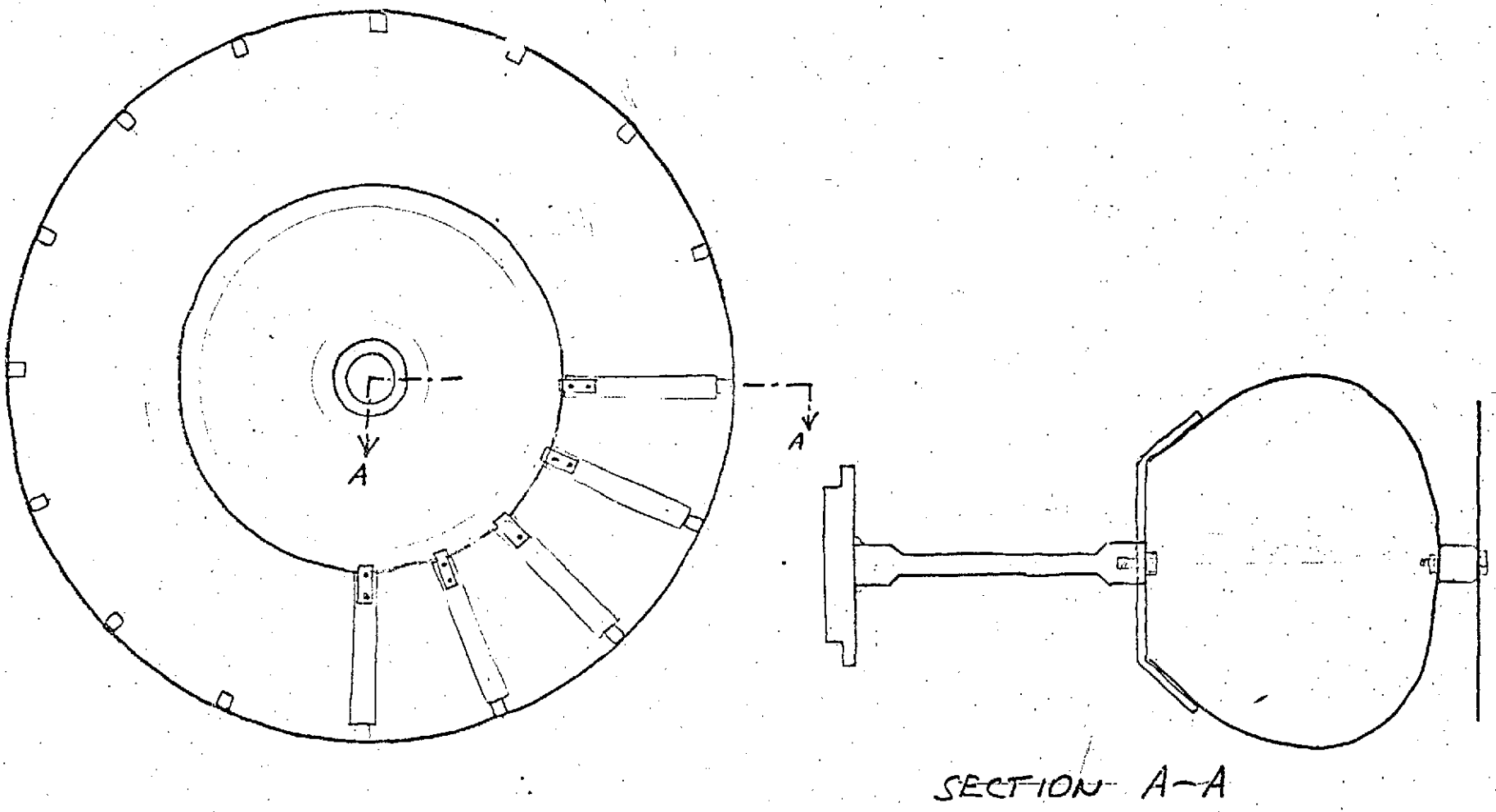

Fig. 12. Proposed Wheel Design

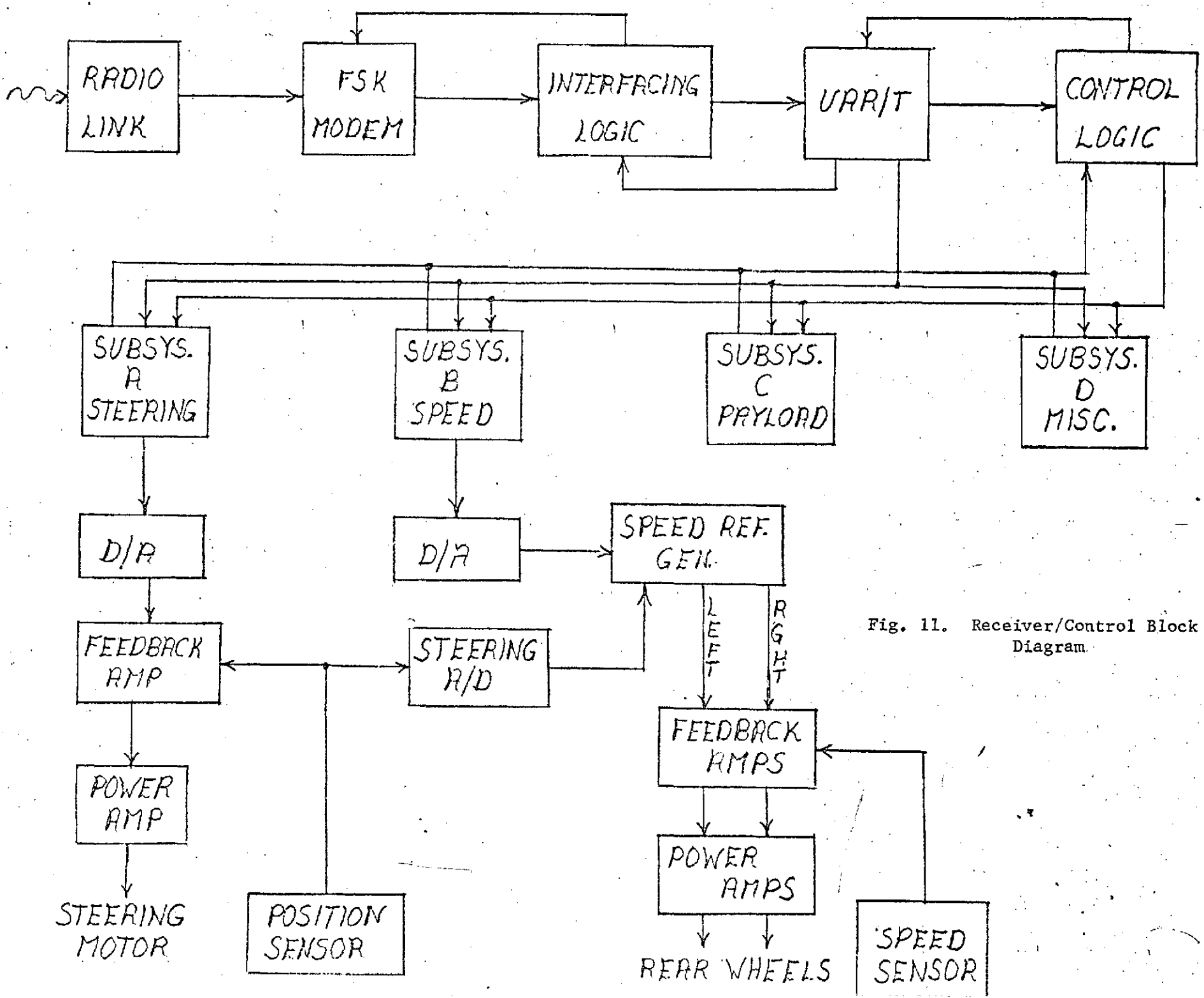

Fig. 11. Receiver/Control Block Diagram

motors. This system is currently under construction and test.

Discussion. The vehicle functions are divided into four subsystems as follows:

Subsystem A - steering

Subsystem B - speed

Subsystem C - payload

Subsystem D - miscellaneous

The steering commands are stored in an analog Read Only Memory (ROM), built out of an operational amplifier and a resistor ladder. The commands are addressed by a 4-bit digital word, and take the form of a reference voltage. This voltage is fed into a position control feedback network which controls the steering motor. The analog ROM has been built and tested for steering angles of 0^{o}, $\pm 5^{o}$, $\pm 20^{o}$, $\pm 30^{o}$, $\pm 45^{o}$, $\pm 60^{o}$, and $\pm 90^{o}$. The design of the motor control is still under study.

The speed voltage reference is generated in a 2-bit plus sign-bit D/A converter. This signal is fed into an electronic differential which uses a signal from the steering subsystem to generate the required differential action in the rear wheels to avoid skidding in a turn. The rear wheel motors are controlled from there by a tachometer feedback scheme. This system is currently under construction.

The two payload motors raise and lower front and rear struts, levelize the payload and activate the deployment sequence. They are controlled in a forward-backward-stop mode. The digital portion of this subsystem is under construction and the analog portion is under study.

The remaining subsystem controls only the emergency maneuver motor in the forward-backward-stop mode. This motor causes the steering post to rotate with respect to the front struts about a transverse horizontal axis. The status of this subsystem is the same as the previous one.

No major problems are foreseen in this area, and construction should be complete by stages running into March.

A.4.b. Radio Link

Objectives. Radio communication with the vehicle and routing of commands to proper subsystem.

Progress Summary. Frequency shift key (FSK) encoding is used with walkie-talkies to provide the necessary link. The entire system has been tested on the bench and is currently under construction, Fig. 14.

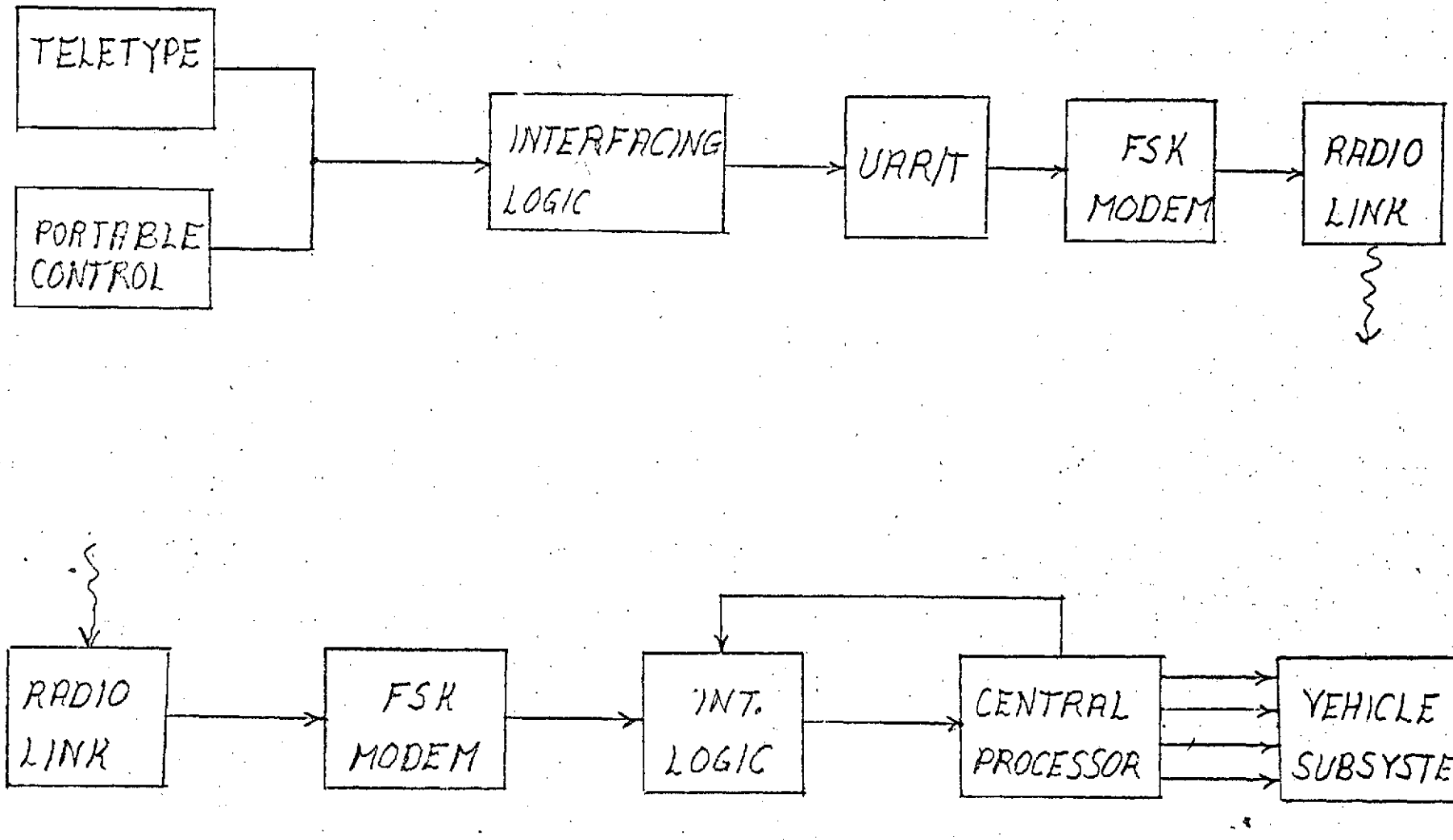

Fig. 14. System Block Diagram

Discussion. The serial output of a Universal Asyncronous Receiver/Transmitter (UAR/T) is fed into an FSK modem modulator/demodulator) which uses a Voltage Controlled Oscillator to generate two audio tones corresponding to the two logic values. These tones are transmitted via the walkie-talkies to the vehicle. They are decoded to voltage levels via a Phase Lock Loop and Comparator. The signal then goes to another UAR/T for decoding. Control logic then checks the validity of the signal and routes the signal to the proper subsystem.

This entire system has been run on the bench and is under construction.

Construction should be finished by the end of January, after which two-way communication will be studied for eventual interfacing with a mini-computer.

A.4.c. Remote Control Station and Transmitter Design

Objectives. Production of human interface with the vehicle.

Progress Summary. Construction is underway on the remote control package. It will interface with the vehicle either by the radio link or via umbilical for bench testing, Fig. 14.

Discussion. There is a rotary switch to select one of the four subsystems and an array of sixteen pushbuttons to select the command desired for each subsystem. Once the command is loaded in with the pushbuttons, it is transmitted by pushing another button. This is to avoid inadvertently sending the wrong command.

In transmitting, the command is loaded into the UAR/T mentioned earlier. The UAR/T then provides a serial signal for the FSK modem and walkie-talkie.

Construction is underway on this module and should be complete by the end of January.

Task B. General Systems Analysis

B.1. System Modeling and Design Optimization - C. Pavarini
Faculty Advisor - Prof. E. J. Smith

Optimal designs have been developed for three major alternative models, i.e. four-wheeled vehicle with either direct earth link or an orbiter-earthlink and a six-wheeled vehicle with a direct earth link. The method by which to obtain optimal design for these and other cases has been developed in general terms. Methods for determining the sensitivity of the optimal designs to perturbation of design parameters have also been developed. This task is now complete and a technical report is scheduled for issuance in February of 1974.

B.2. On-Board Computer Design - B. Fishman
Faculty Advisor: Prof. E. J. Smith

The objective of this task is to develop the software and hardware design specifications for the on-board computer. In addition, support will be provided for the remote control of the 0.5 scale vehicle.

During the 1972-1973 period the on-board computer design was investigated by a statistical approach using queuing theory and random variables to study the average behavior of the computer-vehicle system. The computer-vehicle system interaction was modeled by assuming the computer could be viewed as a queue server, servicing "customers" on two queues, a fixed queue and an interrupt queue. The results of this initial study brought into focus the more important problem of the overall computer design. It was apparent that the computer design specifications, both in regard to software and hardware, were necessary before a logical design process could be initiated. To determine these specifications, it is assumed that all of the control and scheduling decisions will be provided autonomously by the computer. The goal will be to synthesize a design that will meet the lowest realizable specification bound. Since changes in one part of the design can affect other areas, the design process has been initially divided into several steps.

The first step is the identification of what would determine an optimal design. Volume, weight, and cost are the physical restrictions on the computer. Power consumption and heat generation also affect the usefulness of a design. In the process of optimization one can compare the amount of hardware necessary for various approaches to a part of the design. In terms of primary storage, switching networks, and operation features which are fabricated by means of integrated circuit chips the above restrictions are monotonically related so that changes in one of them such as weight gives predeterminable and closely related changes in the others.

Therefore except for changes in input-output devices and possible use of secondary storage the above "costs" can be looked at in one measure, complexity.

The other restriction on the design of the on-board computer is the ability to perform the functions required of it. These functions can be looked at in the general sense as the reading of sensors, performance of operations on the information of sensors, making of decisions which may involve further reading of sensors, and operation until finally a result is stored for later use and/or commands generated for the purpose of control. This could further be reduced to requirements of storage and the amounts of various types of operations performed. Due to the presence of decisions and therefore multiple logical paths the storage and operation requirements may be random variables. The requirements produced by these functions would be how often they need to be done, and the response quickness required.

At this point the initial hardware decisions can be made. Assuming the sequencing method uses little time or storage, the word size or sizes can be chosen in regard to the accuracy needed in calculations and information content of logical variables. The decision of what types of operations should be hardware wired, and how, can be made. The number and types of operations are known. Since the time an operation takes can be balanced against the hardware required, the value of shortening of time vs gain in hardware is not precisely known at this point. However, an estimate should be reasonable knowing that the computer time required cannot be reduced without changing the handling of the functions.

Some of the software decisions can be made at this point. Due to considerations outside the computer, many functions cannot take place simultaneously. This could be due to battery drain as well as physical incompatibility of some functions. The vehicle would not rove and be expected to charge the batteries at the same time. The decisions of the types of modes can be made now since consideration of response times will have been made. This would not significantly effect hardware since even if an operation is used more frequently in a particular mode, its average use remains the same. Changes in mode would be by interrupt, i.e. low battery, or simple completion of mode purpose.

The design so far will have tried to keep the complexity of the software to a minimum. At this stage the amount of hardware needed could be excessive. To reduce the amount of primary storage, paging for each mode could be done using a highly dense (logically) secondary storage. To reduce storage further, paging could be extended to a more frequent basis or even some sort of dynamic primary storage allocation might be considered.

The time required to perform some of the functions might be reduced by the use of queues and interrupts within modes. So far the times of reading measuring devices and control actions were considered fixed or at least predictable enough to be interwoven into a predetermined flow of events and modified only by change of mode or earth initiated procedure. If the initiations of control procedures are queued by the existence of a detected situation, control procedures could be eliminated from periods when values of measuring devices are not changing significantly. This would reduce time spent on the function, but would require a more complex software and hardware.

The control procedures may be more complex in nature due to the fact that they are not initiated at fixed intervals. Also a scheduler would be needed for the modes affected having possibly more than one level of priority. This scheduler would need the hardware to monitor the status of the several sensors and to detect critical situations independently of what the computer is doing at the moment (within a given mode). It would have the ability to time a particular procedure accurately if need be. Also changes in function programs length would not be as harmful to the system timing.

The independence of the scheduler would result in some problems. It would be difficult to detect malfunctions in the additional hardware required to monitor the status of activities to be controlled. Also the activity of the computer over a given period of time would be hard to predict, increasing the difficulty of locating malfunctions in the computer itself. A compromise could be made by having the CPU time used to do the scheduling via the normal input-output devices. This would consume time but not require as much new hardware. In effect this would be redefining the function procedures and with the inclusion of a scheduling function the design procedures used so far would hold.

The computer must have the ability to handle breakdowns in functions of the rover including parts of its own hardware. Important parts of the rover might have alternate procedures which could be brought into play if a component breaks down. Also critical input-output devices, storage blocks, operations and switching networks may be replicated according to their expected lifetime. The function programs could be written in terms of "virtual" operation codes and addresses whose interpretation would be determined by setting of special storage areas. The locating of breakdowns could be done partly from the interpretation of information sent to earth. During rover time or when directed from earth, test programs could be run to locate and bypass problems. Areas where problems are difficult to detect or of importance in detecting problems, such as the direct operation of the computer from earth, might require alternative paths to be used simultaneously and the results compared. These considerations would have to be included at the time decisions relating to the complexity of the hardware are made early in the computer design.

In summary, this task is aimed at developing a framework within which software and hardware specifications can be determined systematically according to the mission requirements.

Task C. Surface Navigation and Path Control

This task is subdivided as follows: design and construction of a laser range finder; surface reflectivity and laser power requirements; three dimensional obstacle recognition; terrain parameter estimation from gradient data; laser range finder scanning systems; and path selection system evaluation.

C.1. Terrain and Obstacle Sensors

C.1.a. Construction of a Laser Range Finder - E. E. Svendsen

Faculty Advisors: Prof. C. N. Shen, Prof. W. Moyer

Objective. The objective of this task is to construct a laser rangefinder transmitter to be used in conjunction with a rangefinding system on a mars rover.

Progress Summary. The project began by researching existing

proposed laser range finder concepts and formulating new ones. After deciding on a particular concept, complete background investigation for all the electronics was undertaken. Most recently, the obtaining of the parts involved and the beginning of actual construction has taken place.

Discussion. Due to the extreme requirements of the range-finder system many refined techniques have been employed in the design of a laser transmitter. The necessity of a fast rise time pulse for accurate ranging has involved the use of state-of-the-art concepts. If a five centimeter accuracy over a range of thirty meters is considered a rise time in the order of nanoseconds is required. In order to meet this criterion, minute detail must be considered in all phases of construction as well as in the choice of the electronic components.

The proposed general circuit finally shown in Figure 15 operates in the following manner. Before the SCR is triggered, the capacitor is charged up by voltage V through the resistor. When the SCR is fired by a trigger pulse applied to the gate, the charge built up on the capacitor will quickly discharge through the SCR and the laser diode. The other diode placed in the reverse direction across the laser diode is to prevent any "backlash" current pulses from damaging this laser diode. A current monitoring probe is placed on the lead to the laser diode to permit monitoring of the current pulses. The actual circuit differs slightly from that shown in Figure 15 and is shown in Figure 16. The difference is designed to reduce circuit inductance which would slow down the rise time. In order to further cut down on the rise time, it has been proposed to construct the transmitter in a radially symmetric fashion as can be seen by the sketch shown in Figure 17. Note that instead of one lumped capacitor, the total capacitance has been split into five smaller parallel capacitors arranged in a radial floral pattern. Three SCR's are used instead of one with the expectation that more current can be pumped more quickly around the circuit. Three SCR's were chosen as a compromise. Too many could introduce excess capacitance into the circuit and cut down on the rise time. It is important to note the overall coaxial symmetry of the entire transmitter as it is hoped that this will significantly affect the overall operation especially with respect to rise time.

These are the actual components finally decided upon and obtained. An approximate 25 Kohm resistor is located in the charging path to fix the RC time constant small enough to allow recharging of the capacitors before the next laser pulse. Five .004 μf. capacitors arranged florally provide a total capacitance of .020 μf. Sprague ceramic disc types were chosen for their low inductance property. Three Unitrode GA-201 thyristors (SCR's), known for their fast rise time are used as pulsers, Ref. 1. An SG-2007 infrared laser diode is used as the actual light pulse transmitter, Ref. 2.

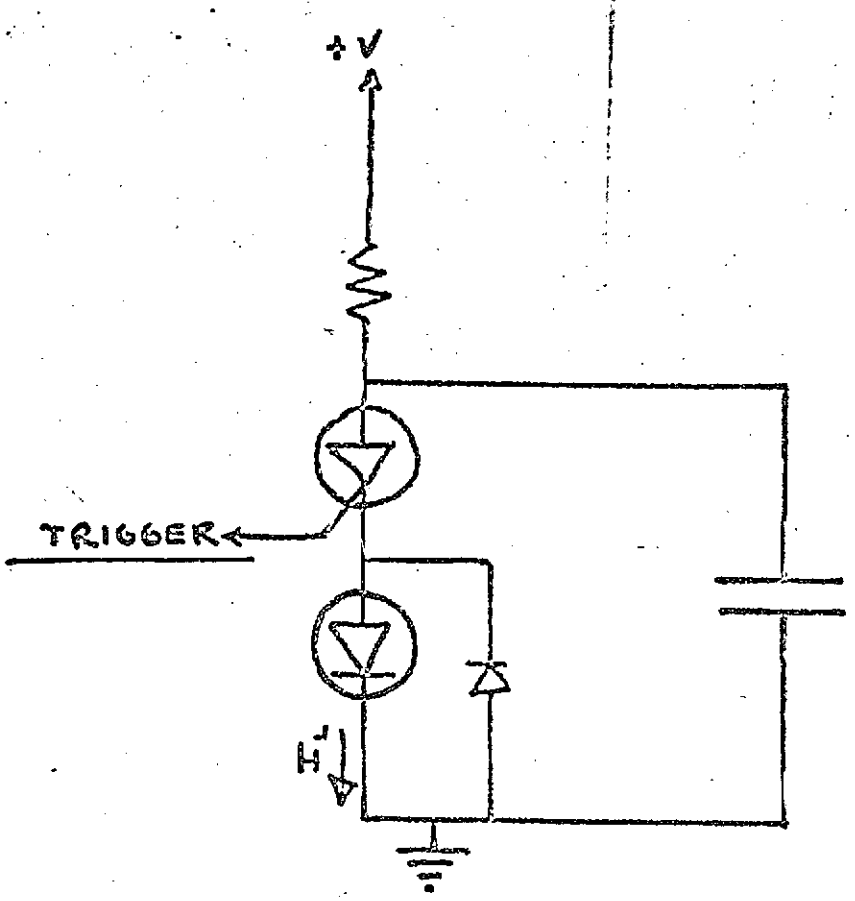

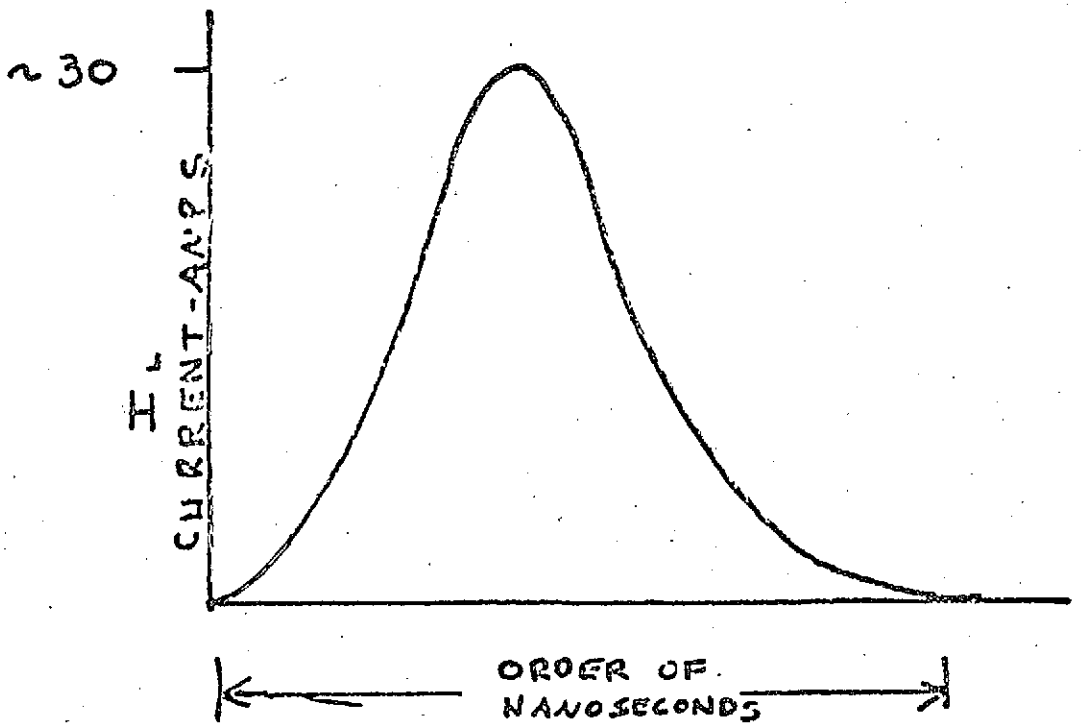

Fig. 15. General Circuit

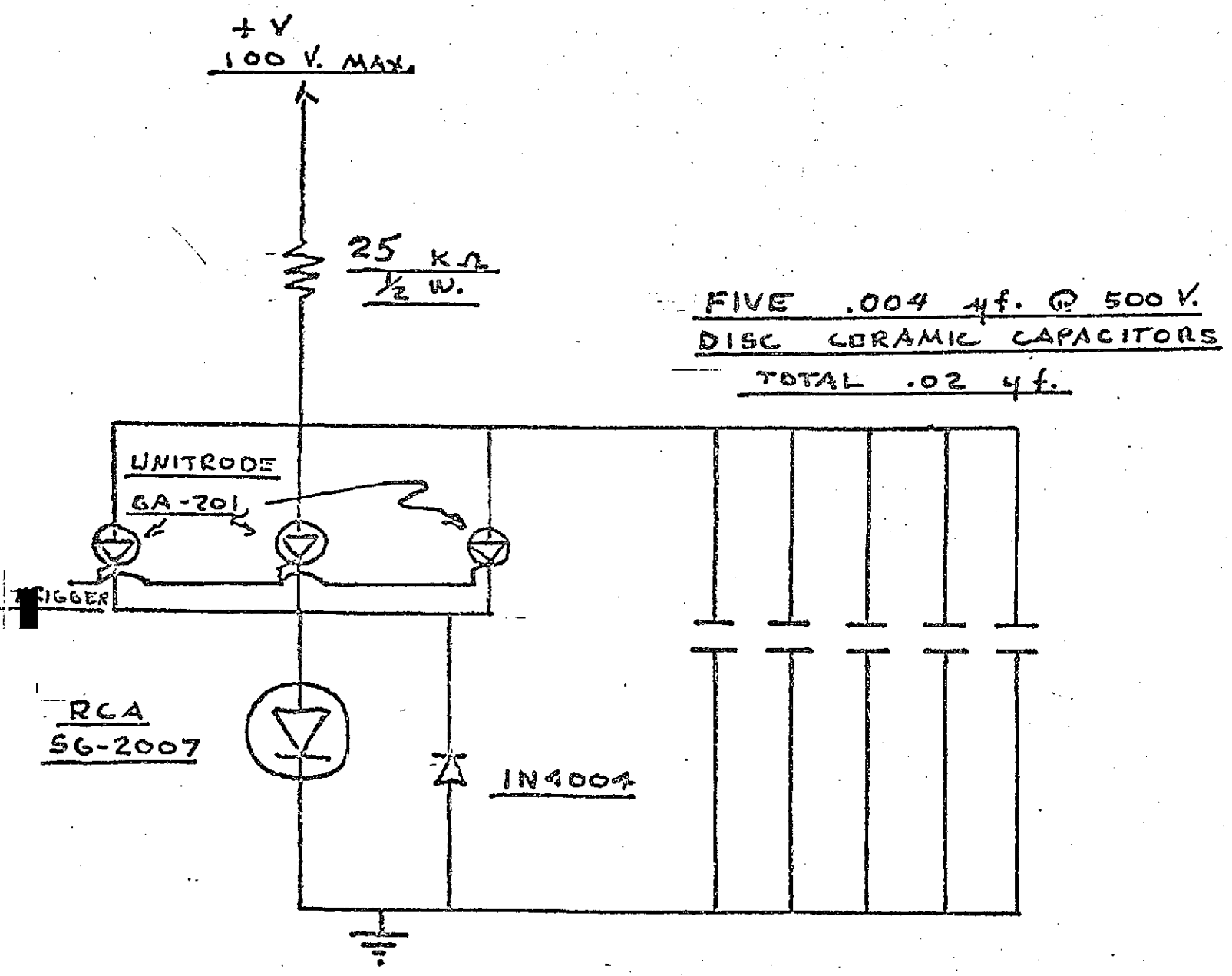

Fig. 16. Circuit Schematic with Actual Parts

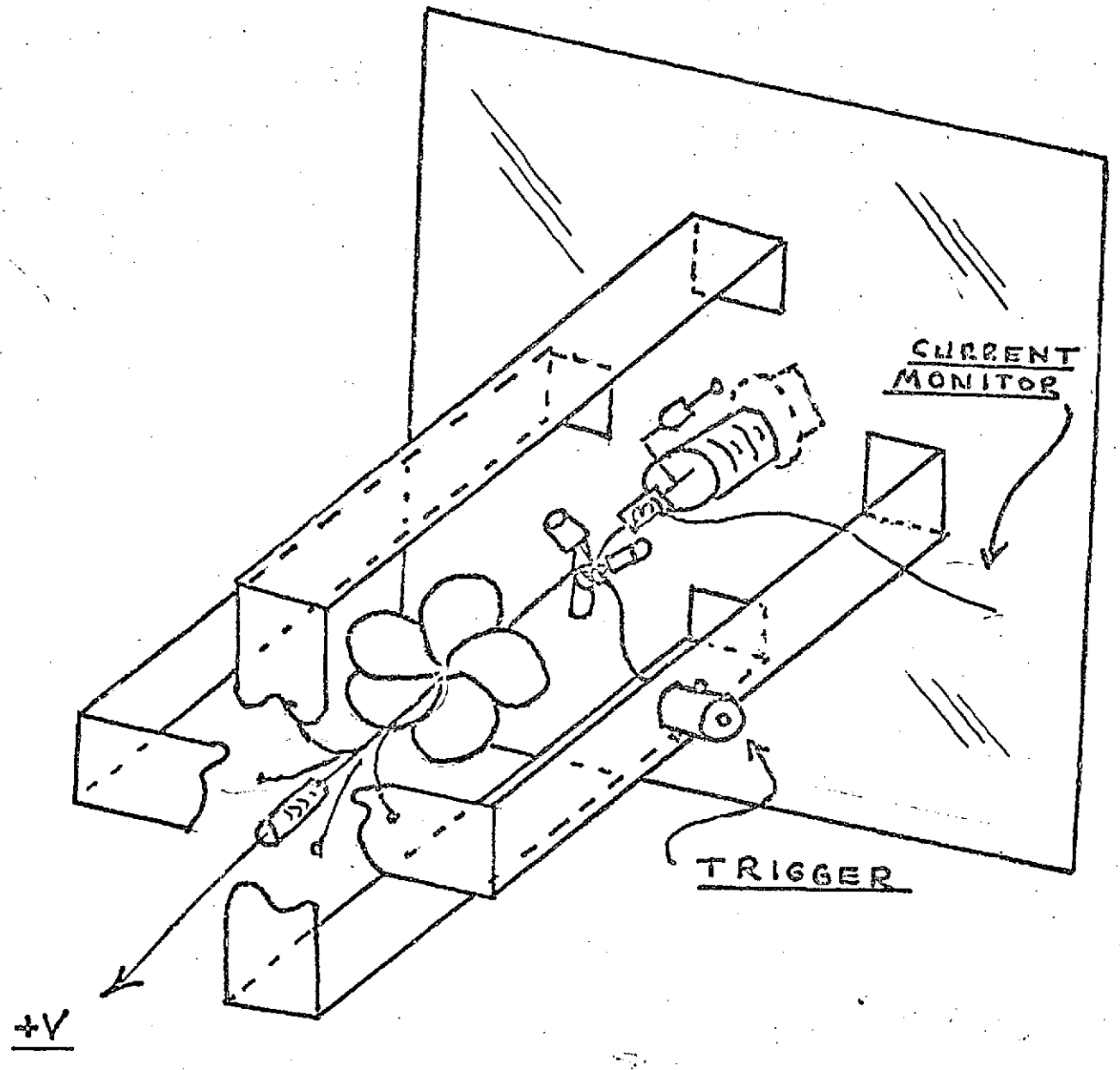

Fig. 17. Sketch of Transmitter - Rear View (Distorted)

The final assembly is very important in cutting down on inductance as previously mentioned. Copper sheeting is used as the return ground path. Flat sheets are less inductive than round wires. The current pulse will go down the center of the assembly and return on the outer path through the copper sheeting.

Most recently, all the parts for the transmitter have been obtained and final assembly is now in progress. Practical considerations such as matching up a triplet of SCR's are being looked into. Before actual pulsing of the laser diode itself, a IN4004 diode will be used to test the circuit. The characteristics of this diode are supposed to be similar to those of laser diodes, Ref. 3. This same type diode is also used for back protection of the laser diode when it is placed in the circuit. By using a substitute diode in initial tests it will be possible to adjust the pulse parameters to fit the limitations of the laser diode. In this way, a burned out laser diode can be prevented.

In the final operation with the laser diode in place, it is hoped that a critical point regarding laser output pulse rise time will prove itself. The current pulse to the laser will certainly be adjusted for the fastest rise time. However, this is not the pulse involved in the time of flight range measurement. The light output pulse of the laser is the critical quantity. It is hoped that with a fast current pulse, a light output pulse with a rise time in the order of nanoseconds will be obtained when the current pulse exceeds the threshold value of the laser diode, Ref. 2. This remains to be seen in the test results.

In the near future, it is hoped that the assembly of the transmitter be completed and put into test operation. A suitable receiver must be constructed to aid in the testing procedure.

PIN photodiodes have been proposed because they lend themselves well to rugged environment. A photomultiplier tube is also being considered. These tubes have good sensitivity and an amplification factor not found in photodiodes.

Also in the immediate future is the consideration of optics for the transmitter and receiver. Questions such as whether or not normal lenses will operate well in the infrared range of the laser is one of many that must be answered.

With transmitter, receiver, and optics finally assembled meaningful range measurement tests can be performed. From this, a subsequent appraisal of this form of ranging can be made.

Shown below if the projected schedule of work to be undertaken.

	Assembly and Operation of Laser Transmitter	Receiver and Optics	Range Testing	Write-up and Considerations for Further Investigation
February	———			
March		———		
April			———	
May				———

C.1.b. Surface Reflectivity, Laser Power Requirements and Receiver Selection - Wesley Dull
Faculty Advisors: Prof. C. N. Shen, Prof. W. Moyer

Objective. The primary objective of this subtask is to experimentally study the characteristics of laser light reflection from surfaces similar to those that might be found on the Martian terrain so as to determine the performance requirements of both the laser rangefinder transmitter and receiver. A second objective will be the optimum choice of receiver considering both electrical power requirements and the expected dynamic range of the reflected laser light.

Progress Summary. Progress to date has been in the determination of what quantities must be experimentally measured to accomplish the stated objective and also in the construction of a test apparatus to perform the desired measurements.

Discussion. The basic problem to be considered is that it is not exactly known what reflected signal levels to expect as the laser rangefinder scans the Martian terrain at ranges varying from three to thirty meters ahead of the vehicle. As can be seen from Figure 18, the incident angles measured with respect to the local surface normal that the rangefinder might encounter can vary anywhere from 0 degrees to 90 degrees. It is thus desired to be able to measure some physical quantity of a given diffuse reflector that will give the received signal level for a given transmitter and receiver as a function of the position of the laser transmitter and receiver with respect to the reflecting surface.

A quantity which can be used to characterize reflections from a diffuse reflector is the bidirectional reflectance ratio. It was decided that the bidirectional reflectance ratio should be measured experimentally rather than calculated analytically for two reasons. First, models for diffuse reflectors from which analytical calculations of the bidirectional reflectance ratio can be made have been developed only recently. As a result, there is not a large amount of data from comparisons between analytically determined and experimentally determined bidirectional reflectance ratios, Ref. 4 and 5. Secondly, the actual analytical calculation of the bidirectional reflectance ratio can be rather involved requiring detailed knowledge of the

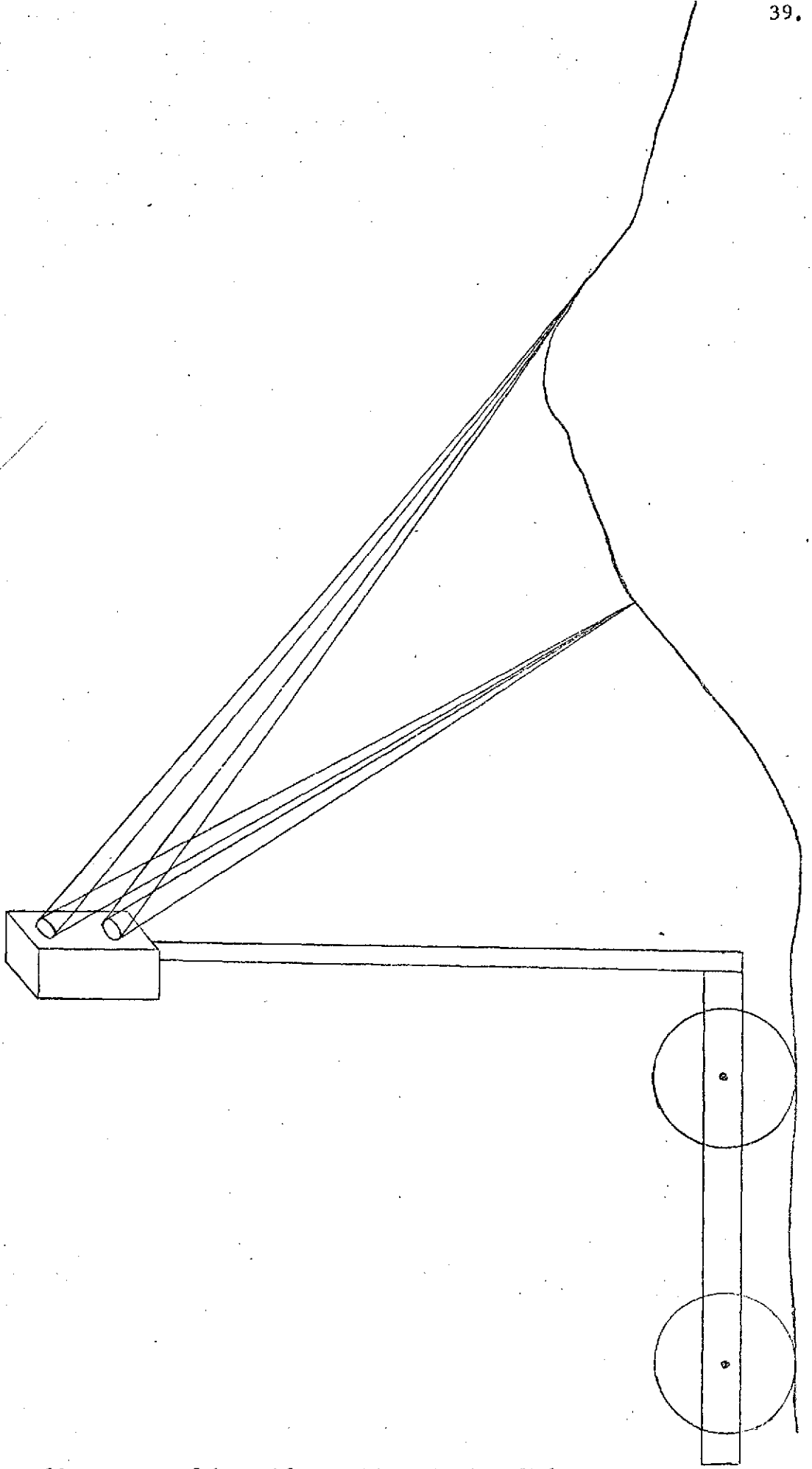

Fig.18. Range of Possible Incident Angles With Respect to the Local Surface Normal

characteristics of the diffuse reflector, Ref. 6.

Figure 19 shows the quantities that define the bidirectional reflectance ratio along with the coordinate system commonly used in association with the bidirectional reflectance ratio. The bidirectional reflectance ratio is according to Ref. 4 defined as

$$\rho(\psi;\theta,\alpha) = \frac{N_r(\psi;\theta,\alpha)}{d\phi_i(\psi)/dA} \qquad (1)$$

where $d\phi_i(\psi)$ and dA are defined in Fig. 19 and $N_r(\psi;\theta,\alpha)$ is the reflected radiance in the directions θ, α due to the incident beam at angle ψ. In terms of quantities defined in Fig. 19

$$N_r(\psi;\theta,\alpha) = \frac{d\phi_r(\psi;\theta,\alpha)}{(d\omega_r)(dA)\cos(\theta)} \qquad (2)$$

Making use of the bidirectional reflectance ratio as defined in Equations 1 and 2 from Ref. 4, the reflectance at any receiver position can be studied. The receiver position of interest to this subtask, however, is one at which the receiver is located in close proximity to the transmitter. Therefore, from examination of Fig. 19, it can be seen that the bidirectional reflectance ratio should be evaluated at approximately the angular position $(\psi;-\psi, 180^\circ)$.

Once $\rho(\psi;-\psi, 180^\circ)$ is evaluated for ψ ranging from 0 degrees to 90 degrees, two useful pieces of information become available. First, if $\rho(\psi;-\psi,180^\circ)$ is normalized over the range of interest for ψ, the complete dynamic range of expected received signals can readily be read from a plot of normalized $\rho(\psi;-\psi, 180^\circ)$ vs ψ. Secondly, if the actual values of $\rho(\psi;-\psi,180^\circ)$ are measured over the range of interest for ψ, the amount of power incident upon a given receiver at a given position can easily be calculated given the transmitter power, assuming that the transmitted power is focused on the reflecting surface.

Since the bidirectional reflectance ratio is defined for differential areas and differential solid angles, any measurement scheme must assure that the illuminated portion of the reflector surface and the light sensitive area of the receiver be kept as small as possible. Although it is important to keep the light sensitive area of the detector as small as possible, it is also important that this light sensitive area be much larger than the illuminated area of the diffuse reflector under test. This is to ensure that the solid angle $d\omega_r$ illustrated in Fig. 19 is a meaningful quantity for the measurement scheme being used. To ensure a meaningful solid angle $d\omega_r$, it was decided to use a small focusing lens ahead of the detector to increase its light sensitive area.

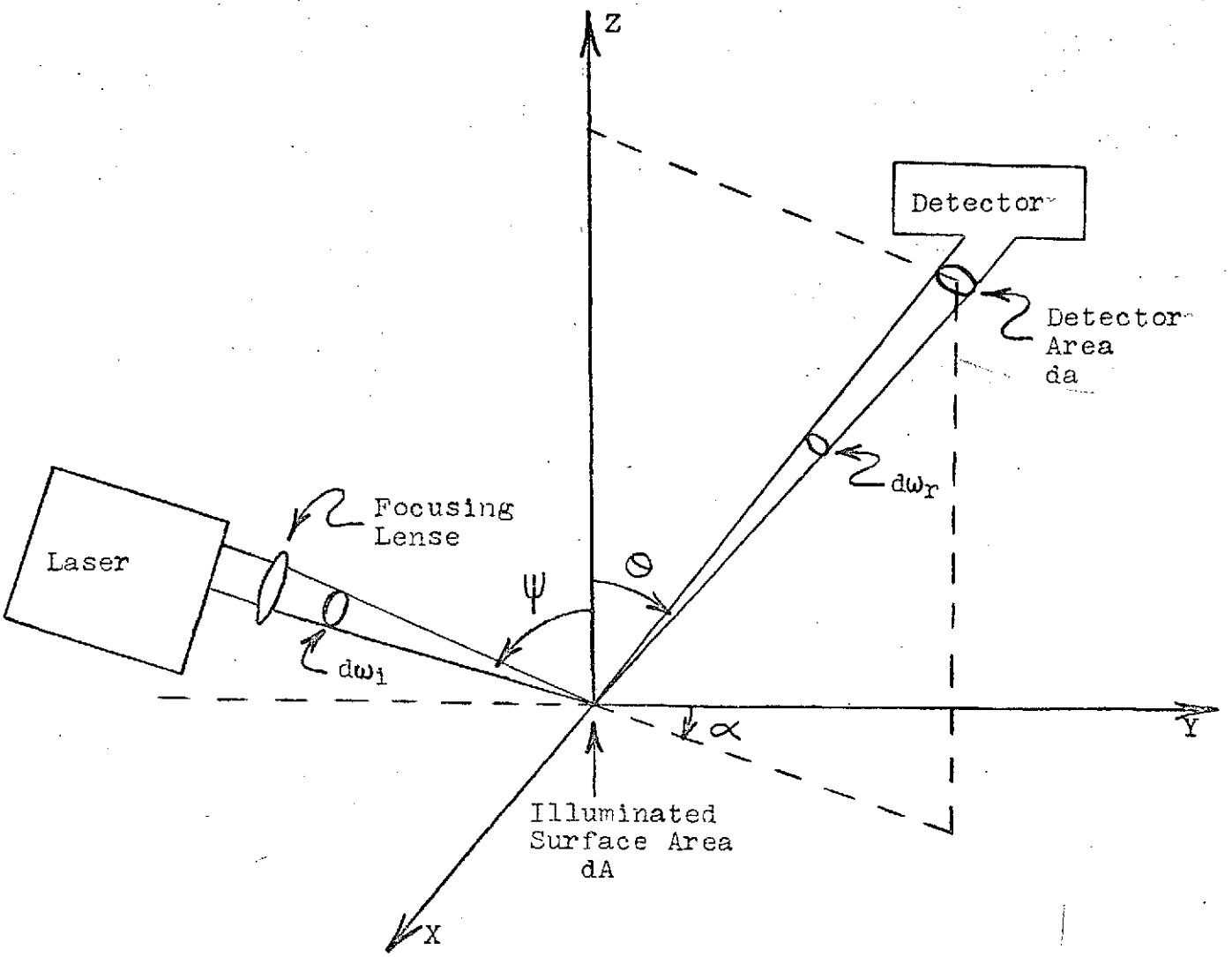

1) The reflecting surface is in the XY plane

2) The incident beam is in the ZY plane

3) $d\omega_i$ - Solid angle of the transmitter as viewed from the reflecting surface

4) $d\omega_r$ - Solid angle of the receiver as viewed from the reflecting surface

5) $d\phi_i(\Psi)$ - Incident radiant flux in units of power that is focused from the source located at angular position Ψ onto the test sample area dA

6) $d\phi_r(\Psi;\Theta,\alpha)$ - Reflected radiant flux in units of power in the direction Θ,α due to the incident beam at angle Ψ

Fig. 19. Bidirectional Reflectance Ratio Coordinate System

It was decided to use a photodiode in a first attempt to measure the bidirectional reflectance ratio. The main reasons for this choice are that the photodiode is inexpensive and a semiconductor, making it highly desirable to use on the Mars rover. To use the photodiode to measure bidirectional reflectance ratios, the device must be biased so as to operate in a nonsaturated mode. As shown in Figure 20, the photodiode operating characteristic that can be used to measure bidirectional reflectance ratios is expressed in Ref. 7 by the equation

$$I = KH \tag{3}$$

where I, K, and H are as defined in Fig. 20.

The light from the laser transmitter used in the measurements will be chopped mechanically so that the detector response due to the laser light reflected from the reflecting surface can easily be distinguished from the detector response due to the background light.

The next problem is to express the quantities used to define the bidirectional reflectance ratio in terms of measurable angles, distances, and detector operating voltages and currents. Figure 21 shows how the photodiode detector circuit of Fig. 20 can be used to measure $d\phi_i(\psi)$. Assuming that the laser beam is approximately uniform in its cross-section and that the cross-sectional area of the laser beam can be measured, the following expression for the radiant flux of the laser beam can be derived:

$$d\phi_i(\psi) = \frac{I_i(\psi)\, dA_1}{K_r} \tag{4}$$

The quantities in Equation 4 are as defined in Fig. 20 and 21. The notation $I_i(\psi)$ is used to indicate that the photodiode current in this case is measured for incident radiation from the laser source at angle ψ.

Figure 22 shows how the photodiode detector circuit of Fig. 20 can be used to measure $N_r(\psi;-\psi,180^\circ)$. Making use of Equations 2 and 3,

$$N_r(\psi;-\psi,180^\circ) = \frac{I_r(\psi;-\psi,180^\circ)\, da}{(K)\, dA\, (d\omega_r)\cos(-\psi)} \tag{5}$$

where the quantities are defined in Fig. 19, 20 and 21. The notation $I_r(\psi;-\psi,180^\circ)$ is used to indicate that the photodiode current in this case is measured for reflected light at the angular position $(\psi;-\psi,180^\circ)$. Equation 6 assumes that all of the light incident upon the focusing lens of cross-sectional area da_1 is focused onto the light sensitive area of the photodiode.

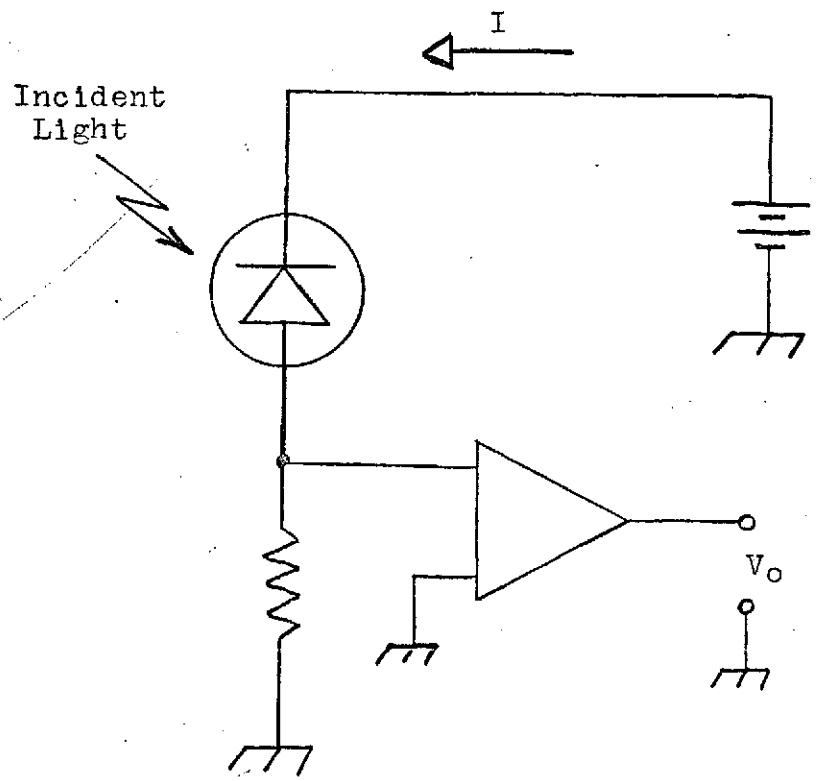

1) I- Back bias diode current flow

2) K- Constant characteristic of the diode

3) H- Total incident radiation on the diode light sensitive area divided by the diode light sensitive area (units of power/area)

4) V_o- Amplifier output

5) V_o is proportional to I

6) I=KH - Nonsaturated operating characteristic of the photodiode

Fig. 20. Photodiode Detector Circuit

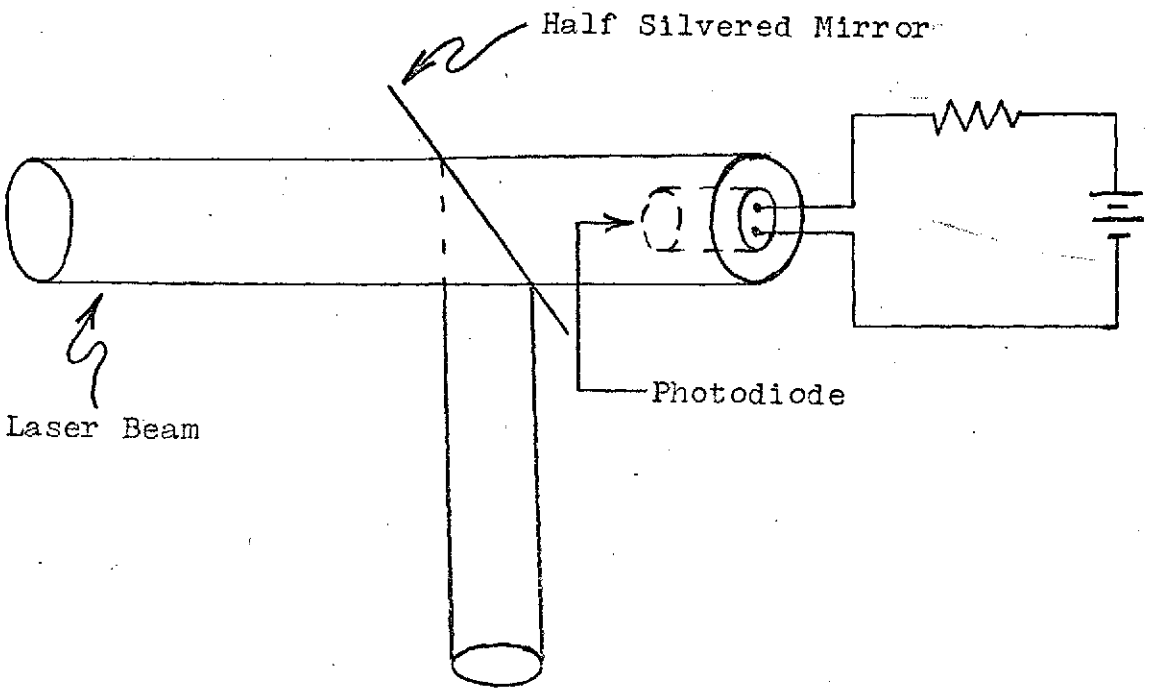

1) da- Light sensitive area of the photodiode

2) dA_1- Cross-sectional area of the incident laser beam

3) r- Fraction of light incident upon the half silvered mirror that is transmitted

4) $d\phi_i(\Psi)$- Radiant flux of the laser beam (units of power)

5) $d\phi_{id}(\Psi)$- Radiant flux of the laser beam (units of power)

Fig. 21. Measuring Incident Radiant Flux

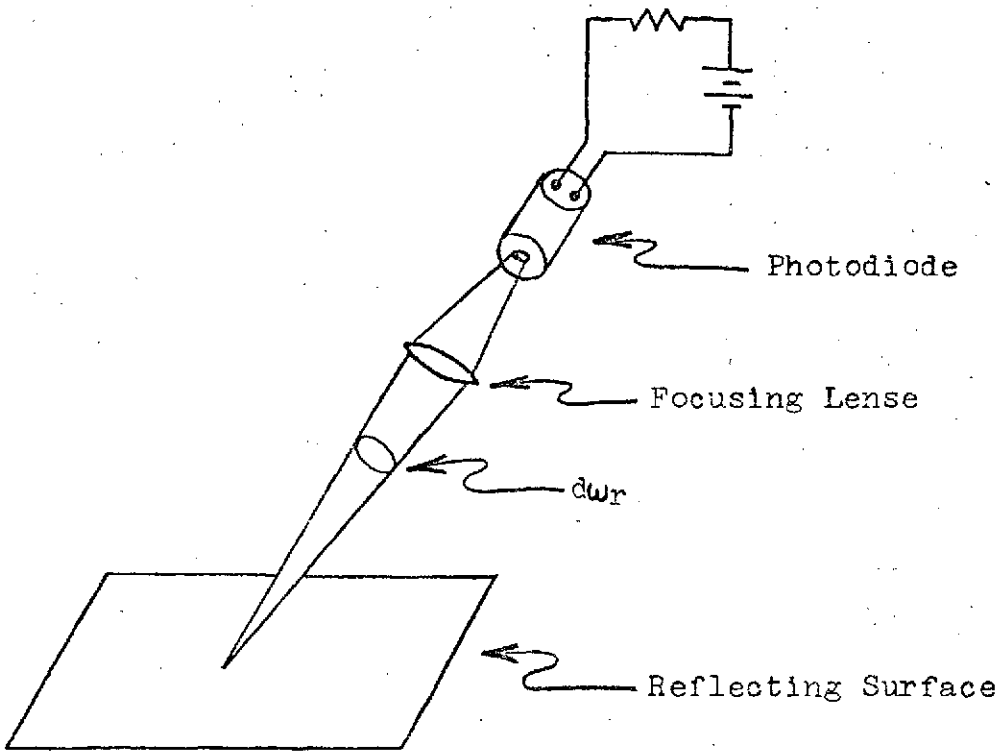

1) $d\omega_r$- Solid angle of the receiver as viewed from the reflecting surface

2) da- Light sensitive area of the photodiode

3) dA- Area of the reflecting surface under test that is illuminated by the laser

4) da_1- Cross-sectional area of the focusing lense

Fig. 22. Measuring Reflected Radiance

the photodiode.

Equations 4 and 5 can be substituted into Equation 1 to arrive at the key equation for measuring the bidirectional reflectance ratio for the receiver located at about the same position as the transmitter:

$$\rho(\psi;-\psi,180^\circ) = \frac{(r)I_r(\psi;-\psi,180^\circ)\,da}{I_i(\psi)\,dA_1(d\omega_r)\cos(-\psi)} \qquad (6)$$

The easiest bidirectional reflectance to measure is the normalized bidirectional reflectance ratio. If ψ_m is the angular position for which $\rho(\psi;-\psi,180^\circ)$ takes on its maximum value as ψ is varied from 0 degrees to 90 degrees, the normalized bidirectional reflectance ratio is given as

$$\rho_N(\psi;-\psi,180^\circ) = \frac{\rho(\psi;-\psi,180^\circ)}{\rho(\psi_m;-\psi_m,180^\circ)} \qquad (7)$$

This normalized bidirectional reflectance ratio can be expressed as

$$\rho_N(\psi;-\psi,180^\circ) = \frac{I_r(\psi;-\psi,180^\circ)\cos(-\psi_m)}{I_r(\psi_m;-\psi_m,180^\circ)\cos(-\psi)} \qquad (8)$$

Figure 23 shows the test apparatus that will be used to measure the normalized bidirectional reflectance ratio. The apparatus is at the present time almost completed. Plate "A" is used to hold the diffuse reflector under tests. Structure "B" holds the focusing lens that focuses the laser light onto the test sample. Box "C" contains the laser transmitter and receiver. The angle ψ is changed by pivoting the two arms holding the laser transmitter, receiver, and focusing lens about the bar to which plate "A" is attached.

Major problems to be faced in the short run future will be in the actual performance of the measurements described above and also in choosing some suitable method of classifying the diffuse reflectors tested.

The following is a projected schedule for the period extending to June, 1974:

	February	March	April	May
Finish Test Apparatus	———			
Perform Measurements		———	———	
Choose Best Receiver Based on Measurement Data				———

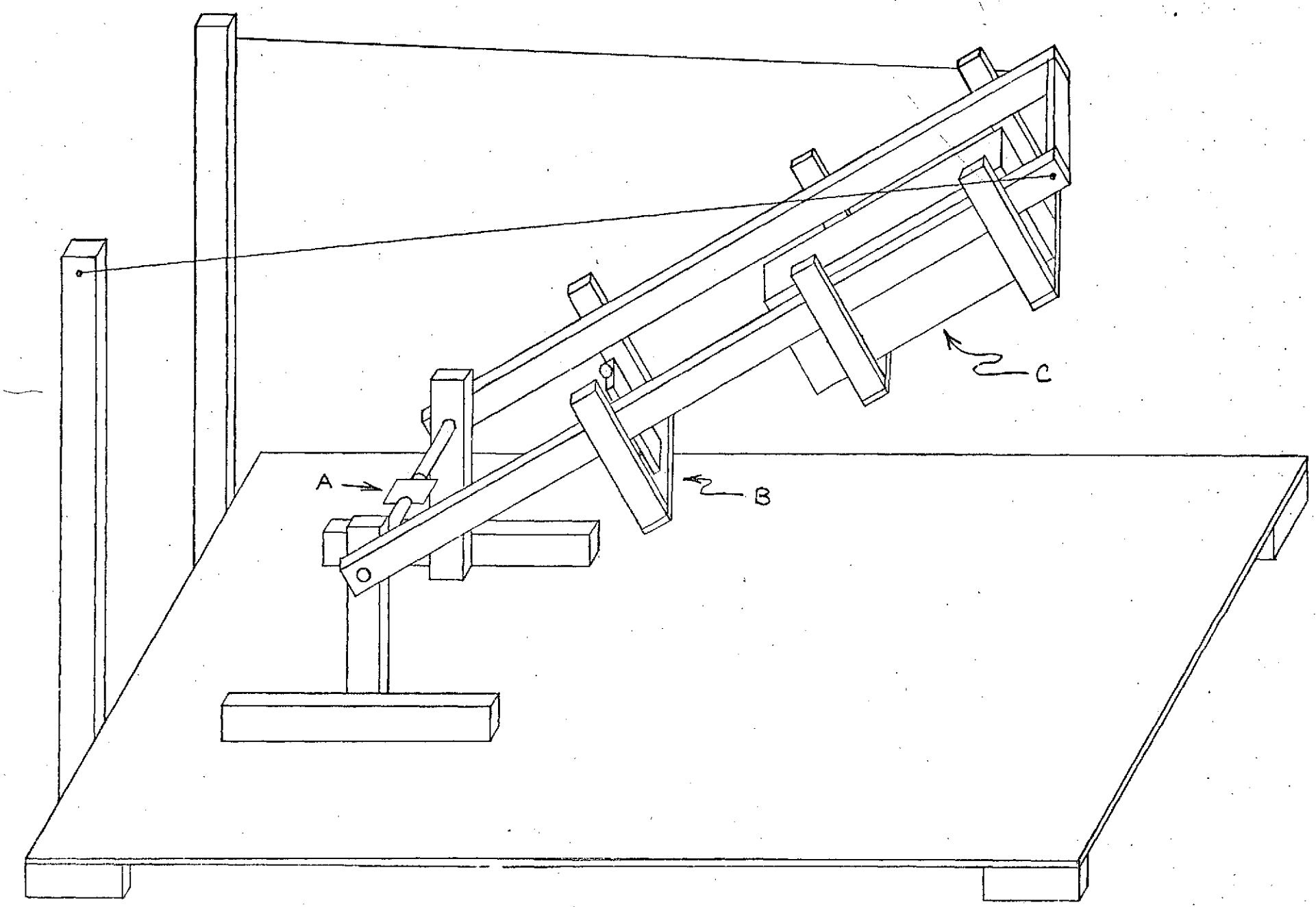

Fig. 23. Bidirectional Reflectance Ratio Test Apparatus

C.2. Obstacle Detection, Terrain Modeling and Scanning Systems

C.2.a. Recognition of Three-dimensional Obstacles by an Edge Detection scheme

Probyl Sanyal, Martin Reed
Faculty Advisor: Prof. C. N. Shen

Objective. In order to navigate autonomously on the Martian surface, the proposed Mars roving vehicle, Ref. 8, must be able to distinguish between passable and impassable terrain by means of a laser rangefinder which scans in a field approximately 3 to 100 meters ahead of the rover. Data obtained by this means will be used to determine an accurate enough "range image" of the terrain in order for the rover to choose the safest path of travel. This task is specifically concerned with the objectives of obstacle classification, identification, and detection. This report discusses work done on an obstacle detection system for this purpose, which is intended to process the information obtained by the laser range finder to provide a basis for a path selection decision.

Progress Summary. Two algorithms, one already existing in the literature and one developed in this effort, were used to obtain the outlines of obstacles from the "range image". Both of these algorithms end with a thresholding operation. A theoretical analysis shows how a proper value of the threshold may be chosen, given the type of irregularity of the terrain to be detected. The analysis also shows how large the statistics of measurement noise can be allowed without leading to false alarms, Ref. 9 and 10. Computer simulation of the schemes for the case of a hemispherical boulder at mid-range have been very encouraging and some typical results have been included. The research finding is summarized in a paper, Ref. 11, entitled "A Practical Obstacle Detection System for the Mars Rover" by Reed, Sanyal and Shen. This paper has been accepted for presentation at the Second Annual Milwaukee Symposium of Automatic Control.

Discussion. It is assumed that a laser rangefinder will be used as the primary sensing device on the rover. The laser is expected to be a much lighter piece of equipment than the T.V. camera. Fig. 24 shows how the laser scan is mounted on the rover and how it works.

The laser is mounted on a mast at a height of 3 meters from ground level. The on-board computer controls the direction of the beam. By varying the elevation angle β and the azimuth angle θ, the laser can scan a desired area.

The time difference between transmitted and reflected beams indicates the range. It is expected that the time required per range reading will not exceed 1 millisecond. Thus, in one second, or in the space of 1 meter traveled by the rover, about a thousand range readings can be obtained and these may be assumed to have been obtained from a stationary point.

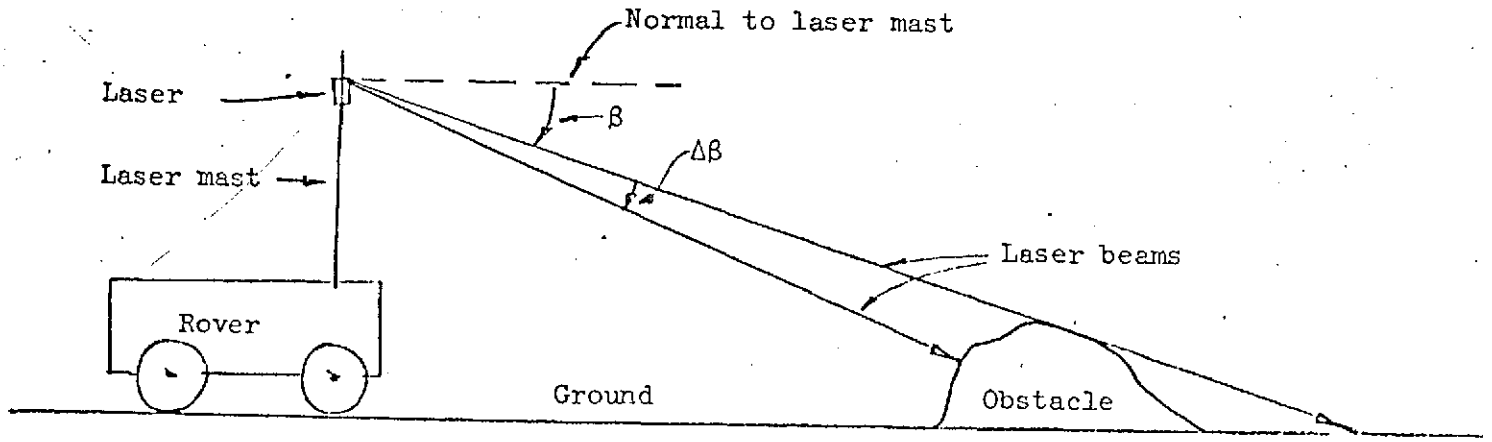

(a) Side view

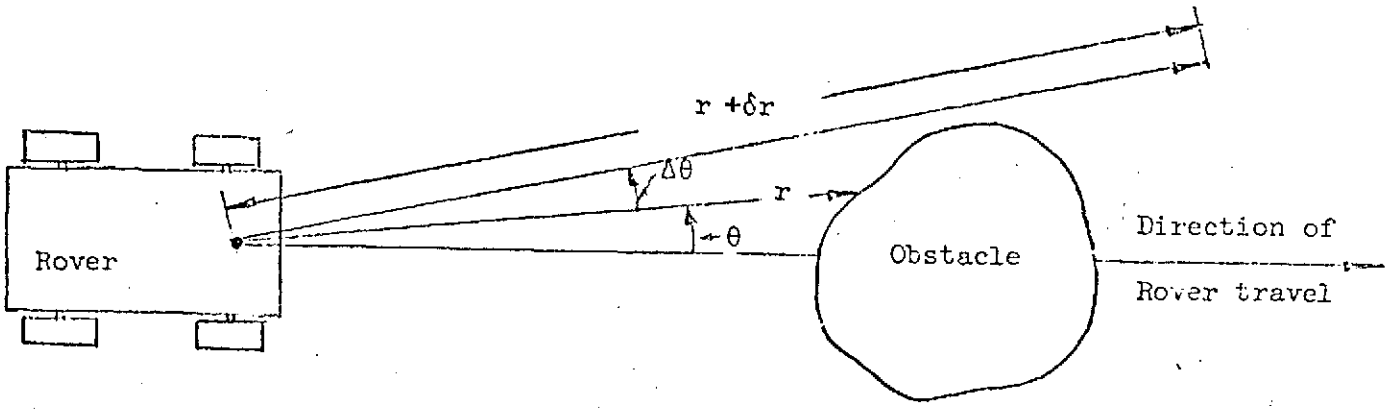

(b) Top view

Fig. 24. The laser range finder

The Range Matrix and Detection Scheme

(a) The Scan

The range data $Z_{i,j}$ obtained by varying the angles β and θ can be stored in a matrix form with the elements ordered according to the values of β and θ. The value of θ changes along the same row with the column index j, while the value of β changes along the same column with the row index i. This matrix, Z, called the measurement matrix, forms a "range image" of the scene ahead. In contrast to a photographic image, where the elements of the image are functions of the brightness of the scene, the "range image" consists of distances of the points on the scene from the point of measurement. Equation 1 shows the Z matrix.

$$Z = \begin{vmatrix} Z_{11} & Z_{12} & \cdots & Z_{1N} \\ \vdots & \vdots & & \vdots \\ & & Z_{i-1,j} & \\ & Z_{i,j-1} & Z_{i,j} \; Z_{i,j+1} & \\ & & Z_{i+1,j} & \\ \vdots & \vdots & & \vdots \\ Z_{M1} & Z_{M2} & & Z_{MN} \end{vmatrix} \qquad (1)$$

(b) The Sharp Change in Range Readings

The presence of sharp changes in the range values on the Z matrix indicate the presence of obstacles. Algorithms used to show up these sharp changes end with a thresholding operation, and the success of the algorithms depend on the relative ease with which a proper threshold can be chosen. Both algorithms tried appear to be quite successful. To apply the normalized Laplacian, Ref. 12, a new matrix Q is obtained by the following operation:

$$Q_{i,j} = \frac{Z_{i-1,j} + Z_{i+1,j} + Z_{i,j-1} + Z_{i,j+1} - Z_{i,j}}{Z_{i-1,j} + Z_{i+1,j} + Z_{i,j-1,} + Z_{i,j+1}} \qquad (2)$$

Alternatively, a four directional ratio can be used with a new matrix S obtained by the operation given below:

$$S_{i,j} = \tfrac{1}{4}\left[\left(\frac{Z_{i-1,j}}{Z_{i,j}}\right)^n + \left(\frac{Z_{i+1,j}}{Z_{i,j}}\right)^n + \left(\frac{Z_{i,j-1}}{Z_{i,j}}\right)^n + \left(\frac{Z_{i,j+1}}{Z_{i,j}}\right)^n\right] \qquad (3)$$

The normalized Laplacian is from the existing literature, while the four directional ratio was developed specifically for this application.

Analysis of the Two Algorithms

Let $Z_{i,j} = r_{i,j} + V_{i,j}$ (4)

where $r_{i,j}$ is the true range measurement and $V_{i,j}$ the additive noise in measurement.

Also let $r_{i-1,j} = (1+\alpha_{i-1,j})\, r_{i,j}$ (5)

where $\alpha_{i-1,j}$ indicates the fractional change in range from point (i-1,j) with respect to point (i,j).

From Equations (4) and (5) one can write

$$Z_{i-1,j} = (1+\alpha_{i-1,j})\, r_{i,j} + V_{i-1,j} \quad (6)$$

The measurements $Z_{i+1,j}$, $Z_{i,j-1}$, and $Z_{i,j+1}$ can also be expressed in terms of $r_{i,j}$.

Using Equations (2) and (6), expanding the resulting fractions in an infinite series, and dropping higher order terms, we get:

For no noise, i.e. $V_{i,j}=0$ for all i,j:

$$\overset{*}{q}_{i,j} \approx \tfrac{1}{4}(\alpha_{i-1,j}+\alpha_{i+1,j}+\alpha_{i,j-1}+\alpha_{i,j+1}) \quad \text{for small } \alpha \quad (7)$$

If somehow all $\alpha = 0$:

$$\overset{*}{q}_{i,j} \approx 1-(1+\frac{V_{i,j}}{r_{i,j}})\left\{1-\tfrac{1}{4}(\frac{V_{i-1,j}}{r_{i,j}}+\frac{V_{i+1,j}}{r_{i,j}}+\frac{V_{i,j-1}}{r_{i,j}}+\frac{V_{i,j+1}}{r_{i,j}})\right\} \quad (8)$$

Assuming that the noise V with each measurement is independent, zero mean, and with the same standard deviation σ, one can write from Equation (8)

$$\text{Var}\,(\overset{*}{q}_{i,j}) \approx \frac{2\sigma^2}{r_{i,j}} \quad (9)$$

In a similar manner for the four directional ratio, using Equations (3) and (6):

If there is no noise:

$$\overset{*}{S}_{i,j} \approx 1+\frac{n}{4}(\alpha_{i-1,j}+\alpha_{i+1,j}+\alpha_{i,j-1}+\alpha_{i,j+1}) \quad (10)$$

If somehow all $\alpha = 0$:

$$\overset{*}{S}_{i,j} \approx 1+\frac{n}{4}(\frac{V_{i-1,j}}{r_{i,j}}+\ldots)-n\frac{V_{i,j}}{r_{i,j}}-n^2(\frac{V_{i,j}}{r_{i,j}})(\frac{V_{i,-1,j}}{r_{i,j}}+\ldots) \quad (11)$$

With the assumption of independent, zero mean noise with standard deviation σ, a first order approximation of the variance of $S^{\mp}_{i,j}$ can be shown to be:

$$\mathrm{Var}(\overset{\mp}{S}_{i,j}) \approx 2n^2 \frac{\sigma^2}{r^2_{i,j}} \tag{12}$$

The foregoing analysis gives the means of choosing the proper threshold, given the values of α. For example, if two of the outer points (i-1,j) and (i,j-1) lay outside the obstacle and the other three points, including the central point (i,j), lay on the obstacle, then one may assume

$$\alpha_{i-1,j}, \alpha_{i,j-1} > 0 \text{ and } \alpha_{i+1,j} \approx \alpha_{i,j+1} \approx 0 \tag{13}$$

Then from Equation (7) with $\alpha_{i-1,j} \approx \alpha_{i,j-1} \approx 0.04$

$$\overset{*}{Q}_{i,j} \approx \tfrac{1}{4}(0.004+0+0.04+0) = 0.02 \tag{14}$$

Thus, the threshold may be set just below 0.02 if the point in consideration is to be detected, i.e.

$$Tq \approx 0.019 \tag{15}$$

If the central point is assumed to be just outside the obstacle with the other points as before, then one will have a negative threshold value, and this is used to determine points just outside the object.

If the four directional ratio method is used, then from Equation (10):

$$\overset{*}{S}_{i,j} \approx 1 + \frac{n}{4}(0.04+0+0.04+0) = 1 + \frac{n}{4}(0.08) \tag{16a}$$

For n= 2: $\overset{*}{S}_{i,j} \approx 1 + \tfrac{1}{2}(0.08) = 1.04$ (16b)

Notice that by increasing n, the apparent threshold value can be amplified.

The variances given in Equations (9) and (12) give an indication of how large a measurement noise may be accommodated by the algorithms. Suppose it is desired that the threshold lies outside the one σ limit of the variation in q. Then from Equations (9) and (15)

$$\sqrt{\frac{2\sigma^2}{r^2_{i,j}}} = 0.019 \tag{17}$$

or $\sigma = 0.019 \sqrt{2}\, r_{i,j}$

Obviously, at longer ranges, higher measurement noise may be allowed.

The values of α may be obtained from a physical model

obstacles and terrains.

Simulation Results

Fig. 25 illustrates the case study for all computer simulations to date. The rover is on a perfectly flat terrain, with a hemispherical boulder of one meter radius directly in its path of travel, located 30 meters horizontally from the laser mast. A computer program was written to generate the range data points in the "range image", given the elevation angles β and the azimuth angles θ as inputs. Fig. 26 shows the resultant "range image", both when the measurements are undistorted and when they are contaminated by zero mean, 5 cm standard deviation, Gaussian noise. The reason for selection of σ_V = 5 cm was that this was one of the desired accuracies of the laser rangefinder. The limits on β and θ should also be noted; they were chosen so as to scan the entire boulder plus a small area of terrain surrounding the boulder.

In Fig. 27 we have the matrix of $\alpha_{i-1,j}$ values, which is the same for the noiseless and noisy cases. The fact that they are the same should be expected, since from Equation (17), for $r_{i,j}$ = 30 meters, we have that $\sigma_{allowable} = Tq\sqrt{2}\, r_{i,j}$. With Tq on the order of .02, this gives $\sigma_{allowable} \approx .9$ whereas the σ used is only .05. An error this small will obviously have little effect on the edge detection algorithms used.

Fig. 28, 29 and 30 illustrate the resulting matrices after the three algorithms (four directional ratio with n=1 and n=2, and normalized Laplacian) have been applied to the "range image". Once again, the results are the same for both the noiseless and noisy cases.

Finally, in Fig. 31, 32 and 33 we see outline of the boulder after the thresholding operation has been applied to the previous matrices. By proper choice of thresholds, all three algorithms yield the same picture. The lack of a bottom edge is a characteristic outcome of these algorithms, and will have to be approached by a different method.

Future Problems

1) As mentioned at the end of the last section, the bottom edge is completely missed by the algorithms used. This can be a serious problem for without a bottom reference the rover will have a difficult time trying to decide how far and how high one front of the boulder is, and thus how much of an obstacle it represents. An alternate scheme must be devised to detect this bottom edge with the same accuracy as the rest of the obstacle.

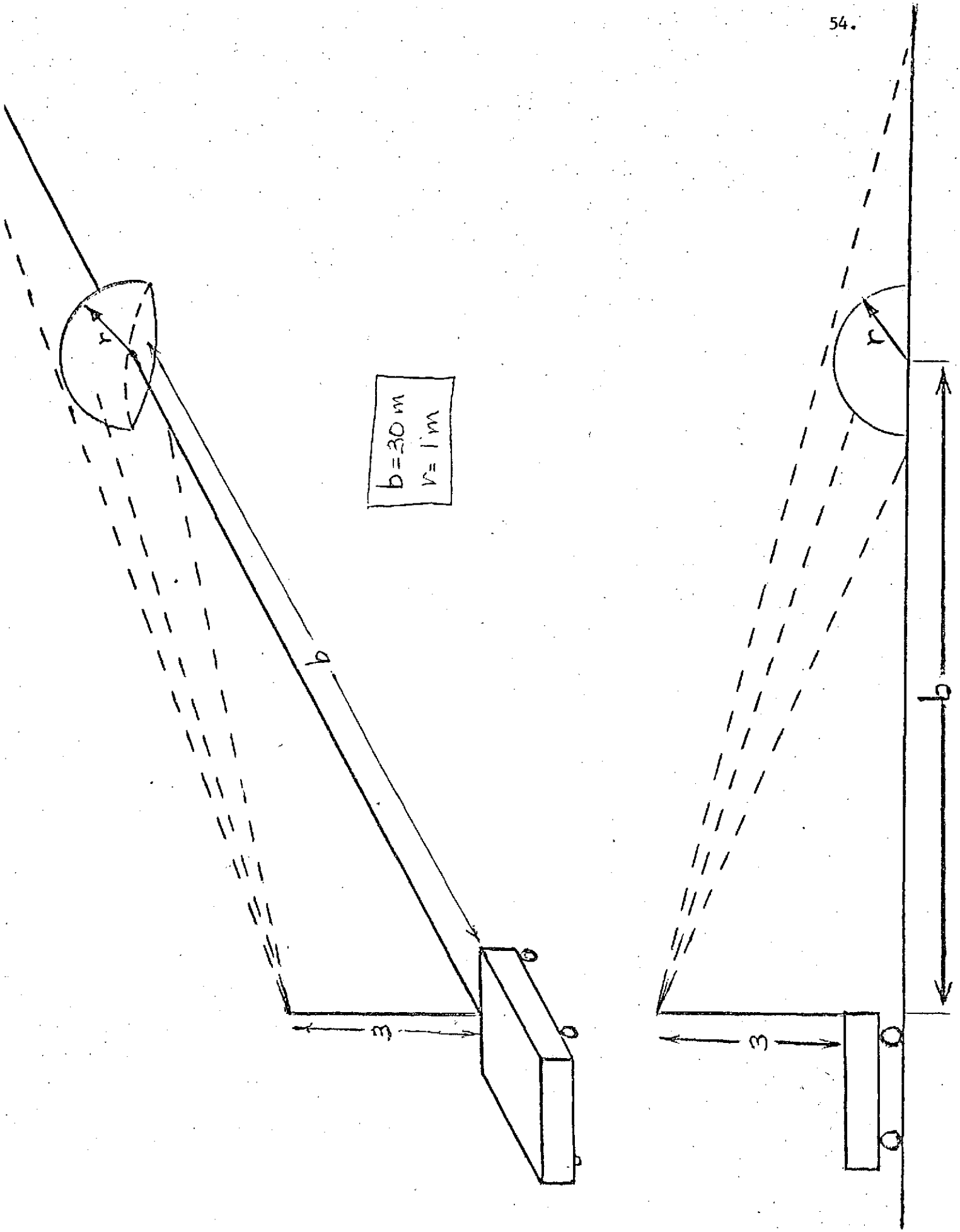

Fig. 25. Case Study for Computer Simulations

CALCULATED RANGE DATA FOR A HEMISPHERICAL BOULDER (1.0 METER RADIUS) AT A DISTANCE OF 30 METERS FROM MARS ROVER

BETA MAX = 6.6 DEGREES BETA MIN = 3.0 DEGREES BETA INCREMENT = .15 DEGREES
THETA MAX = 2.0 DEGREES THETA MIN =-2.0 DEGREES THETA INCREMENT = .20 DEGREES

R(1,1)-----(BETA MIN, THETA MIN) R(1,21)-----(BETA MIN, THETA MAX)
R(25,1)-----(BETA MAX, THETA MIN) R(25,21)-----(BETA MAX, THETA MAX)

UNDISTORTED BY NOISE

57.25	57.25	57.25	57.25	57.25	57.25	57.25	57.25	57.25	57.25	57.25	57.25	57.25	57.25	57.25	57.25	57.25	57.25	57.25	57.25	57.25	57.25	57.25
54.63	54.63	54.63	54.63	54.63	54.63	54.63	54.63	54.63	54.63	54.63	54.63	54.63	54.63	54.63	54.63	54.63	54.63	54.63	54.63	54.63	54.63	54.63
52.13	52.13	52.13	52.13	52.13	52.13	52.13	52.13	52.13	52.13	52.13	52.13	52.13	52.13	52.13	52.13	52.13	52.13	52.13	52.13	52.13	52.13	52.13
49.88	49.88	49.88	49.88	49.88	49.88	49.88	49.88	49.88	49.88	49.88	49.88	49.88	49.88	49.88	49.88	49.88	49.88	49.88	49.88	49.88	49.88	49.88
47.75	47.75	47.75	47.75	47.75	47.75	47.75	47.75	47.75	47.75	47.75	47.75	47.75	47.75	47.75	47.75	47.75	47.75	47.75	47.75	47.75	47.75	47.75
45.88	45.88	45.88	45.88	45.88	45.88	45.88	45.88	45.88	45.88	45.88	45.88	45.88	45.88	45.88	45.88	45.88	45.88	45.88	45.88	45.88	45.88	45.88
44.13	44.13	44.13	44.13	44.13	44.13	44.13	44.13	29.91	29.84	29.84	29.84	29.91	44.13	44.13	44.13	44.13	44.13	44.13	44.13	44.13	44.13	44.13
42.50	42.50	42.50	42.50	42.50	42.50	29.88	29.77	29.69	29.66	29.66	29.66	29.69	29.77	29.88	42.50	42.50	42.50	42.50	42.50	42.50	42.50	42.50
40.94	40.94	40.94	40.94	40.94	29.83	29.70	29.63	29.56	29.55	29.53	29.55	29.56	29.63	29.70	29.83	40.94	40.94	40.94	40.94	40.94	40.94	40.94
39.50	39.50	39.50	39.50	29.83	29.67	29.58	29.52	29.47	29.45	29.44	29.45	29.47	29.52	29.58	29.67	29.83	39.50	39.50	39.50	39.50	39.50	39.50
38.25	38.25	38.25	29.91	29.69	29.58	29.49	29.44	29.40	29.38	29.38	29.38	29.40	29.44	29.49	29.58	29.69	29.91	38.25	38.25	38.25	38.25	38.25
37.06	37.06	37.06	29.75	29.59	29.50	29.42	29.38	29.34	29.32	29.31	29.32	29.34	29.38	29.42	29.50	29.59	29.75	37.06	37.06	37.06	37.06	37.06
35.88	35.88	29.88	29.66	29.52	29.44	29.38	29.32	29.29	29.27	29.27	29.27	29.29	29.32	29.38	29.44	29.52	29.66	29.88	35.88	35.88	35.88	35.88
34.75	34.75	29.77	29.59	29.48	29.39	29.33	29.29	29.25	29.23	29.23	29.23	29.25	29.29	29.33	29.39	29.48	29.59	29.77	34.75	34.75	34.75	34.75
33.75	33.75	29.70	29.54	29.43	29.36	29.30	29.25	29.22	29.21	29.20	29.21	29.22	29.25	29.30	29.36	29.43	29.54	29.70	33.75	33.75	33.75	33.75
32.75	29.91	29.65	29.50	29.40	29.33	29.27	29.23	29.20	29.18	29.18	29.18	29.20	29.23	29.27	29.33	29.40	29.50	29.65	29.91	32.75	32.75	32.75
31.88	29.84	29.62	29.48	29.38	29.31	29.25	29.21	29.18	29.17	29.16	29.17	29.18	29.21	29.25	29.31	29.38	29.48	29.62	29.84	31.88	31.88	31.88
31.06	29.81	29.60	29.46	29.37	29.30	29.24	29.20	29.18	29.16	29.15	29.16	29.18	29.20	29.24	29.30	29.37	29.46	29.60	29.81	31.06	31.06	31.06
30.25	29.80	29.59	29.46	29.36	29.29	29.24	29.20	29.17	29.15	29.15	29.15	29.17	29.20	29.24	29.29	29.36	29.46	29.59	29.80	30.25	30.25	30.25
29.44	29.44	29.44	29.44	29.37	29.29	29.24	29.20	29.18	29.16	29.15	29.16	29.18	29.20	29.24	29.29	29.37	29.44	29.44	29.44	29.44	29.44	29.44
28.69	28.69	28.69	28.69	28.69	28.69	28.69	28.69	28.69	28.69	28.69	28.69	28.69	28.69	28.69	28.69	28.69	28.69	28.69	28.69	28.69	28.69	28.69
28.03	28.03	28.03	28.03	28.03	28.03	28.03	28.03	28.03	28.03	28.03	28.03	28.03	28.03	28.03	28.03	28.03	28.03	28.03	28.03	28.03	28.03	28.03
27.38	27.38	27.38	27.38	27.38	27.38	27.38	27.38	27.38	27.38	27.38	27.38	27.38	27.38	27.38	27.38	27.38	27.38	27.38	27.38	27.38	27.38	27.38
26.69	26.69	26.69	26.69	26.69	26.69	26.69	26.69	26.69	26.69	26.69	26.69	26.69	26.69	26.69	26.69	26.69	26.69	26.69	26.69	26.69	26.69	26.69
26.13	26.13	26.13	26.13	26.13	26.13	26.13	26.13	26.13	26.13	26.13	26.13	26.13	26.13	26.13	26.13	26.13	26.13	26.13	26.13	26.13	26.13	26.13

CONTAMINATED BY ZERO MEAN, .05 METER STANDARD DEVIATION, GAUSSIAN NOISE

57.22	57.25	57.27	57.26	57.23	57.24	57.21	57.26	57.22	57.30	57.20	57.29	57.35	57.22	57.28	57.24	57.36	57.27	57.35	57.27	57.26
54.61	54.62	54.69	54.61	54.57	54.60	54.58	54.56	54.61	54.67	54.64	54.63	54.69	54.57	54.72	54.62	54.67	54.65	54.68	54.61	54.74
52.21	52.16	52.26	52.14	52.04	52.14	52.13	52.10	52.08	52.05	52.19	52.03	52.20	52.10	52.17	52.06	52.15	52.14	52.16	52.12	52.15
49.87	49.92	49.90	49.89	49.77	49.88	49.89	49.95	49.87	49.94	49.87	49.91	49.94	49.84	49.88	49.93	49.84	49.78	49.99	49.88	49.96
47.80	47.76	47.77	47.72	47.77	47.82	47.69	47.64	47.78	47.73	47.74	47.63	47.67	47.81	47.86	47.73	47.78	47.75	47.78	47.91	47.70
45.99	45.85	45.89	45.87	45.94	45.90	45.88	45.79	45.93	45.89	45.85	45.91	45.87	45.93	45.95	45.81	45.97	45.90	45.84	45.77	45.87
44.10	44.11	44.12	44.12	44.12	44.16	44.12	44.09	29.93	29.82	29.75	29.84	29.84	44.11	44.10	44.06	44.17	44.09	44.10	44.12	44.13
42.51	42.45	42.50	42.47	42.51	42.41	29.89	29.79	29.64	29.67	29.69	29.71	29.59	29.77	29.87	42.47	42.47	42.58	42.44	42.53	42.51
40.96	40.91	40.98	41.05	40.88	29.85	29.79	29.53	29.47	29.53	29.59	29.47	29.58	29.63	29.73	29.79	40.86	40.90	40.94	40.88	40.89
39.44	39.49	39.55	39.47	29.82	29.75	29.56	29.47	29.41	29.41	29.49	29.46	29.53	29.57	29.60	29.69	29.85	39.49	39.47	39.53	39.41
38.21	38.18	38.27	29.98	29.70	29.58	29.44	29.45	29.38	29.33	29.36	29.36	29.42	29.39	29.56	29.64	29.71	29.93	38.30	38.25	38.35
37.07	37.11	37.11	29.72	29.59	29.48	29.36	29.29	29.32	29.34	29.36	29.18	29.42	29.40	29.47	29.48	29.59	29.67	37.06	36.95	37.07
35.87	35.87	29.68	29.69	29.50	29.42	29.33	29.25	29.27	29.26	29.35	29.29	29.25	29.32	29.33	29.34	29.48	29.60	29.82	35.93	35.84
34.71	34.75	29.73	29.59	29.40	29.32	29.31	29.13	29.23	29.25	29.26	29.23	29.29	29.28	29.35	29.25	29.45	29.61	29.79	34.73	34.79
33.77	33.69	29.66	29.57	29.41	29.32	29.41	29.29	29.22	29.28	29.27	29.20	29.23	29.29	29.33	29.36	29.46	29.57	29.61	33.79	33.72
32.69	29.83	29.69	29.49	29.49	29.29	29.18	29.16	29.23	29.30	29.24	29.22	29.12	29.24	29.35	29.25	29.41	29.53	29.58	29.96	32.80
31.79	29.80	29.61	29.44	29.43	29.36	29.19	29.17	29.18	29.12	29.13	29.10	29.14	29.20	29.28	29.31	29.32	29.45	29.64	29.78	31.80
31.11	29.82	29.67	29.46	29.35	29.30	29.30	29.14	29.12	29.20	29.18	29.15	29.20	29.20	29.19	29.31	29.36	29.51	29.55	29.82	31.01
30.25	29.72	29.59	29.40	29.29	29.20	29.20	29.12	29.12	29.20	29.17	29.16	29.14	29.17	29.30	29.28	29.37	29.35	29.54	29.96	30.22
29.51	29.49	29.47	29.47	29.37	29.26	29.24	29.17	29.25	29.10	29.09	29.15	29.30	29.15	29.27	29.26	29.33	29.32	29.48	29.45	29.49
28.72	28.77	28.63	28.68	28.72	28.77	28.79	28.82	28.68	28.69	28.63	28.69	28.72	28.68	28.67	28.61	28.75	28.69	28.79	28.60	28.75
27.94	27.99	28.00	28.05	27.97	27.95	28.07	28.03	28.00	27.95	28.00	28.02	28.01	28.12	28.00	28.05	28.08	28.05	28.09	27.98	27.97
27.38	27.38	27.32	27.42	27.34	27.28	27.36	27.34	27.47	27.36	27.37	27.41	27.41	27.31	27.31	27.36	27.39	27.35	27.28	27.39	27.48
26.71	26.69	26.78	26.74	26.70	26.80	26.65	26.66	26.68	26.73	26.79	26.68	26.69	26.70	26.64	26.70	26.69	26.71	26.62	26.68	26.71
26.24	26.12	26.12	26.08	26.20	26.06	26.10	26.12	26.14	26.13	26.21	26.16	26.04	26.15	26.07	26.28	26.15	26.10	26.12	26.13	26.12

Fig. 26. The "Range Image" Matrices

MATRIX OF ALPHA(I-1,J) VALUES

I = 2 TO 25 ↓ J = 1 TO 21 →

0.048	0.048	0.048	0.048	0.048	0.048	0.048	0.048	0.048	0.048	0.048	0.048	0.048	0.048	0.048	0.048	0.048	0.048	0.048	0.048	0.048
0.048	0.048	0.048	0.048	0.048	0.048	0.048	0.048	0.048	0.048	0.048	0.048	0.048	0.048	0.048	0.048	0.048	0.048	0.048	0.048	0.048
0.045	0.045	0.045	0.045	0.045	0.045	0.045	0.045	0.045	0.045	0.045	0.045	0.045	0.045	0.045	0.045	0.045	0.045	0.045	0.045	0.045
0.045	0.045	0.045	0.045	0.045	0.045	0.045	0.045	0.045	0.045	0.045	0.045	0.045	0.045	0.045	0.045	0.045	0.045	0.045	0.045	0.045
0.041	0.041	0.041	0.041	0.041	0.041	0.041	0.041	0.041	0.041	0.041	0.041	0.041	0.041	0.041	0.041	0.041	0.041	0.041	0.041	0.041
0.040	0.040	0.040	0.040	0.040	0.040	0.040	0.040	0.534	0.537	0.537	0.537	0.534	0.040	0.040	0.040	0.040	0.040	0.040	0.040	0.040
0.038	0.038	0.038	0.038	0.038	0.038	0.477	0.482	0.007	0.006	0.006	0.006	0.007	0.482	0.477	0.038	0.038	0.038	0.038	0.038	0.038
0.038	0.038	0.038	0.038	0.038	0.425	0.006	0.005	0.004	0.004	0.004	0.004	0.004	0.005	0.006	0.425	0.038	0.038	0.038	0.038	0.038
0.036	0.036	0.036	0.036	0.372	0.005	0.004	0.004	0.003	0.003	0.003	0.003	0.003	0.004	0.004	0.005	0.372	0.036	0.036	0.036	0.036
0.033	0.033	0.033	0.321	0.005	0.003	0.003	0.003	0.002	0.003	0.002	0.003	0.002	0.003	0.003	0.003	0.005	0.321	0.033	0.033	0.033
0.032	0.032	0.032	0.005	0.003	0.003	0.002	0.002	0.002	0.002	0.002	0.002	0.002	0.002	0.002	0.003	0.003	0.005	0.032	0.032	0.032
0.033	0.033	0.241	0.003	0.002	0.002	0.002	0.002	0.002	0.002	0.002	0.002	0.002	0.002	0.002	0.002	0.002	0.003	0.241	0.033	0.033
0.032	0.032	0.004	0.002	0.002	0.002	0.002	0.001	0.001	0.001	0.001	0.001	0.001	0.001	0.002	0.002	0.002	0.002	0.004	0.032	0.032
0.030	0.030	0.002	0.002	0.001	0.001	0.001	0.001	0.001	0.001	0.001	0.001	0.001	0.001	0.001	0.001	0.001	0.002	0.002	0.030	0.030
0.031	0.129	0.002	0.001	0.001	0.001	0.001	0.001	0.001	0.001	0.001	0.001	0.001	0.001	0.001	0.001	0.001	0.001	0.002	0.129	0.031
0.027	0.002	0.001	0.001	0.001	0.001	0.001	0.001	0.001	0.001	0.001	0.001	0.001	0.001	0.001	0.001	0.001	0.001	0.001	0.002	0.027
0.024	0.001	0.001	0.001	0.000	0.000	0.000	0.000	0.000	0.000	0.000	0.000	0.000	0.000	0.000	0.000	0.000	0.001	0.001	0.001	0.026
0.027	0.000	0.000	0.000	0.000	0.000	0.000	0.000	0.000	0.000	0.0	0.000	0.000	0.000	0.000	0.000	0.000	0.000	0.000	0.000	0.027
0.023	0.012	0.005	0.001	-0.000	0.0	0.0	0.0	-0.000	-0.000	0.0	-0.000	-0.000	0.0	0.0	0.0	-0.000	0.001	0.005	0.012	0.028
0.026	0.026	0.026	0.026	0.024	0.021	0.019	0.018	0.017	0.016	0.016	0.016	0.017	0.018	0.019	0.021	0.024	0.026	0.026	0.026	0.026
0.023	0.023	0.023	0.023	0.023	0.023	0.023	0.023	0.023	0.023	0.023	0.023	0.023	0.023	0.023	0.023	0.023	0.023	0.023	0.023	0.023
0.024	0.024	0.024	0.024	0.024	0.024	0.024	0.024	0.024	0.024	0.024	0.024	0.024	0.024	0.024	0.024	0.024	0.024	0.024	0.024	0.024
0.026	0.026	0.026	0.026	0.026	0.026	0.026	0.026	0.026	0.026	0.026	0.026	0.026	0.026	0.026	0.026	0.026	0.026	0.026	0.026	0.026
0.022	0.022	0.022	0.022	0.022	0.022	0.022	0.022	0.022	0.022	0.022	0.022	0.022	0.022	0.022	0.022	0.022	0.022	0.022	0.022	0.022

Fig. 27. Matrix of $\alpha(i-1,j)$ Values

FOUR DIRECTIONAL RATIO EDGE DETECTION SCHEME, WITH N=1

1.00	1.00	1.00	1.00	1.00	1.00	1.00	1.00	1.00	1.00	1.00	1.00	1.00	1.00	1.00	1.00	1.00	1.00	1.00
1.00	1.00	1.00	1.00	1.00	1.00	1.00	1.00	1.00	1.00	1.00	1.00	1.00	1.00	1.00	1.00	1.00	1.00	1.00
1.00	1.00	1.00	1.00	1.00	1.00	1.00	1.00	1.00	1.00	1.00	1.00	1.00	1.00	1.00	1.00	1.00	1.00	1.00
1.00	1.00	1.00	1.00	1.00	1.00	1.00	1.00	1.00	1.00	1.00	1.00	1.00	1.00	1.00	1.00	1.00	1.00	1.00
1.00	1.00	1.00	1.00	1.00	1.00	1.00	0.92	0.92	0.92	0.92	0.92	1.00	1.00	1.00	1.00	1.00	1.00	1.00
1.00	1.00	1.00	1.00	1.00	0.93	0.85	1.25	1.13	1.14	1.13	1.25	0.85	0.93	1.00	1.00	1.00	1.00	1.00
1.00	1.00	1.00	1.00	0.86	1.22	1.12	1.00	1.00	1.00	1.00	1.00	1.12	1.22	0.86	1.00	1.00	1.00	1.00
1.00	1.00	1.00	0.88	1.20	1.00	1.00	1.00	1.00	1.00	1.00	1.00	1.00	1.00	1.20	0.87	1.00	1.00	1.00
1.00	1.00	0.89	1.17	1.00	1.00	1.00	1.00	1.00	1.00	1.00	1.00	1.00	1.00	1.00	1.17	0.89	1.00	1.00
1.00	0.95	1.15	1.00	1.00	1.00	1.00	1.00	1.00	1.00	1.00	1.00	1.00	1.00	1.00	1.00	1.15	0.94	1.00
1.00	0.91	1.06	1.00	1.00	1.00	1.00	1.00	1.00	1.00	1.01	1.00	1.00	1.00	1.00	1.00	1.06	0.91	1.00
0.95	1.11	1.00	1.00	1.00	1.00	1.00	1.00	1.00	1.00	1.00	1.00	1.00	1.00	1.00	1.00	1.00	1.11	0.96
0.96	1.04	1.00	1.00	1.00	1.00	1.00	1.00	1.00	1.00	1.00	1.00	1.00	1.00	1.00	1.00	1.00	1.04	0.97
0.95	1.03	1.00	1.00	1.00	1.00	1.00	1.00	1.00	1.00	1.00	1.00	1.00	1.00	1.00	1.00	1.00	1.04	0.95
1.05	1.00	1.00	1.00	1.00	1.00	1.00	1.00	1.00	1.00	1.00	1.00	1.00	1.00	1.00	1.00	1.00	1.00	1.05
1.02	1.00	1.00	1.00	1.00	1.00	1.00	1.00	1.00	1.00	1.00	1.00	1.00	1.00	1.00	1.00	1.00	1.00	1.02
1.01	1.00	1.00	1.00	1.00	1.00	1.00	1.00	1.00	1.00	1.00	1.00	1.00	1.00	1.00	1.00	1.00	1.00	1.01
1.00	1.00	1.00	1.00	1.00	1.00	1.00	1.00	1.00	1.00	1.00	1.00	1.00	1.00	1.00	1.00	1.00	1.00	1.00
1.00	0.99	0.99	0.99	1.00	1.00	1.00	0.99	1.00	1.00	1.00	0.99	1.00	0.99	1.00	0.99	1.00	0.99	1.00
1.00	1.00	1.00	1.00	1.00	1.00	0.99	1.00	1.00	1.00	1.00	1.00	1.00	1.00	1.00	1.00	1.00	1.00	1.00
1.00	1.00	1.00	1.00	1.00	1.00	1.00	1.00	1.00	1.00	1.00	1.00	1.00	1.00	1.00	1.00	1.00	1.00	1.00
1.00	1.00	1.00	1.00	1.00	1.00	1.00	1.00	1.00	1.00	1.00	1.00	1.00	1.00	1.00	1.00	1.00	1.00	1.00
1.00	1.00	1.00	1.00	1.00	1.00	1.00	1.00	1.00	1.00	1.00	1.00	1.00	1.00	1.00	1.00	1.00	1.00	1.00

Fig. 28. Four Directional Ratio Edge Detection Scheme, with n = 1

FOUR DIRECTIONAL RATIO EDGE DETECTION SCHEME, WITH N=2

1.00	1.00	1.00	1.00	1.00	1.00	1.00	1.00	1.00	1.00	1.00	1.00	1.01	1.00	1.00	1.00	1.00	1.00	1.00
1.00	1.00	1.00	1.01	1.00	1.00	1.00	1.00	1.01	1.00	1.01	1.00	1.00	1.00	1.01	1.00	1.00	1.00	1.00
1.00	1.00	1.00	1.01	1.00	1.00	1.00	1.00	1.00	1.00	1.00	1.00	1.00	1.00	1.00	1.00	1.01	1.00	1.00
1.00	1.00	1.01	1.00	1.00	1.01	1.01	1.00	1.01	1.00	1.01	1.01	1.00	1.00	1.01	1.00	1.00	1.00	1.00
1.00	1.00	1.00	1.00	1.00	1.00	1.00	0.87	0.88	0.88	0.87	0.88	1.00	1.00	1.01	1.00	1.00	1.00	1.01
1.00	1.00	1.00	1.00	1.00	0.89	0.75	1.62	1.34	1.35	1.34	1.63	0.75	0.89	1.00	1.00	1.01	1.00	1.00
1.00	1.00	1.00	1.00	0.77	1.55	1.29	1.00	1.00	1.00	1.00	1.01	1.30	1.55	0.77	1.00	1.00	1.01	1.00
1.00	1.00	1.00	0.79	1.47	0.99	1.01	1.00	1.00	1.00	1.01	1.00	1.00	1.00	1.48	0.79	1.00	1.00	1.01
1.00	1.00	0.81	1.40	1.00	1.00	1.00	1.00	1.00	1.00	1.00	1.00	1.00	1.00	1.00	1.40	0.80	1.01	1.00
1.00	0.90	1.34	1.00	1.00	1.00	1.00	1.00	1.00	1.00	1.00	1.00	1.01	1.00	1.00	1.00	1.34	0.90	1.00
1.00	0.84	1.14	1.00	1.00	1.00	1.00	1.00	1.00	1.00	1.01	0.99	1.00	1.00	1.00	1.00	1.14	0.84	1.01
0.93	1.24	1.00	1.00	1.00	1.00	1.00	1.00	1.00	1.00	1.00	1.01	1.00	1.00	1.00	1.00	1.00	1.25	0.92
0.93	1.09	1.00	1.00	1.00	1.00	1.01	1.00	1.00	1.00	1.00	1.00	1.00	1.00	1.01	1.00	1.00	1.08	0.94
0.91	1.07	1.00	1.00	1.00	0.99	1.00	1.00	1.00	1.00	1.00	1.00	1.00	1.00	1.00	1.00	1.00	1.08	0.90
1.12	1.00	1.00	0.99	1.00	1.01	1.00	1.00	0.99	1.00	1.00	1.01	1.00	0.99	1.01	1.00	1.00	1.01	1.11
1.03	1.00	1.00	1.00	1.00	1.00	1.00	1.00	1.01	1.00	1.00	1.00	1.00	1.00	1.00	1.00	1.00	1.00	1.04
1.02	1.00	1.00	1.00	1.00	0.99	1.00	1.00	1.00	1.00	1.00	1.00	1.00	1.01	1.00	1.00	0.99	1.01	1.02
1.01	1.00	1.00	1.00	1.00	1.00	1.00	1.00	1.00	1.00	1.00	1.00	1.00	1.00	1.00	1.00	1.01	1.00	0.99
0.99	0.99	0.98	0.99	0.99	0.99	1.00	0.98	1.00	0.99	0.99	0.98	1.00	0.99	0.99	0.99	0.99	0.99	0.99
1.00	1.00	1.00	1.00	0.99	1.00	0.99	1.00	0.99	1.00	1.00	1.00	1.00	1.00	1.01	1.00	1.00	1.00	1.01
1.00	1.00	1.00	1.00	1.01	1.00	1.00	1.00	1.00	1.00	1.00	1.00	0.99	1.00	1.00	1.00	1.00	1.00	1.00
1.00	1.00	1.00	1.00	1.01	1.00	1.00	0.99	1.00	1.00	1.00	1.00	1.01	1.00	1.00	1.00	1.00	1.01	1.00
1.00	1.00	1.00	1.01	0.99	1.01	1.00	1.01	1.00	1.00	1.01	1.00	1.00	1.00	1.00	1.00	1.00	1.01	1.00

Fig. 29. Four Directional Ratio Edge Detection Scheme, with n = 2

NORMALIZED LAPLACIAN EDGE DETECTION SCHEME

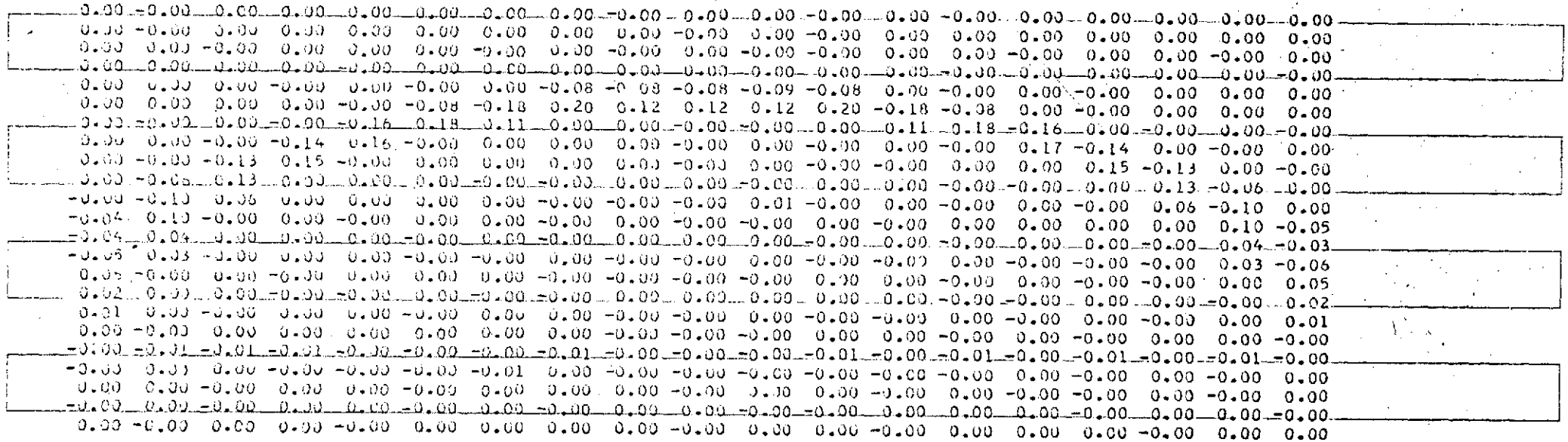

Fig. 30. Normalized Laplacian Edge Detection Scheme

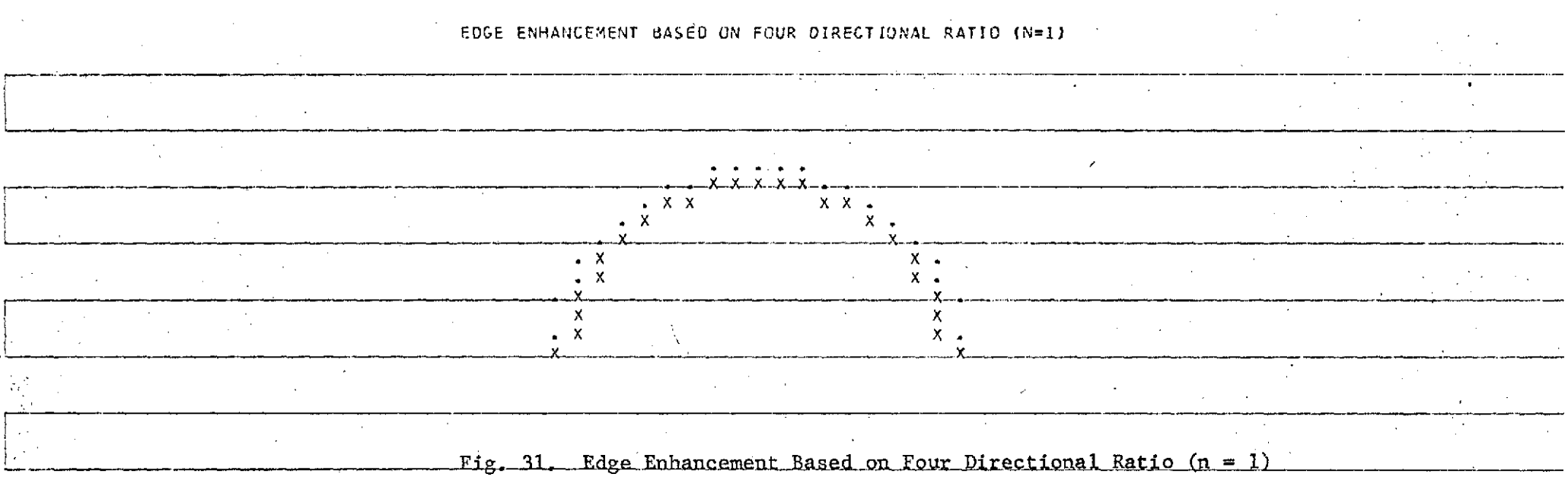

Fig. 31. Edge Enhancement Based on Four Directional Ratio (n = 1)

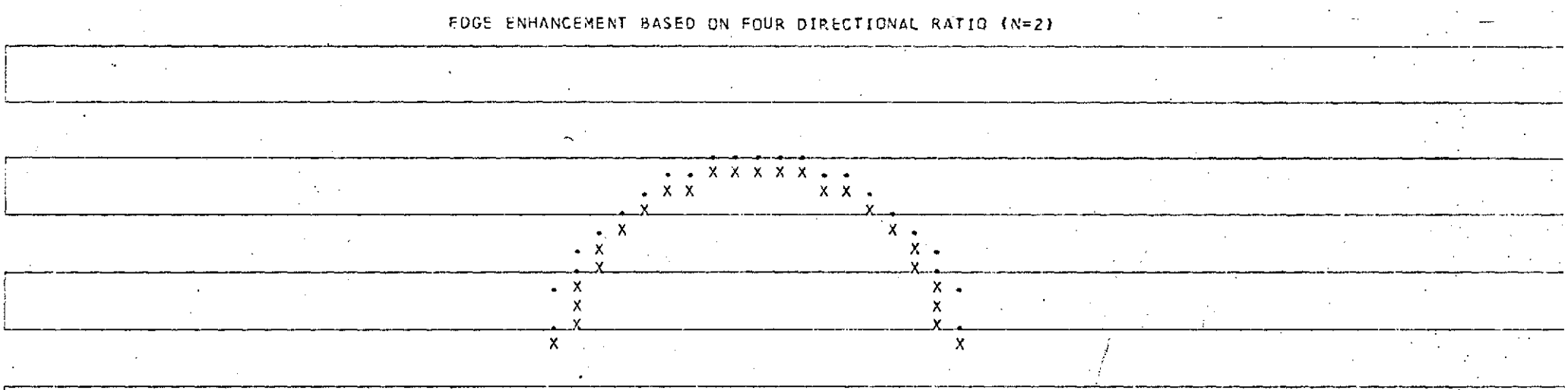

Fig. 32. Edge Enhancement Based on Four Directional Ratio (n = 2)

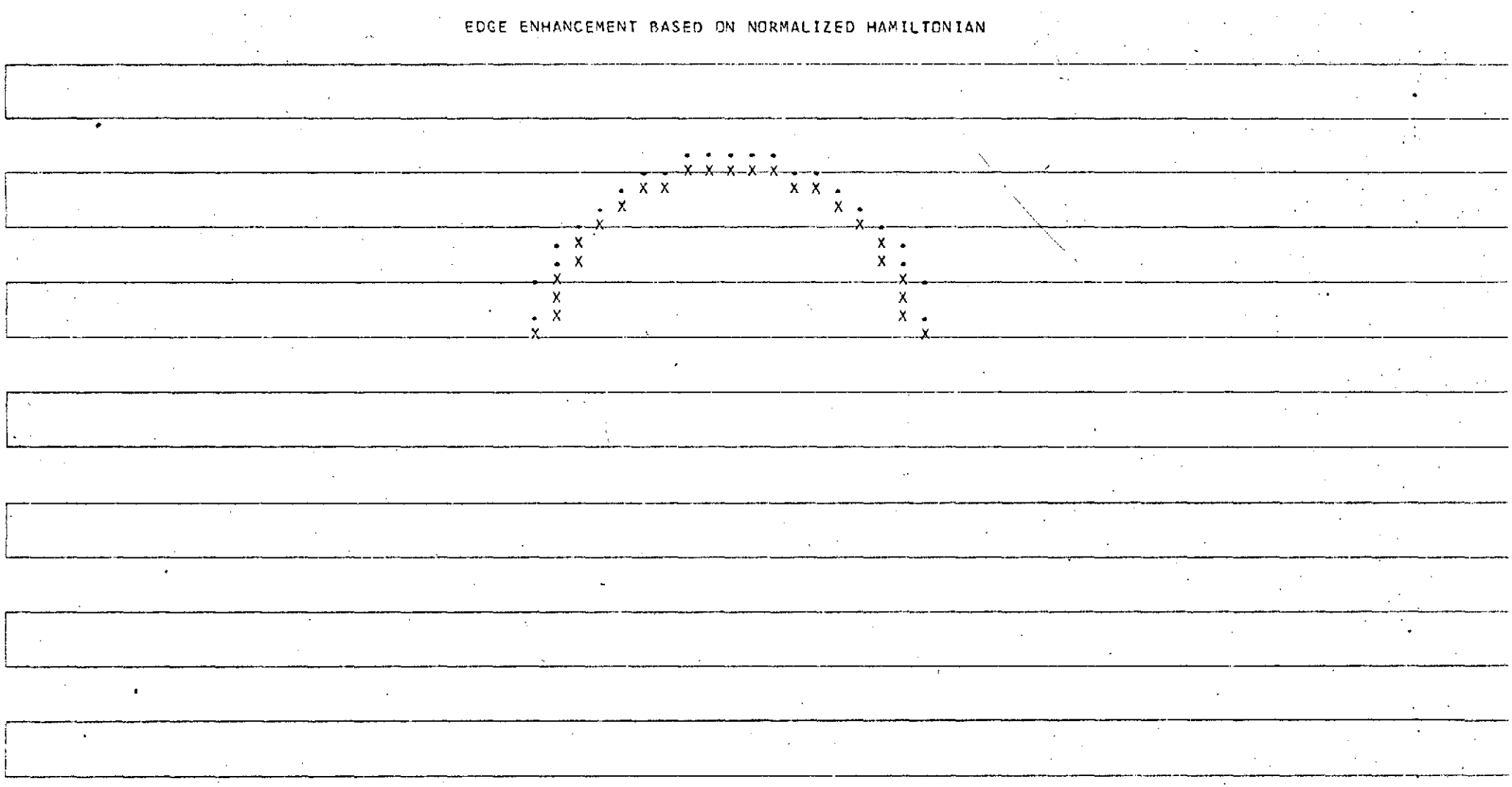

Fig. 33. Edge Enhancement Based on Normalized Laplacian

2) The elevation and azimuth angles were intentionally limited to include only the boulder and a small border surrounding it in the "range image". 21 separate azimuth angles, each .20 degrees apart, and 25 separate elevation angles, each .15 degrees apart, were implemented. This gave the "range image" the characteristics of high point density, but over a very limited region. Future requirements from the group working on the measurement scanning scheme may decrease the available point density, due to restrictions on the laser scan capability or in order to widen the field of view, and the algorithms may be affected by this limitation.

3) The algorithms have only been tested for the one specific case given. What will happen for bigger or smaller boulders, closer or farther away? Will one algorithm then work better than the others? These questions will have to be investigated.

Timetable for future work

	February	March	April	May
Introduce different size and location boulders	———			
Develop an algorithm for the bottom edge of obstacle	———	———		
Introduce other obstacles		———	———	
Determine minimum "range image" point density requirements			———	
Write final report				———

C.2.b. Parameter Estimation for Terrain Modeling from Gradient Data -
K. R. D'Angelo
Faculty Advisor: Prof. C. N. Shen

Objective. There were two primary objectives undertaken in the area of terrain modeling. One objective was to develop a method for representing sections of the Martian terrain by curved surfaces, using two successive laser scans. The second was to find a way of evaluating the proposed model and establishing limits for the scanning parameters.

Progress Summary. A two step modeling procedure was developed. The method uses height, location and gradient data found from sixteen data points. The model formed is a third degree, two dimensional polynomial. A complete error analysis of the modeling method was carried out. The computer program to implement the analysis is now being completed.

Discussion

a) Modeling Procedure - Step 1

The first step in the modeling procedure is to model stochastically a plane from frou data points, Ref. 13. This plane is formed in the (h", a", b") coordinate system attached to the vehicle and then transformed to the (h,a,b) coordinate system which is aligned with the local vertical, Fig. 34. Four planes are modeled in this way. Each plane yields the height, location, cross-path slope, $\partial h/\partial a$, and in-path slope, $\partial h/\partial b$, at the center point, p,n, Fig. 35.

b) Modeling Procedure - Step 2

Once four planes have been modeled, a new coordinate system is formed, by shifting the axis so that the point P' is located at (0,0) in the $a^{\mp}b^{\mp}$ system, Fig. 35. This shift improves the model's accuracy and simplifies calculations.

To represent the terrain, the two dimensional third degree polynomial

$$h = f(a^{\mp}, b^{\mp}) = C_{00}^{\mp} + C_{10}^{\mp} a^{\mp} + C_{01}^{\mp} b^{\mp} + C_{20}^{\mp} a^{\mp 2}/2 + C_{11}^{\mp} a^{\mp} b^{\mp} + C_{02}^{\mp} b^{\mp 2}/2 + C_{30}^{\mp} a^{\mp 3}/6 + C_{21}^{\mp} a^{\mp 2}/2\, b^{\mp} + C_{12}^{\mp} a^{\mp} b^{\mp 2}/2 + C_{03}^{\mp} b^{\mp 3}/6 \qquad (1)$$

was chosen where the C_{ij}'s are unknown parameters which must be determined in order to represent the surface. Expressions for $\partial h/\partial a^{\mp}$ and $\partial h/\partial b^{\mp}$ can easily be found. Because of the coordinate shift, three parameters are found immediately

$$h_1 = C_{00}^{\mp}, \quad (\partial h/\partial a^{\mp}) = C_{10}^{\mp}, \quad (\partial h/\partial b^{\mp}) = C_{01}^{\mp} \qquad (2)$$

Since there are four P^n points and at each P^n point the height, $\partial h/\partial a$, and $\partial h/\partial b$ are known, 12 equations can be written. If we eliminate the three above equations, Eq. (2), then a matrix equation

$$\underline{h}^{\mp} = \underline{A}^{\mp}\, \underline{C}^{\mp} \qquad (3)$$

can be written where $\underline{h}^{\mp}$ is a 9 element vector containing h_i, $(\frac{\partial h}{\partial a^{\mp}})_i$, $(\frac{\partial h}{\partial b^{\mp}})_i$ and $C_{00}^{\mp}$, $C_{10}^{\mp}$, $C_{01}^{\mp}$, where i = 2,3,4. $\underline{A}^{\mp}$ is the coefficient matrix, and $C^{\mp}$ is the vector containing the 7 remaining unknown parameters.

This system of equations is overdetermined and must be solved stochastically. This is done by least square approximation which results in

$$\underline{C}^{\mp} = (A^{\mp T} A^{\mp})^{-1} A^{\mp T} h^{\mp} \qquad (4)$$

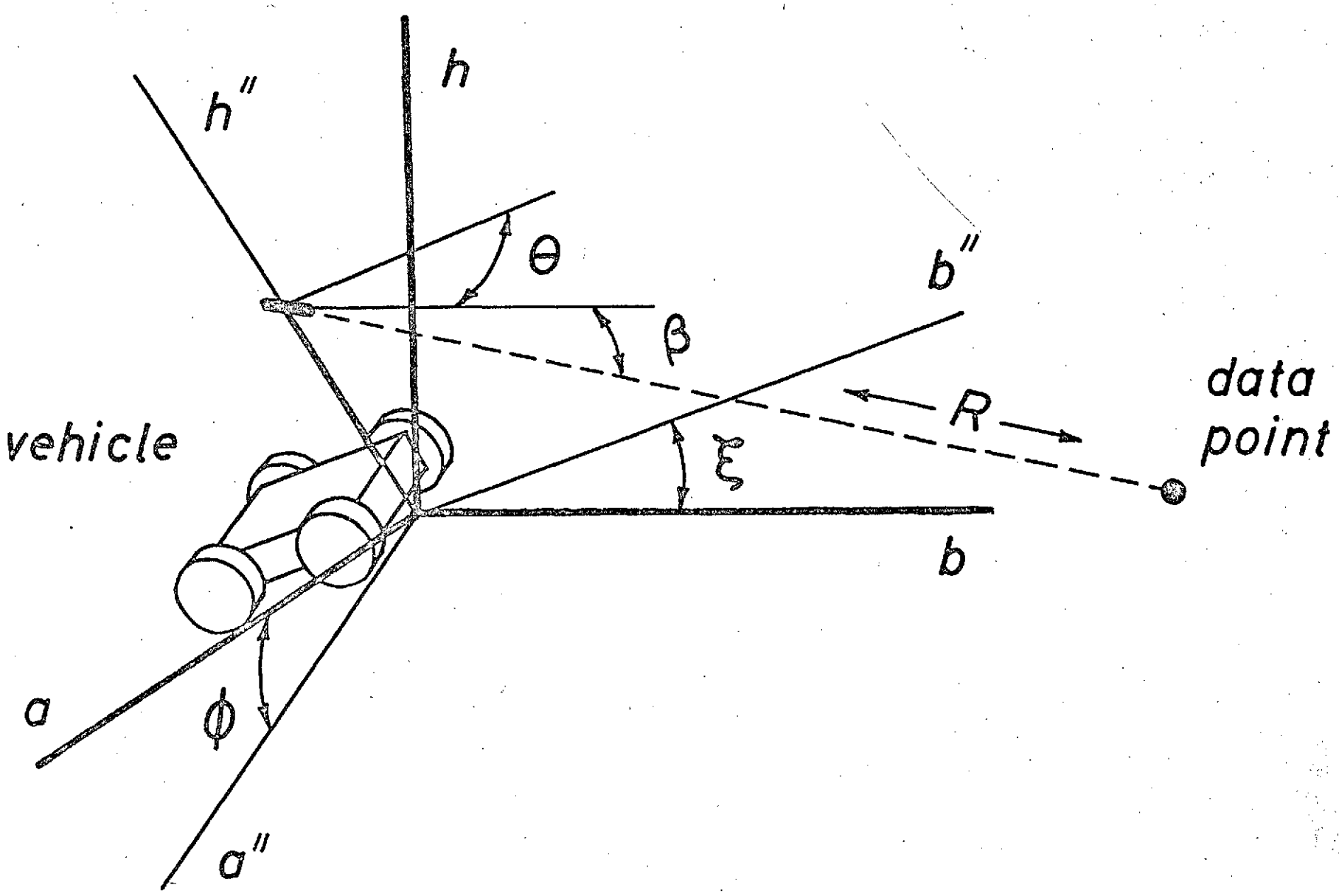

Fig. 34. Thi figure shows the three measured quantities, R, β and θ, the two coordinate systems, and the transformation angles ϕ and ξ.

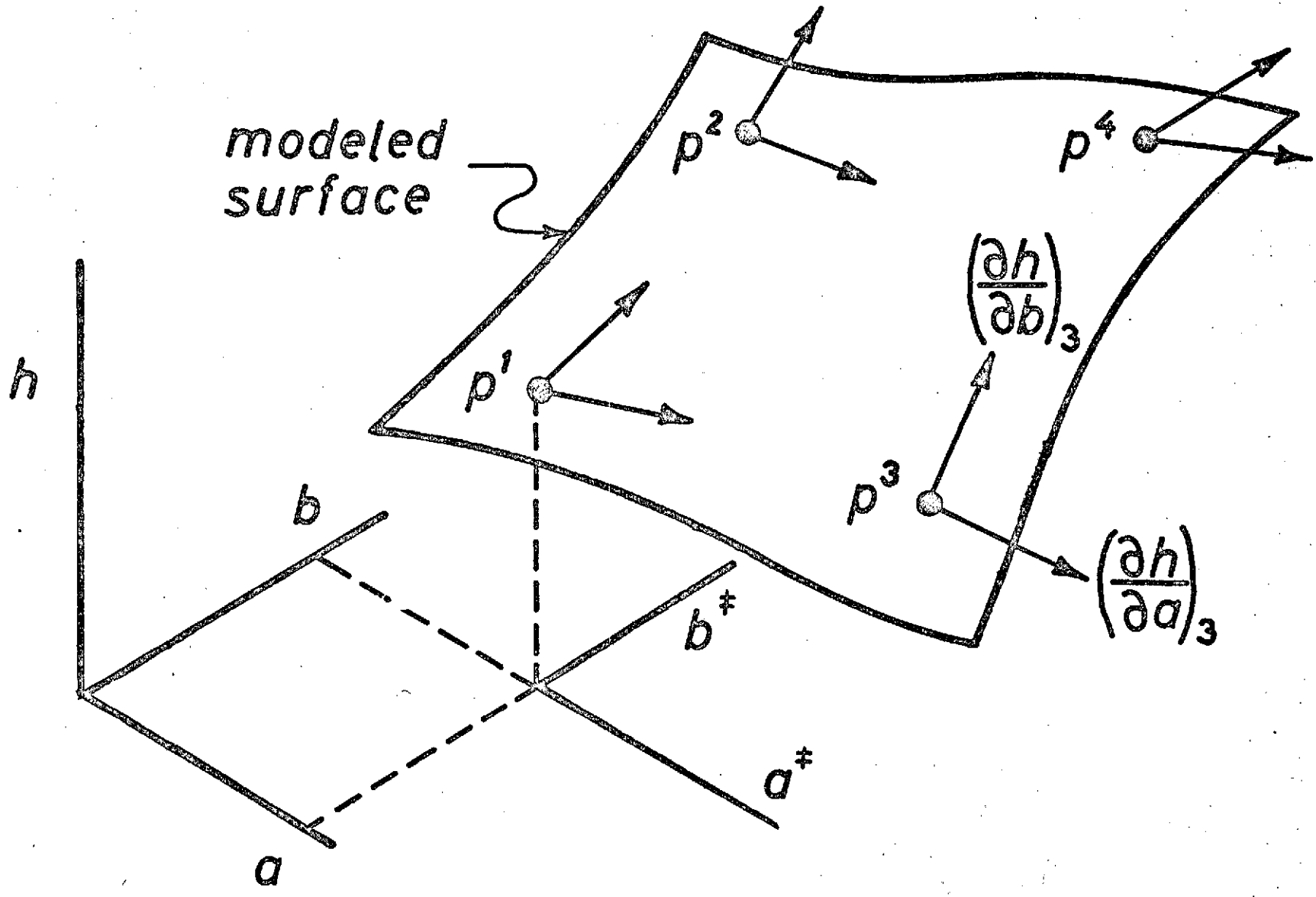

Fig. 35. This illustration shows the location, height and two directional derivatives for each center point. It also shows the position of the $a^{\mp}$, $b^{\mp}$-coordinate system.

Once C has been found by Equation 4 then the surface polynomial, Equation 1, can be written. The gradient of this surface can then be determined immediately as:

$$S = \text{Gradient} = \left[\left(\partial h/\partial a^{\mp}\right)^2 + \left(\partial h/\partial b^{\mp}\right)^2\right]^{\frac{1}{2}} \qquad (5)$$

c) Error Analysis - Step 1. - Error covariance matrix for the data points. This and the following sections outline the procedure for finding the standard deviation of the gradient for the modeled surface.

The first step is to find the covariance matrix for the coordinates, a", b", h" at each of the sixteen raw data points. This is found as a function of the standard deviation of the measured quantities, R, β and θ.

d) Error Analysis - Step 2 - Error covariance matrix for modeled planes. The covariance matrix for the slopes of the modeled planes are found next. These four matrices are a function of those found in Step 1.

e) Error Analysis - Step 3 - Error covariance matrix for the center points. This step involves finding the covariance matrices for the center points, p^n. To do this we must first find the covariance matrix of the variables at the center point (a''^n_p, b''^n_p, h''^n_p, $\partial h/\partial a''^n$, $\partial h/\partial b''^n$) in the (h",a",b") coordinate system.

Next we must transform this matrix into the (h,a,b) coordinate system. This is done by use of a transformation involving a matrix D, which is a function of the angles ϕ and ξ, Fig. 34.

f) Error Analysis - Step 4 - Error covariance matrix the model parameters. This step nvolves finding the covariance matrix for the C_{ij} parameters found in Equation 1. This involves use of all four covariance matrices found in Step 3.

g) Error Analysis - Step 5 - Error covariance matrix for the gradient. This step yields the covariance of the gradient. To do this, first the covariance matrix of the slopes, $\partial h/\partial a$ and $\partial h/\partial b$, must be found. This matrix is a function of the matrix found in Step 4.

Finally, the covariance matrix of the gradient is found using the above covariance matrix. The standard deviation can then be found directly. Note the standard deviation of the gradient is a function of the point under consideration and varies accordingly.

Conclusion

The modeling method described above provides a means for modeling the terrain, which makes efficient use of the data points. This is important since there is a limit to the number of data points which may be used. The data point spacing may be varied to change the amount of detail.

This procedure also requires a relatively small amount of calculations. Since time is an important factor in the path selection system and the number of data points are high, calculations must be performed quickly.

By using the two values for slope at a data point it is believed that this model will follow the slope contour more closely than a model using height data only.

With the standard deviation of height and gradient at points on this surface found, limits can be set on the parameters used to determine data point spacing and location. It will also be used to determine which method of arranging the data points is optimum for modeling. These applications are presently being evaluated and the results should be available soon.

Future Problems

The computer program for the error analysis will have to be debugged before meaningful data can be produced. Once the data is available, the problem of parameter optimization and data point spacing can be investigated.

Once the data point spacing has been set the resolution of the proposed model can be tested to see what range of obstacles it can detec.

Time Schedule

	February	March	April	May
Computer program for error analysis	———			
Parameter optimization		———		
Investigate model resolution			———	
Project report				———

C.2.c. Scanning Scheme for a Laser Rangefinder - D. Scanlon
Faculty Advisor: Prof. C. N. Shen

Objective. The major objective is to develop a comprehensive scheme by which the terrain will be scanned by the MRV's laser rangefinder. In other words, given certain constraints the goal is to find the best way of collecting the range data via the laser scanning system. Some of the constraints being dealt with are errors due to data point spacing, the vehicles physical capabilities, limitations caused by the laser scanning hardware, and the time necessary to collect and process the data. At the present time there are two different methods of processing the range information: terrain modeling and edge detection. The needs of the two methods being quite different, they will have to be treated separately, at least for the present.

Progress Summary. The progress that has been made so far is with the study of a scanning scheme for use in terrain modeling. Briefly, an attempt was made to design a scheme in which the transmitting angles of the laser changed by equal increments for each scan. With this feature the scheme is more readily implementable by some physical scanning systems. This goal proved impossible to realize, resulting in a scheme somewhat less than desired. The chief reason for the difficulty encountered lies in the fact that the standard deviation of the gradient (important in terrain modeling, meaningless for edge detection) rises sharply as the measurement point spacing becomes smaller, and as the points are taken closer to the vehicle. This also means that there is a trade-off involved between obtaining a high point density for maximum information and reducing the point density for greater accuracy in calculating the gradient.

Discussion. Fig. 36 shows the proposed method of a single scan for terrain modeling. The dots of the figure signify "measurement points" or points where range and angle information is known as a direct result of the laser scan. The rectangles represent "data points" which are determined by four surrounding measurement points and have associated with them a height, an in-path slope, and a cross-path slope. It is desirable that the measurement points be taken in the "W" format so that the data points are determined by four measurement points obtained very close together in time thereby eliminating error due to movement of the vehicle. Four data points are then used to model a section of the terrain (shown in dotted lines) with a polynomial. Fig. 37, a view looking down on the rover, essentially defines Δa and Δb (in meters) and $\Delta\theta$ (in degrees). It has been determined that the scan is to be from three to thirty meters in front of the vehicle. The rover should be able to see enough terrain at the three meter range to at least equal its own width. If the vehicle is 2 to 3 meters wide then a 60 degree scan would be needed to accomplish this. For the present time this sweep should be no larger than this due to angle limitations of scanning hardware.

A side view of the rover, Fig. 38, defines $\Delta\phi$ (degrees) and shows the laser height to be three meters. A major assumption

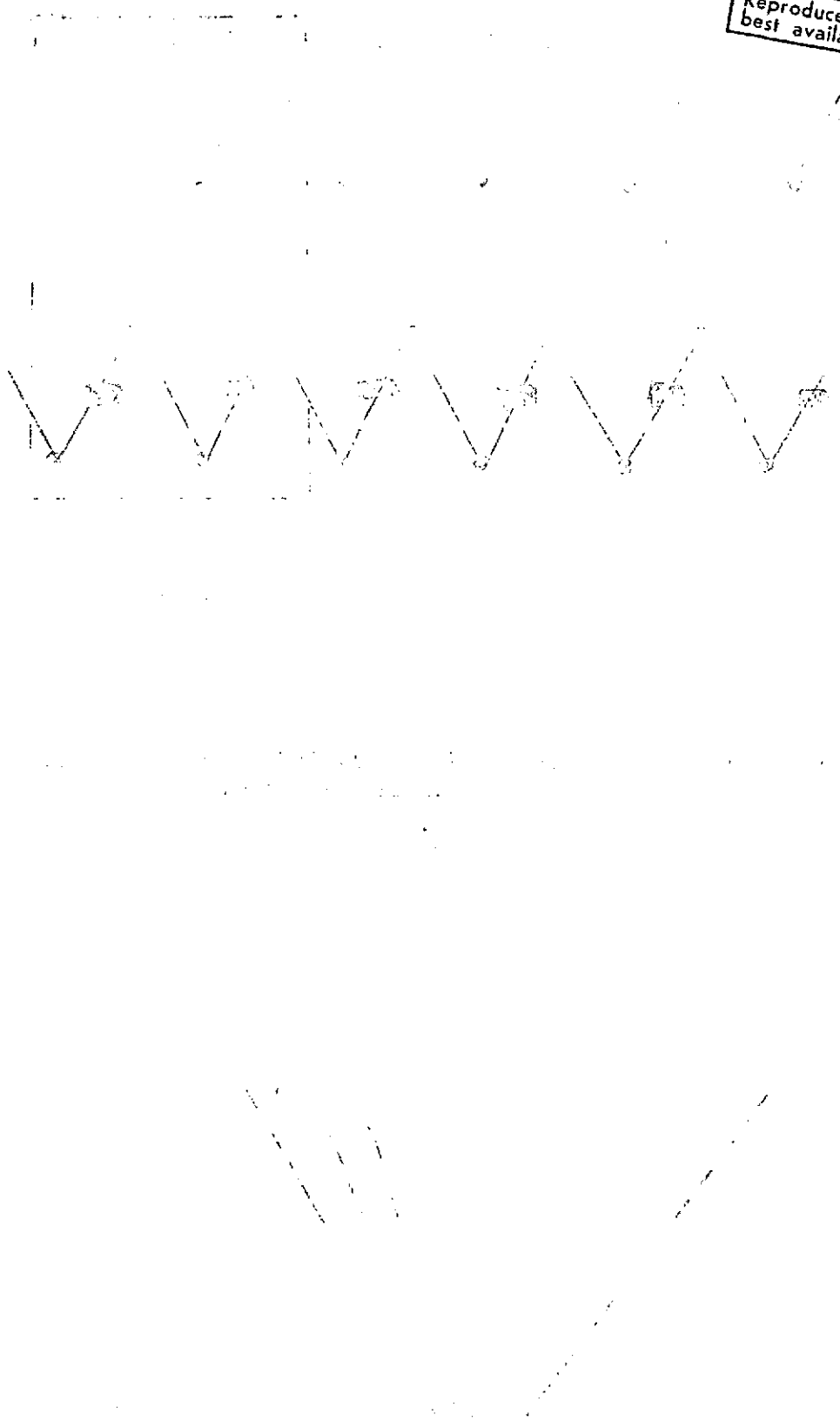

Fig 37. Top View

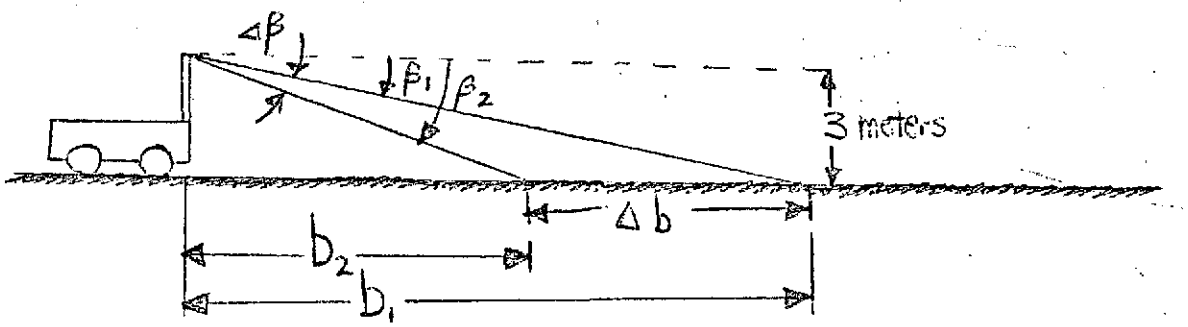

Fig. 38. Side View

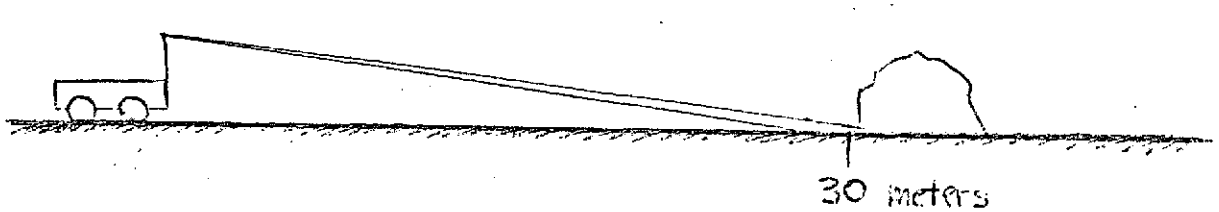

Fig. 39. Rover will not know if boulder is too high to climb until it is 10 meters closer

which should be noted is that all calculations and results are derived here for level ground for our preliminary study only.

Given that we want to model the terrain from three to thirty we run into the problem pictured in Fig. 39 assuming a boulder or steep incline is located at the thirty meter point. Knowing also that the vehicle is capable normally of climbing a 0.4 meter step, it can be shown that the rover will not be able to recognize the boulder as being or not being 0.4 meters high until it is at least ten meters closer. This effect tends to reduce the rover's decision-making ability in the 20-30 meter range. As will be seen later in Table I, one extra scan beyond thirty meters fits nicely into the scheme by extending the rover's view by the needed ten meters and allowing the scans to be doubled-up as required by the modeling scheme. Along the same line of thought, the measurement point spacing should be such that "boulders" of height over 0.4 meters are not totally bypassed by the scan, Fig. 40. The scheme of Table I is shown to have the necessary measurement point spacing to avoid this problem. The boulder heights listed in the last column were calculated from the relation $3\Delta b/b$.

Certainly the most important figure is Fig. 41, a set of curves of standard deviation of gradient versus distance from vehicle, Ref. 10. The standard deviation of the elevation (β) and azimuth (θ) angles was assumed to be one minute, an obtainable accuracy, and the standard deviation of the range was set at five cm., an accuracy hopefully obtainable. Associate with each curve of course is an increasing measurement point spacing as the distance from the vehicle is increased. Starting with the curve on the left the measurement point spacings represented are:

	4a	4b
Curve No. 1	.45 - .8	0.4 - 1.0
Curve No. 2	.45 - .65	.5 - .9
Curve No. 3	.38 - 1.4	.2 - 2.4
Curve No. 4	.4 - .8	.25 - 1.0

Although it is desirable to get as much information as possible, it can be seen that making the measurement point spacing too small results in a large uncertainty in the gradient. On the other hand, placing the points far apart for a small standard deviation in gradient gives less meaningful results since much terrain has been overlooked. Table I represents a possible compromise. It can be seen that equal angle increments are not wholly obtainable and the major region of difficulty is that from 3 to 9 meters. It should be noted that the $\sigma_{\frac{\Delta b}{b}}$ column is a rough estimate. Since the goal of equal angle increments is not met anyway, the sections that are now equally incremented do not have to be religiously kept that way. A slightly better measurement point spacing is obtainable at the expense of breaking up

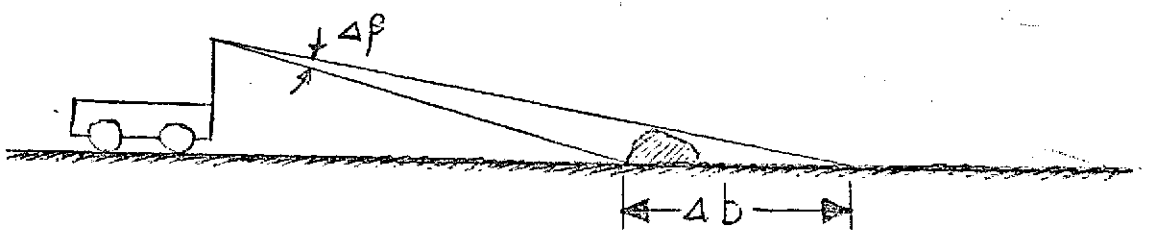

Fig. 40. Scan misses boulder because $\Delta\beta$ is too large

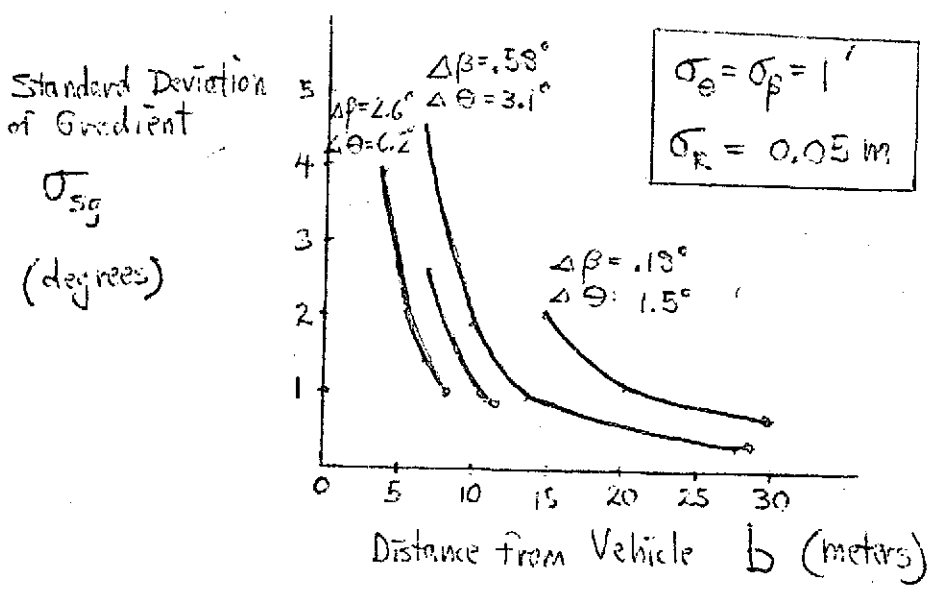

Fig. 41. Standard deviation in gradient vs distance from vehicle on flat surface

TABLE I

SCANNING SCHEME FOR TERRAIN MODELING

UTILIZING EQUAL ANGLE INCREMENTS

deg. β	deg. $\Delta\beta$	deg. $\Delta\theta$	meters b	meters Δb	meters Δa	degrees σ_{sg}	meters MAX. BOULDER HEIGHT THAT CAN BE MISSED
45.0 40.0	5		3.0 3.6	0.6	0.2	5	0.5
35.5 32.0	3.5		4.2 4.8	0.6	0.3	4	0.4
28.8 27.0			5.5 5.9	0.4	0.4	4	0.2
25.2 23.4	1.8		6.4 6.9	0.5	0.5	3	0.2
21.6 19.8			7.6 8.3	0.7	0.6	2	0.3
18.0 16.2			9.2 10.3	1.1	0.7	1	0.3
15.6 15.0			10.8 11.2	0.4	0.8	2	0.1
14.4 13.8			11.7 12.2	0.5	0.9	2	0.1
13.2 12.6		4.3	12.8 13.4	0.6	1.0	1	0.1
12.0 11.4			14.1 14.9	0.8	1.1	1	0.2
10.8 10.2	0.6		15.7 16.7	1.0	1.2	1	0.2
9.6 9.0			17.8 18.9	1.1	1.4	½	0.2
8.4 7.8			20.3 21.8	1.5	1.6	½	0.2
7.2 6.6			23.8 26.0	2.2	1.9	½	0.3
6.0 5.4			28.5 31.7	3.2	2.3	½	0.3
4.8 4.2			35.5 41.2	5.7	2.7	½	0.4

the equal increments. The Δa column is based on fifteen points per line or thirty points per scan resulting in a total of 480 measurement points. Hence, at the estimated time needed per point of one millisecond, the entire scan will take only one-half second, making the vehicle movement during that time a nearly negligible one-half meter maximum. The rover can then be given five seconds for computation purposes as it travels along before the next scan. This will give it a chance to scan an area from 23-30 meters three times before crossing it. Due to the inherent inaccuracies from fairly large measurement point spacing this kind of repetition is desirable. Provisions can easily be made for a higher scanning frequency during turning or traversing steep slopes.

Future Work. A scanning scheme suitable for terrain modeling does not lend itself well to the edge detection approach. Based on current work with edge detection, Ref. 11, the total number of points in the rover's field of vision would be on the order of five to ten thousand. This represents a new problem and it is intended to study scanning as related to edge detection in the near future. The first step I would like to take is to experiment with data point spacings at various ranges to find the minimum number of data points we can get by with and still have effective detection. Second, the effects of the 1 m/sec travel speed and the .63 rad/sec turning rate have on the results. Computation times for the two different schemes are also of interest.

Proposed Schedule.

	February	March	April	May
Data point spacing for edge detection	———			
Speed and turning effects		———	———	
Final scheme proposal				———
Report				———

C.3. Path Selection System Simulation and Evaluation -
R. R. Simonds, R. Campbell
Faculty Advisor: Prof. D. K. Frederick

Previous efforts concerning this area of investigation have concentrated upon the development of a computer package for the simulation and evaluation of proposed path-selection systems. The objective of the present effort is twofold. The first is the development of standard test terrains and a testing procedure to facilitate the analysis capability of the simulation package. The second is the simulation and evaluation of a path selection system proposed several years ago by the navigational computer group at Cornell University.

The development of test terrains has proceeded through the structuring of several initial test sequences and the analysis of the early

Cornell system has been performed using these test sequences. The progress in the two areas of study is discussed below, followed by a statement of future work.

C.3.a. Development of Standard Test Terrains and Evaluation Procedures

To facilitate the use of the computer simulation package as an evaluation tool, the development of a standard testing procedure has been undertaken. This testing procedure consists of investigating the obstacle avoidance behavior of a path-selection system by simulating the system's performance on a sequence of test terrains in the presence of random effects.

In developing this testing sequence an effort was made to determine general rules for the structuring of test terrains, the use of random effects, and the examination of system characteristics that would provide the most information from each simulation. It is hoped that the developed testing sequence will not only provide the program user with a set of terrains and techniques to meet his analysis needs but also a set of guidelines for incorporating additional test situations into the sequence as the need arises.

Noise

The testing procedure outlined below employs the noise capability of the simulation package to create the effect of high-frequency rubble strewn over the test terrain. This effect is obtained by adding filtered white noise to the vehicle's in-path and cross-path slopes, thereby randomly tilting the vehicle and perturbing the sensor orientation accordingly. Knowledge of the damping ratios and natural frequencies of the rover's pitch and roll modes is used to specify the filter's characteristics. The capability of adding noise to the laser range measurements exists and can be used at the user's discretion. Generally the effect of a tipping sensor mast, referred to as attitude noise, had a more pronounced effect on system performance than that of range measurement noise for the terrain sensing systems studied to date.

The procedure used in the test sequences has been to first examine the functioning of the system in the absence of noise and, if the performance is satisfactory, to repeat the sequence with the addition of noise effects.

Obstacles

The principle types of obstacles available in the simulation are spherical or drum shaped boulders and spherical craters. The boulders selected for use in the test terrains have height-to-diameter ratios of unity. Boulders with heights of 2/3 and 2 meters, respectively, were used for analysis purposes. The 2/3 meter size is roughly on the order of the maximum step height that the rover can handle and represents a lower bound on boulder obstacle sizes. The 2 meter size is on the order of the vehicle's dimensions. Larger sizes were not used as it was

felt that they would be too easily detected to be useful.

The craters selected for use in the test terrains have depth-to-diameter ratios of 1/3 and are used in diameters of 1, 3, and 9 meters. The first case represents a lower bound for the crater to be considered an obstacle, whereas the second case has dimensions on the order of the vehicle's dimensions. The largest size is roughly three times the size of the vehicle and is therefore large enough and deep enough to represent a serious hazard to the vehicle.

Standard Testing Procedure

The sequence of test terrains outlined below examines the obstacle avoidance behavior of a path selection system under a variety of ideal and non-ideal conditions. The testing begins with relatively simple avoidance problems involving a single boulder or crater and proceeds to more complicated situations. Each avoidance problem is repeated on several different base terrains in order to enable assessment of the effects of in-path and cross-path slopes on the system's functioning. In every case the noiseless performance of the system is first examined. If the performance is satisfactory, the case is repeated with the addition of noise.

1. Single Obstacle Encounters with Flat Base Terrain

In this basic avoidance situation shown in Fig. 42, a single boulder or crater is placed directly on the anticipated line of travel from the vehicle's initial position to the specified target position. The initial position is chosen such that the boulder or crater is beyond the sensor range on the first scan. The target is positioned so as to be attainable and also minimize the length of the anticipated vehicle path. This shortens the amount of computer time necessary for the simulation and thereby reduces its cost. If the performance is satisfactory, the same cases are repeated with the addition of noise effects. The range at which the system begins active avoidance and the closest approach of the vehicle to the obstacle are recorded for each case.

2. Single Obstacle Encounters with Rolling Base Terrains

a) Gently Rolling Terrain

In this testing sequence the terrain shown in Fig. 43 is used to examine system performance in the presence of the type of non-zero in-path and cross-path slopes found in a gently undulating terrain. The system's noiseless functioning is examined first. The initial position and target position are chosen to provide either non-zero in-path and cross-path slopes by angling across the terrain, or just in-path slopes by moving in the x-direction only. A case with no obstacles is run to determine the vehicle path to the target and to serve as a base line in predicting when avoidance behavior begins. A single boulder or

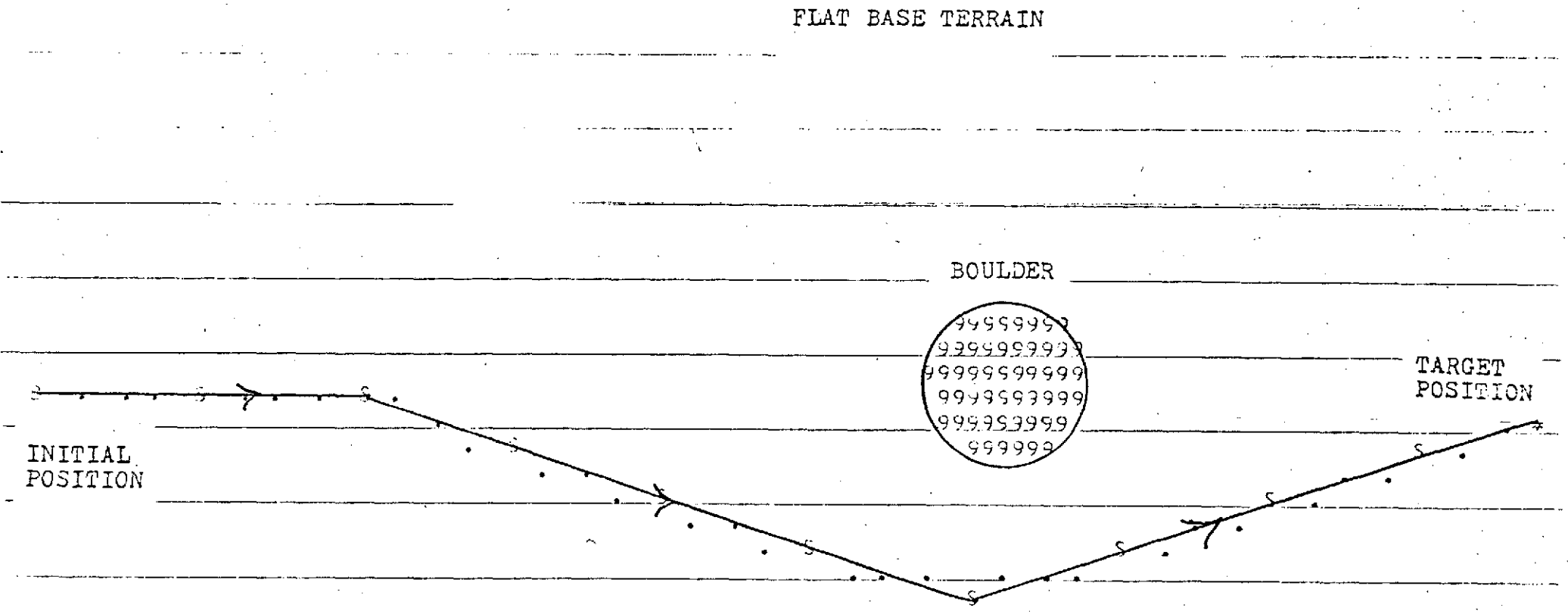

Fig. 42. Single Obstacle Encounter (Flat Base Terrain)

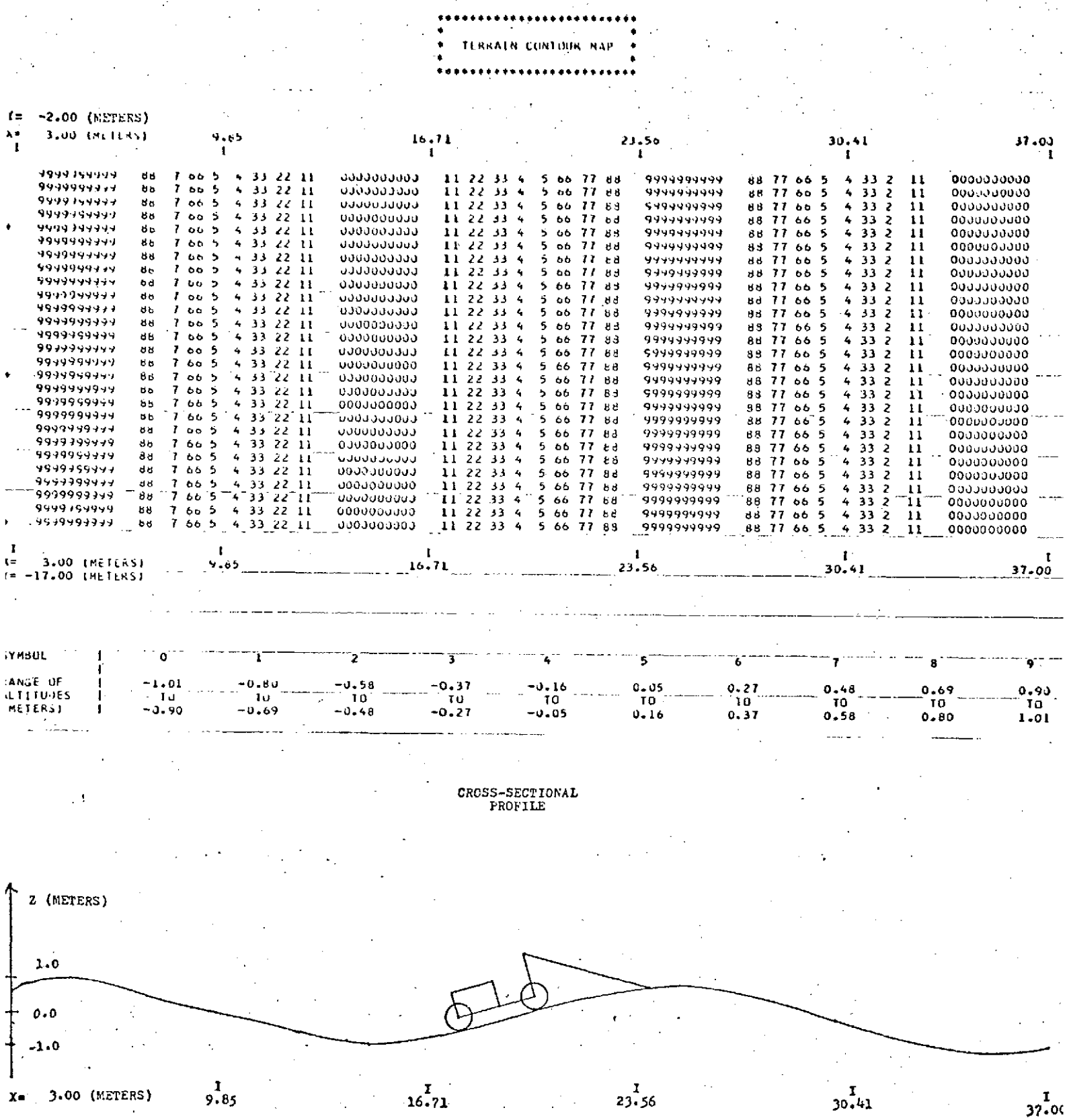

CROSS-SECTIONAL PROFILE

Fig. 43. Gently Rolling Terrain

crater is then placed directly in the vehicle's path to the target and the procedure outlined for the flat base terrain sequence is followed. If the performance is satisfactory the same cases are repeated with the addition of noise.

b) Rolling Incline

In this testing sequence the terrain shown in Fig. 44 is used to examine system performance in the presence of the type of non-zero in-path and cross-path slopes encountered on the size of a hill. The incline has a maximum in-path slope of 18° to 20° and presents no hazard to vehicle travel. Both uphill and downhill approaches are possible. The choices of initial vehicle position and target position allow a variety of in-path and cross-path slopes to be encountered as the vehicle proceeds to the target. A case without obstacles is run to determine the path to the target and to serve as a base line in establishing when avoidance behavior begins. A single boulder or crater is then placed on the vehicle's path and the procedure outlined in the flat base terrain sequence is followed. The choice of the obstacle's position is based upon finding situations along the vehicle path to target where the effects of in-path and cross-path slopes make detection difficult. Fig. 45 shows two possible uphill cases for a path parallel to the x-axis. In the first situation the presence of the boulder is masked by the hill in the background. In the second situation the sensor beam is tilted above the obstacle's location.

3. Multi-Obstacle Cases

The previous sequences examined the system's performance in avoiding single obstacles in a variety of slope settings and in the presence and/absence of noise. The next sequence of terrains assumes the system has proved it can successfully avoid single obstacles, and presents the system with more complicated avoidance problems to solve. All these cases are run in the presence of noise.

a) Boulder-Crater Field

Figure 46 shows a maze-like arrangement of boulders and craters of various sizes lying at the base of a 25 meter hill. There are several possible paths through the field and the average path length to the target is anticipated to be 50 to 80 meters. Filtered white noise is used during the simulation to create the effect of rubble strewn on the base terrain varying in size up to a maximum of 0.1 meters. The indicators of system performance in this simulation are the time to travel to the target, the length of the chosen path, and the closest approach to an obstacle.

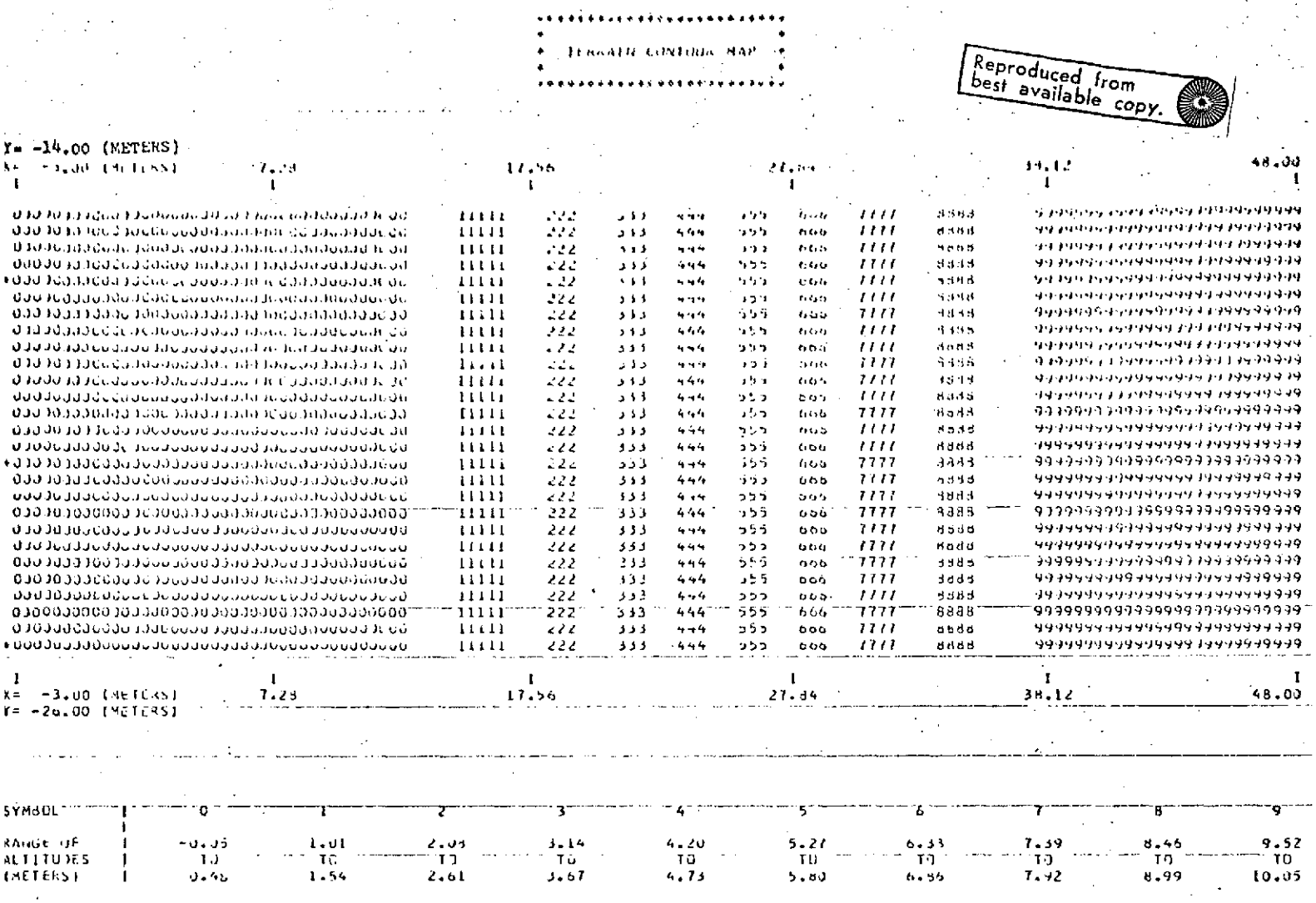

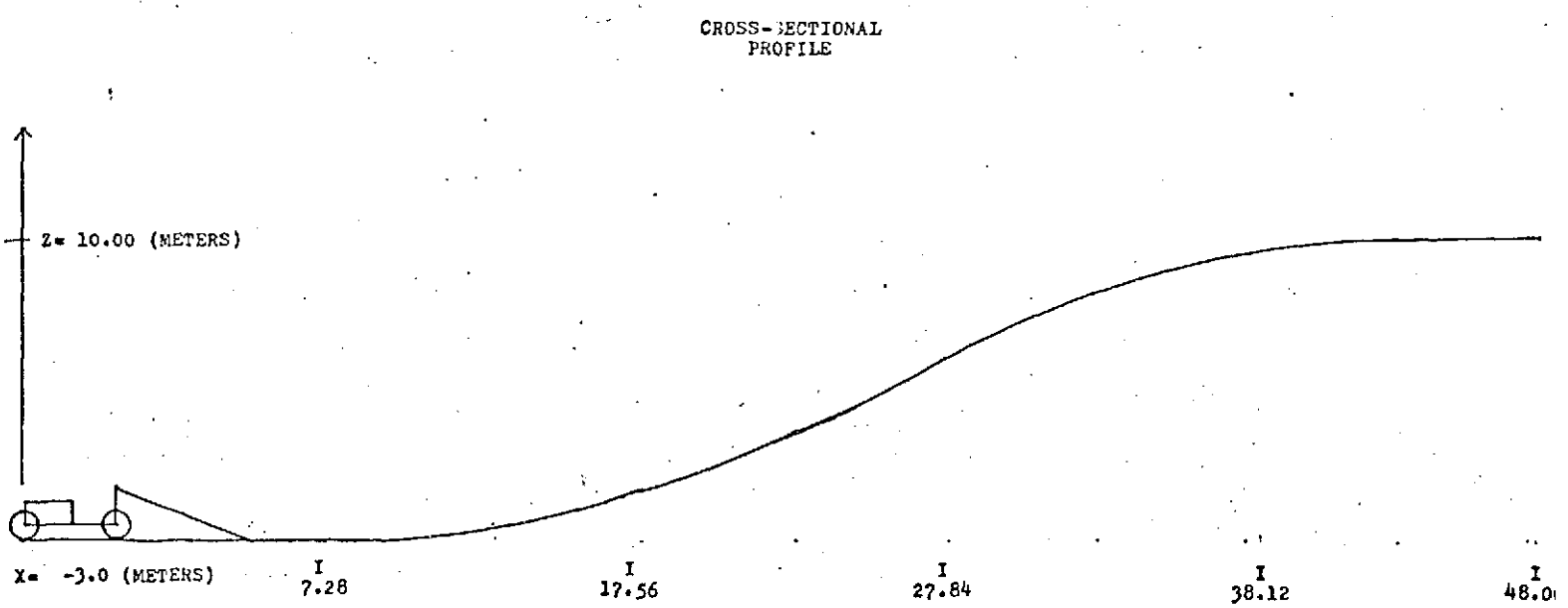

Fig. 44. Rolling Incline

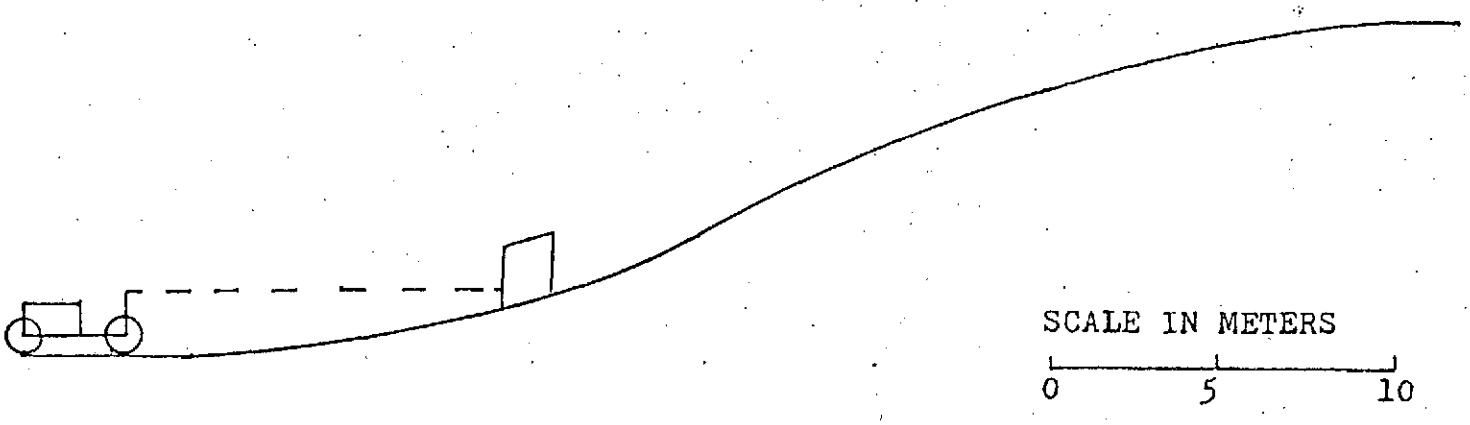

CASE 1

CASE 2

Fig. 45. Single Obstacle Encounters
(Rolling Incline)

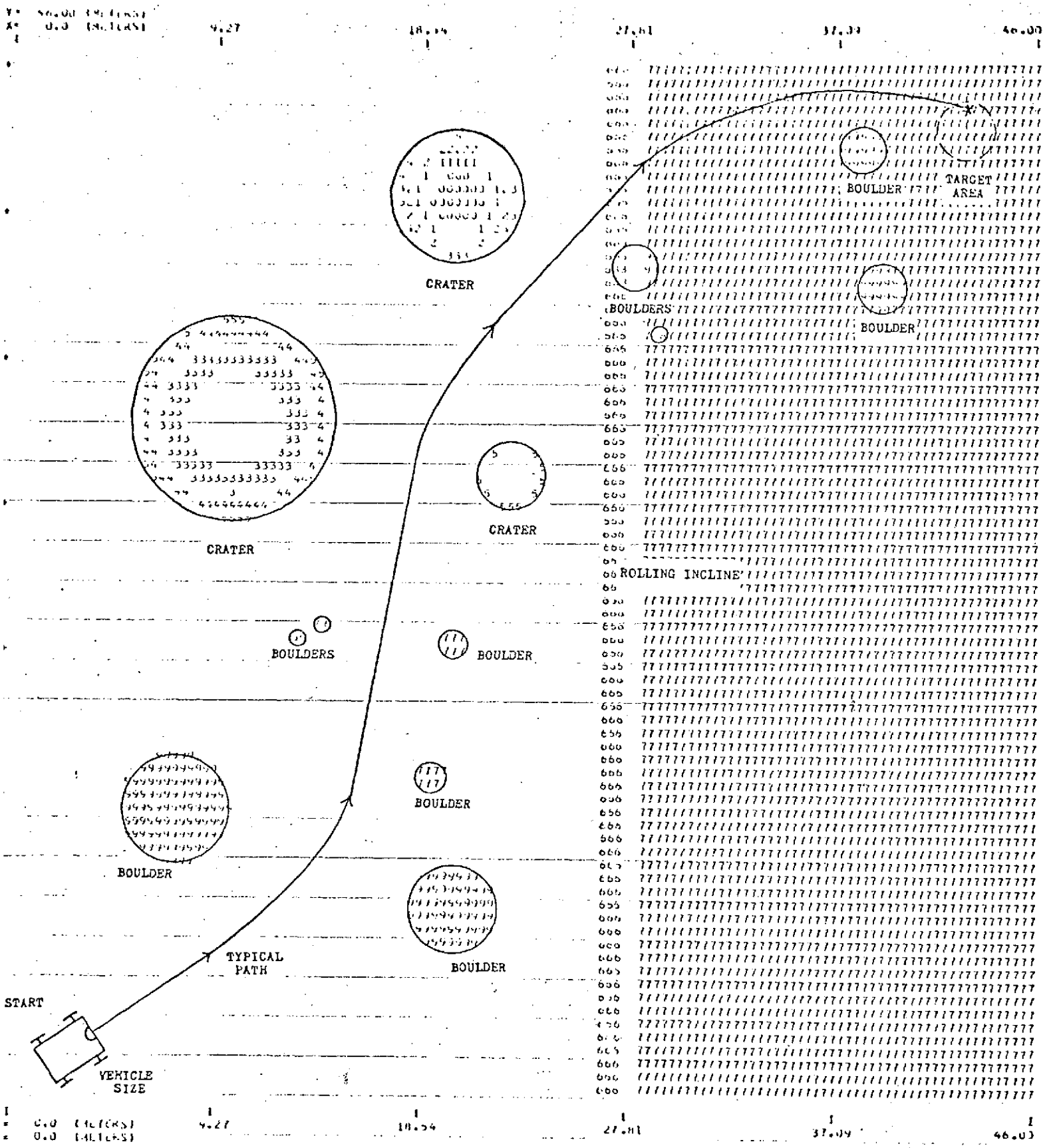

Fig. 46. Boulder-Crater Field

b) Box Canyon
Figure 47 shows a box canyon formed by three Gaussian hills, each too steep to be climbed. The vehicle must back out of the canyon and circle the hills to reach target.

Conclusions and Recommendations

The test terrains that have been developed to date place heavy emphasis on single obstacle encounters in a variety of slope settings and in the presence and absence of noise effects. Satisfactory performance on these basic terrains is required before performance on more complicated multi-obstacle terrains is examined. The development of single obstacle encounter terrains has been essentially completed and future work should concentrate on the development of additional multi-obstacle terrains.

To date, the use of noise effects in the testing procedure has been confined to the employment of attitude noise. Future work should examine the use of range measurement noise and the combined use of range measurement and attitude noise.

C.3.b. Early Cornell System Evaluation

The first step in the analysis of the early Cornell path-selection system was the incorporation of the system design into the computer simulation package. After this was accomplished an analysis procedure was formulated in accordance with the standard testing sequence which has been developed concurrently and carried out. Finally, based on the simulation results, several recommendations directed at system improvements have been made.

A brief description of the early Cornell system, the simulation procedure, and the results of the evaluation are presented below.

System Description
The early Cornell path-selection system as modeled in the simulation package is divided into three distinct operations: the sensor, the terrain modeling process, and the path-selection algorithm. A description of each operation is given below.

(i) Sensor - A sensor mounted on a vertical mast fixed to the front of the vehicle is simulated. The sensor mast height above ground is specified by the program user. The orientation of the sensor is calculated by taking into account the effects of in-path and cross-path slopes at the vehicle's current position.

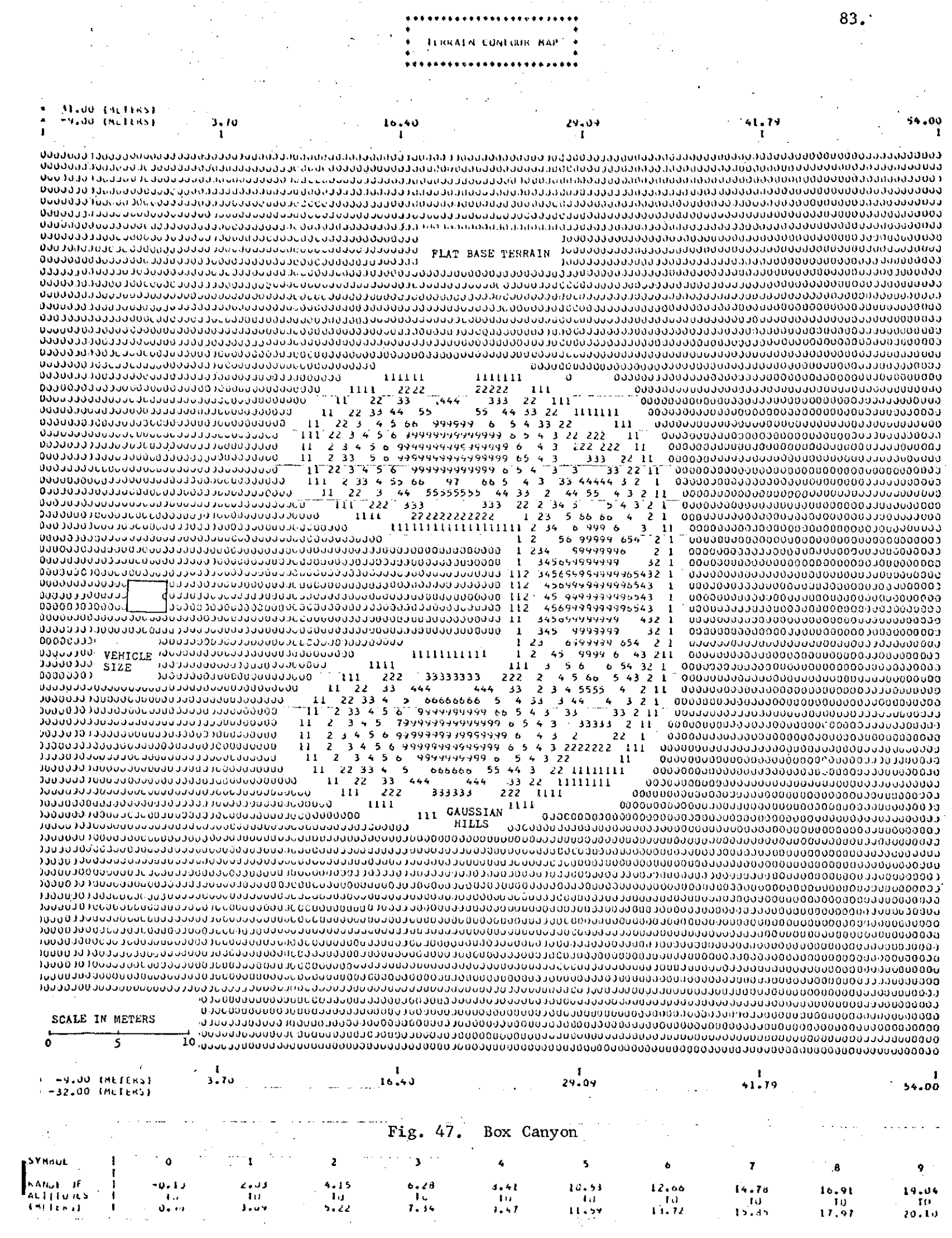

Fig. 47. Box Canyon

SYMBOL	0	1	2	3	4	5	6	7	8	9
RANGE OF ALTITUDES (METERS)	-10.10 TO 0.00	2.03 TO 3.09	4.15 TO 5.22	6.28 TO 7.34	8.41 TO 9.47	10.53 TO 11.59	12.66 TO 13.72	14.78 TO 15.85	16.91 TO 17.97	19.04 TO 20.10

A single beam which moves in a plane perpendicular to the mast is simulated. The scan time is assumed to be instantaneous and the time between scans is uniform. At each sensor scan 29 range measurements are made in a uniform sweep of the area in front of the vehicle, as indicated in Fig. 48.

(ii) Terrain Modeling Process - This process operates on the range measurements received from the sensor simulator. The result is a go/no go map generated along the fifteen forward paths P1, P2,...,P15 by comparing the range measurements with the minimum ranges required for a clear path. The vehicle width and specified buffer zone are incorporated in the calculations.

(iii) Path-Selection Algorithm - In normal operation the path-selection algorithm chooses the closest "safe" path to target. If all of the paths are blocked the emergency mode is called and the following steps are taken:

1) the vehicle is backed up in a straight line,
2) a new sensor scan is taken,
3) the seven forward paths P5 through P11, are blocked,
4) the closest "safe" path to target is again selected.

A special feature of the path-selection algorithm is the concave obstacle mode. This mode was specifically designed to aid the vehicle in reaching its destination if trapped by obstacles forming a concave blockade. When in this mode the minimum range values are reduced and generally either the extreme left or extreme right path is chosen. A more detailed description of the early Cornell path-selection may be found in Ref. 14.

Simulation Procedure

The simulation and evaluation of the early Cornell system was performed in a systematic fashion, corresponding to the guidelines of the standard test procedures described under Task C.3.a. A total of 38 simulation runs have been made examining the system's deterministic performance and its performance in the presence of attitude noise. No examination of the effects of range measurement noise have been made to date.

On the single boulder encounters and rolling incline cases three system parameters were varied, namely, the sensor mast height, the specified buffer zone, and the azimuth

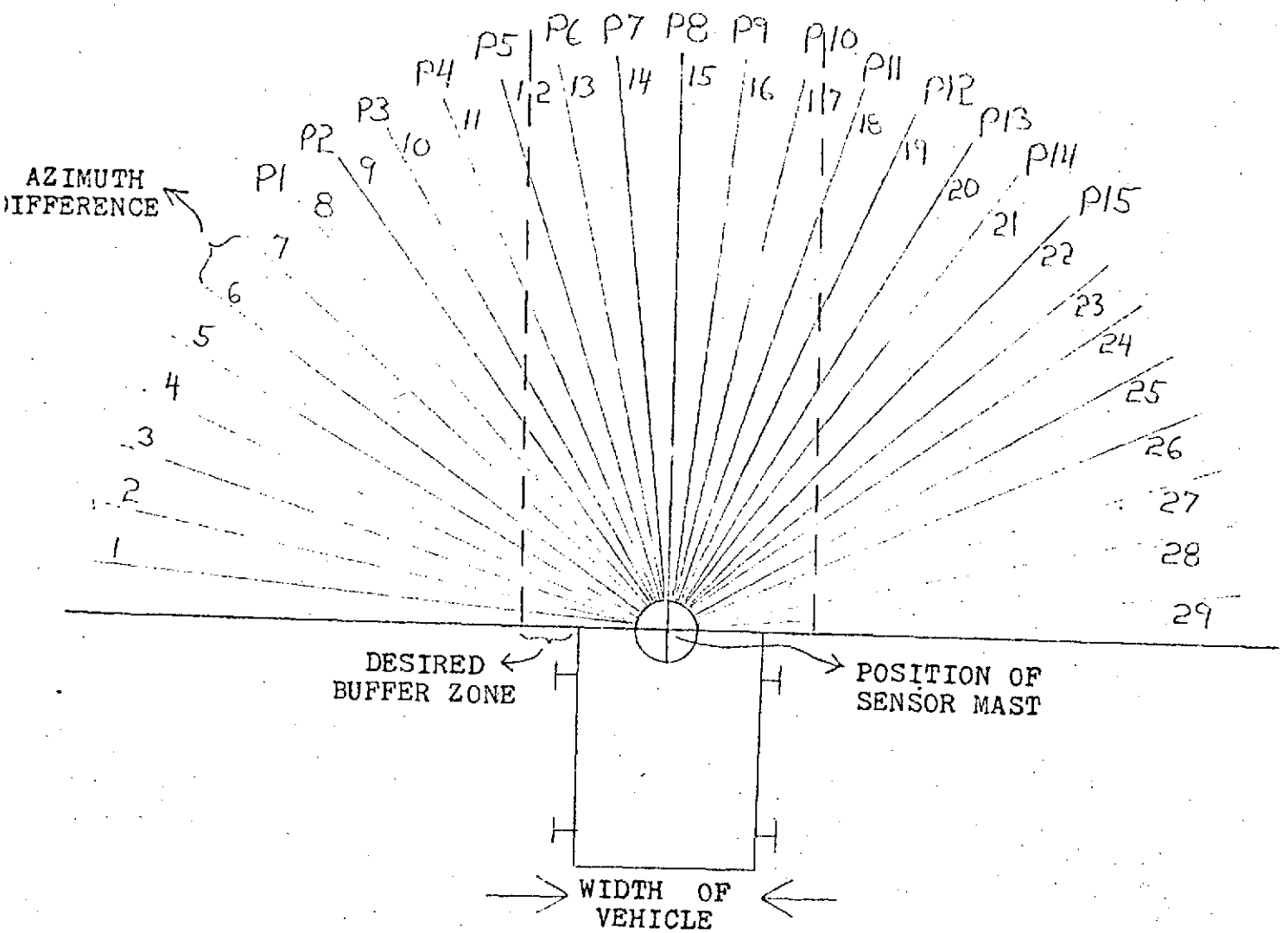

Fig. 48. Sensor Scan (Top View)

difference between adjacent beams, see Fig. 48. The highlights of these simulations will now be discussed.

Simulation Results

As an example of a single obstacle encounter in the presence of noise consider Fig. 49. The system detects the boulder when the vehicle is 7 meters away and steers gently left. However, at the next scan attitude noise has tilted the sensor mast 10 degrees forward, driving the scans into the ground. As a result, the vehicle is fooled into believing there is an obstacle directly in front of itself and steers sharply left.

Fig. 50 is an overlay of two runs with identical system parameters but with different noise characteristics. The upper path was made in the presence of noise and the path-selection system called for two emergency backup maneuvers, whereas the lower path was the result of an absence of noise, with the vehicle moving directly to target. It should be mentioned, however, that with the small boulder of dimensions 2/3 x 2/3 meters the vehicle more often than not failed to avoid the boulder because it lost sight of it between sensor shots. Even when the azimuth difference was reduced by 33% the system still failed to avoid the obstacle.

On the rolling incline cases, when the boulders were placed at the top of the hill they were never detected by the system because as the vehicle approached the obstacle the scans were pointing over it due to the in-path slope of the hill. Fig. 51 is an example of the case where the boulder is placed near the bottom of the hill, where the system was able to see and avoid the boulder.

Special Terrains

The terrain depicted in Fig. 52 of 3 boulders and a cliff was designed to challenge the emergency mode of the algorithm. As originally implemented, the early Cornell system failed to navigate the terrain, as the emergency algorithm repeatedly steered the vehicle back into the trouble area. As an improvement to the emergency procedure a memory capability was added, thereby enabling the system to temporarily remember where the trouble area is located. The path in Fig. 52 illustrates the behavior of the modified system. The new emergency mode, which was only triggered once in the simulation, enabled the vehicle to find the only safe path to the target.

In a deterministic run through a field of ten large boulders the vehicle was able to find a short and safe path to target. However, when the system was simulated over a realistic boulder-crater field which included a small rise and noise, the performance was not as efficient, Fig. 53. For this simulation a one meter mast height and ½ meter buffer zone were specified. The vehicle was eventually able to reach its target despite misinterpreting the small rise as an unnegotiable obstacle and using the emergency mode 13 times.

Conclusions and Recommendations

The analysis of the early Cornell system performed to date

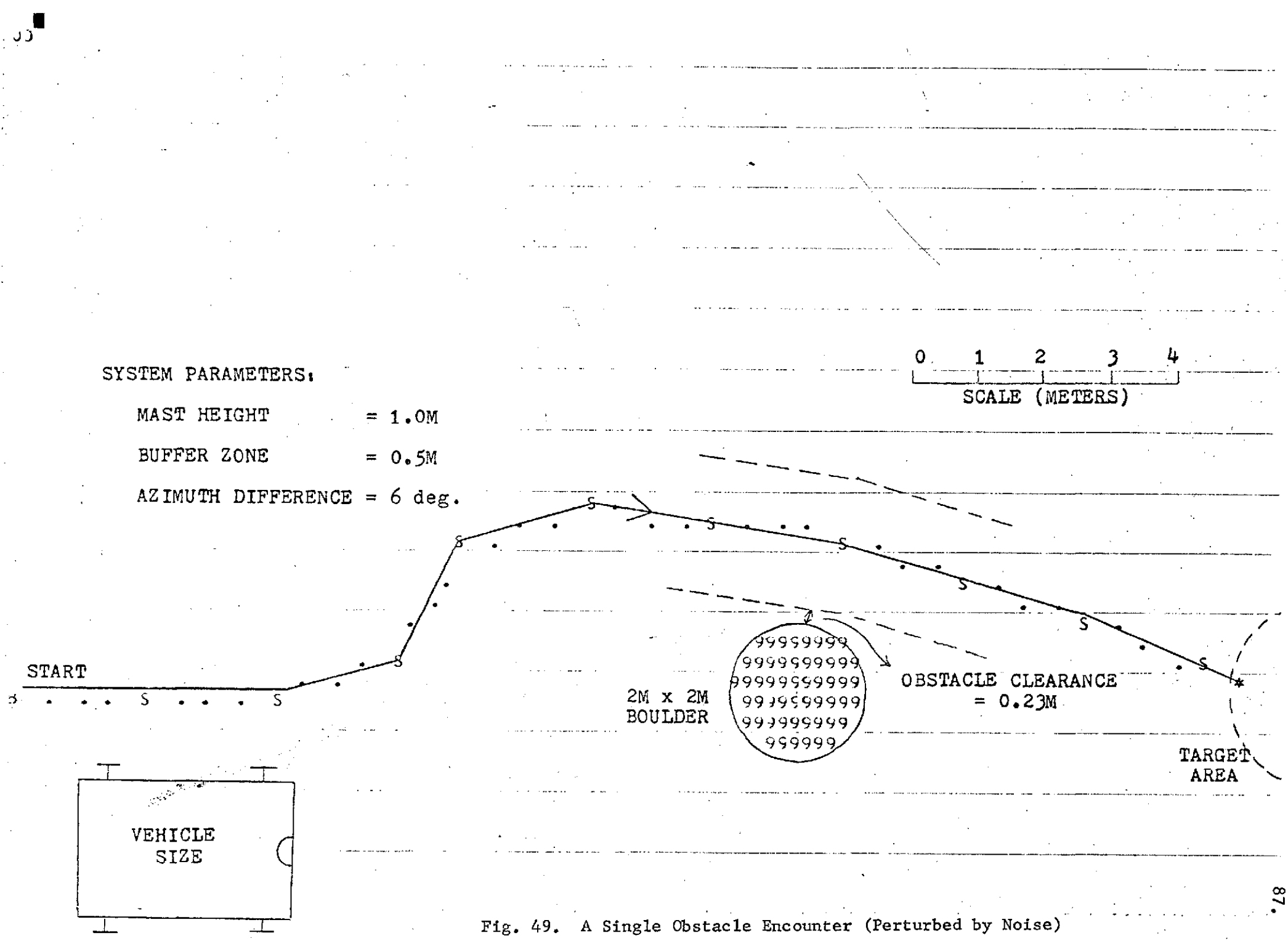

Fig. 49. A Single Obstacle Encounter (Perturbed by Noise)

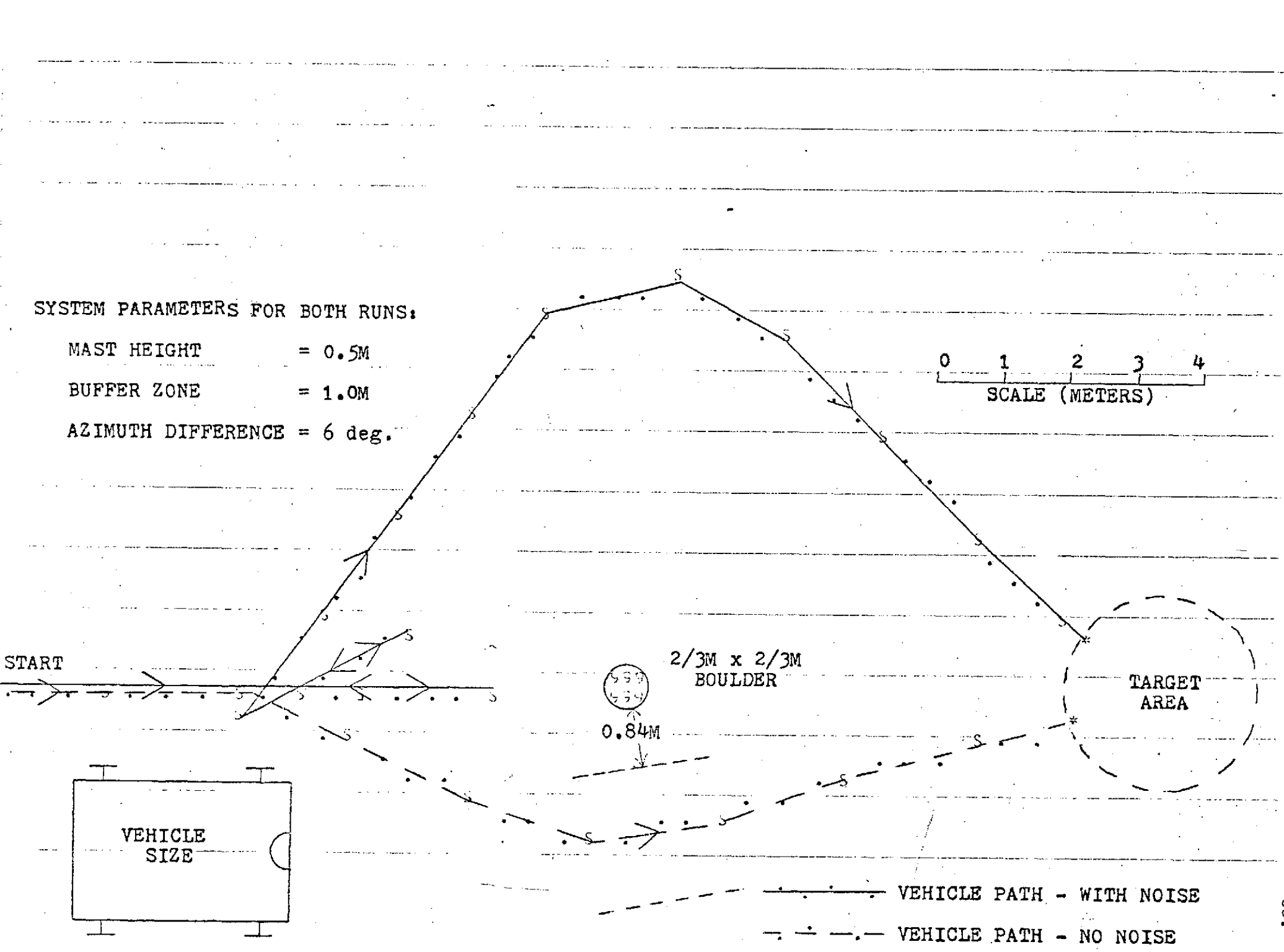

Fig. 50. A Comparison of System Performance With and Without Noise

SYSTEM PARAMETERS:

MAST HEIGHT = 2.0M

BUFFER ZONE = 0.5M

AZIMUTH DIFF. = 6 deg.

OBSTACLE CLEARANCE
= 0.67M

TARGET
AREA

CROSS SECTIONAL PROFILE

TARGET

0 2 4 6 8 10

SCALE (METERS)

Fig. 51. A Rolling Incline - Boulder Near Bottom

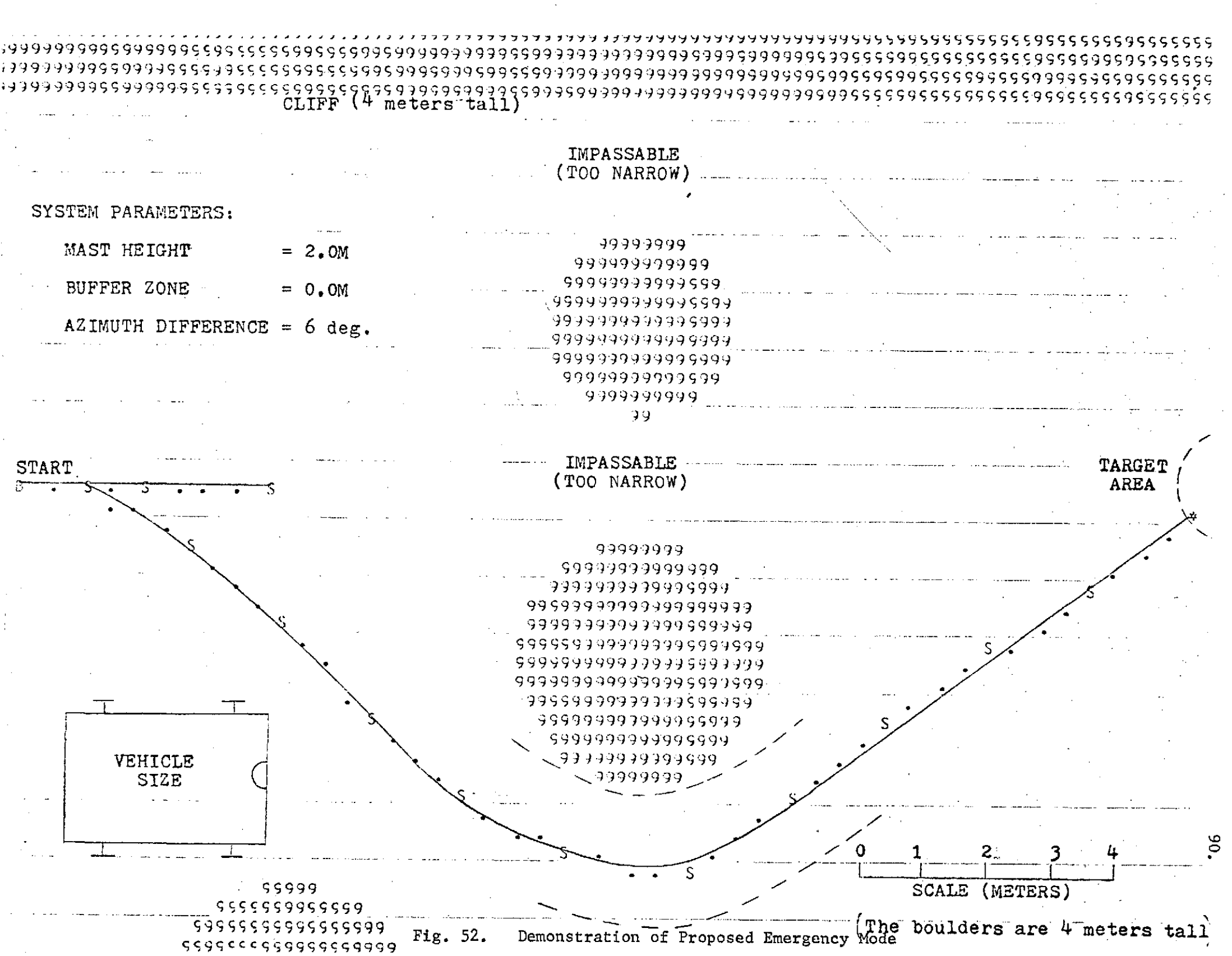

Fig. 52. Demonstration of Proposed Emergency Mode (The boulders are 4 meters tall

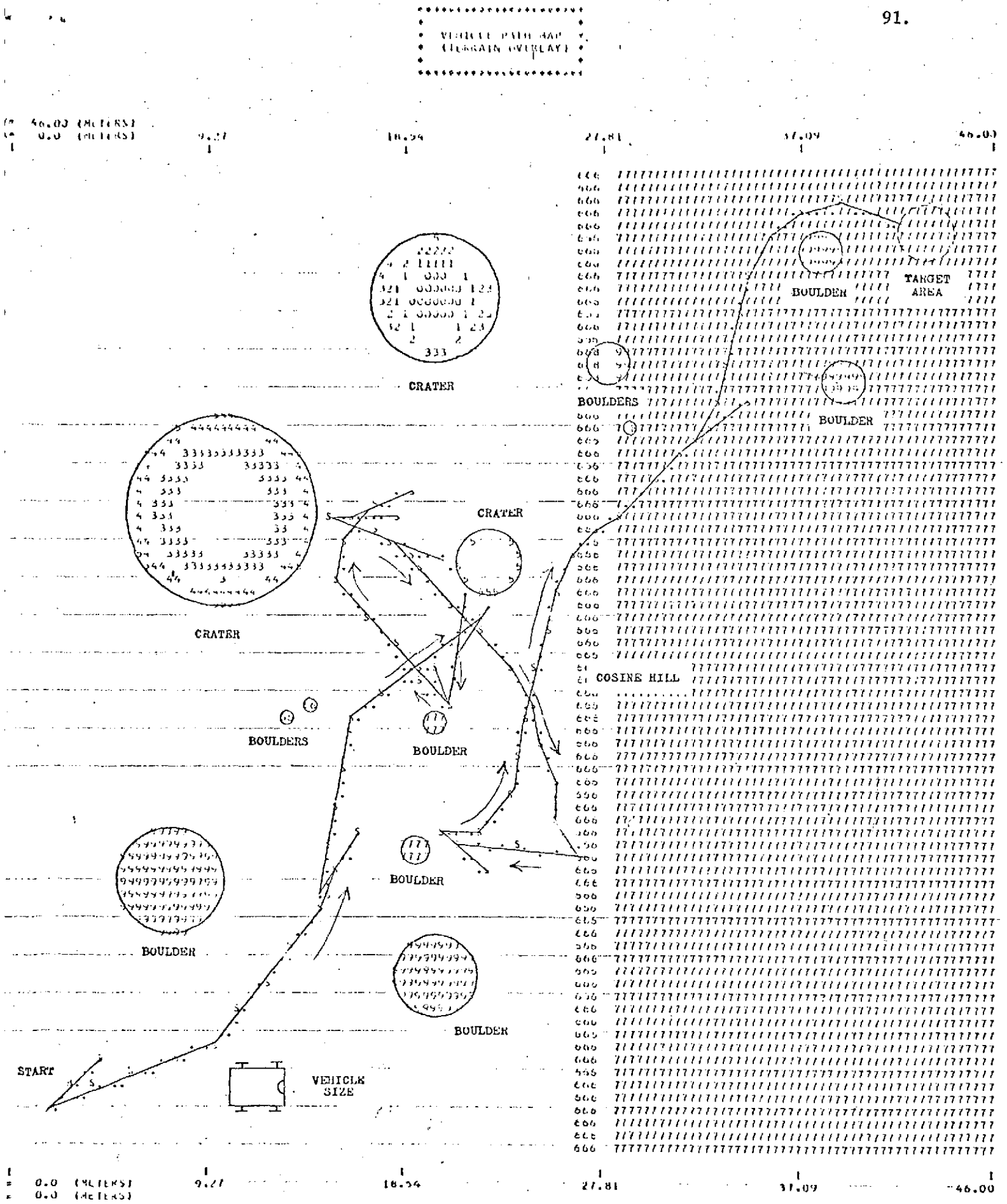

Fig. 53. Navigation over a Boulder - Crater Field

YMODE	0	1	2	3	4	5	6	7	8	9
ANGLE OF	-5.64	-4.62	-3.60	-2.58	-1.56	-0.54	1.47	1.53	2.52	3.54

has shown that it has the ability to navigate successfully on most simple and clearly defined obstacle encounters, but has limited ability on realistic terrains and in the presence of random effects. However, the system is not capable of negotiating small obstacles of 2/3 x 2/3 meters or less, even when not perturbed by noise.

The size of those obstacles which are detectable is a function of the mast height. With small mast heights, noise disturbances frequently trigger the emergency mode, when no emergency really exists. Larger mast heights result in a failure to detect smaller obstacles. A mast height between 1 to 2 meters appears to be about the best compromise, particularly if an ideal mechanical sensor is assumed that can detect small obstacles.

The additional obstacle clearance obtained as the buffer zone is increased beyond 1 meter is small, with a ½ to 1 meter buffer recommended. This specification should produce an actual obstacle clearance of 0.4 to 0.85 meters in most cases.

To increase the system's capability to negotiate realistic terrains the following path-selection system modifications are recommended as items for future study:

(i) The addition of a dual or multi-beam sensor scheme incorporating different elevation angles or sensor heights. The purpose of varying the orientation or position of sensor locations would be to divorce the function of detecting large positive obstacles from that of detecting small boulders and craters.

(ii) The use of non-uniform sensor scanning with the greatest density of scans being taken directly in front of the vehicle.

(iii) The incorporation of an emergency mode which has the ability to remember where a trouble area exists until the vehicle has safely passed the problem.

Future Work

Future work is planned in the following areas:

(i) Completion of early Cornell System Evaluation - Work will include the study of recommended improvements and the addition of range measurement noise to the simulation of random effects.

(ii) Investigation of Short Range Path Selection System - Work will include development of a path-selection algorithm, terrain modeler, and sensor configuration for a system that has sensing capabilities on the

order of 3 to 5 meters. The design will be analyzed by simulating the system's performance on standard test terrains.

(iii) Continued Development of Test Terrains - Work in this area will concentrate on the improvement of testing procedures and the development of additional test terrains that will enhance the analysis function of the simulation package.

(iv) Software Refinement and Documentation - There is an ongoing effort to improve the efficiency of existing software and updating and improving the program documentation will be continued.

The work described in (i), (ii), and (iii) is scheduled for completion in May 1974.

Task D. Chemical Analysis of Specimens

One important phase of the initial missions to Mars is the search for organic matter and living organisms on the martian surface. The present concept for attaining this objective consists of subjecting samples of the atmosphere and surface material to certain chemical and biochemical reactions and thereafter analyzing the products produced, probably in a combination gas chromatograph/mass spectrometer (GC/MS). The gas chromatograph is proposed for separating complex mixtures evolved from the experiments into small groups of similar chemical species. Chemical analysis of these groups would be accomplished in the mass spectrometer. It is the objective of this task to provide engineering techniques and criteria for designing such a system.

Most of the previous effort has involved the systems analysis of the gas chromatograph using simulation, Ref. 15 and 16. This technique uses mathematical models, which incorporate fundamental parameters evaluated from reported experiments, to explore various concepts and to direct further experimental research. Application of prior work to multicomponent chemical systems and improvement of the mathematical model are currently being studied.

The task problems are being attacked by a three-member team, each of whom is pursuing a specific assignment:

1. Chromatograph system characteristics

2. Chromatograph simulation development

    a. Multicomponent chromatography
    b. Chromatograph model improvement

D.1. Chromatograph System Characteristics - A. N. Stovall
Faculty Advisor: Prof. P. K. Lashmet

It is the objective of this subtask to develop techniques for designing chromatograph systems using simulation models currently under study. As the purpose of the chromatograph is to separate

chemical species, the initial effort involves a quantitative definition of resolution or the degree of separation obtained in a specific design under particular operating conditions. A large value of resolution should imply a chromatogram having distinct peaks, whereas a low value should suggest poor separation or overlapping peaks. Resolution should be a function of the physical parameters of the chromatograph, and use of moment analysis seems logical.

Based on the concepts of Fig. 54, the resolution R has been defined in the literature, Ref. 20, as

$$R = \frac{T_2 - T_1}{(W_1 + W_2)/2}$$

where

T_1, T_2 = peak times for first and second component, respectively

W_1, W_2 = base widths for first and second component peaks, respectively

For almost symmetrical peaks, resolution of unity corresponds to peak bases immediately adjacent to one another with no overlapping. Overlapping peaks give resolution of less than unity. The above parameters may be approximated by the moments, Ref. 17 and 18:

$$T \sim \mu(1)$$

$$W \sim 4\sqrt{\bar{\mu}(2)}$$

where

$\mu(1)$ = first moment about the origin or the peak mean

$\bar{\mu}(2)$ = second moment about the mean or the variance

Resolution now becomes

$$R = \frac{0.5\left[\mu(1)_2 - \mu(1)_1\right]}{\sqrt{\bar{\mu}(2)_2} + \sqrt{\bar{\mu}(2)_1}}$$

These moments may be calculated from the model equations and are functions of the system parameters, Ref. 17.

Further investigation showed this definition to be independent of sample size or composition. Figure 55 shows that the chromatograms of the same chemical but of different sample sizes are different although they have the same moments. Because of this characteristic, resolution as defined above appears inadequate to represent separation in mixtures of components having widely

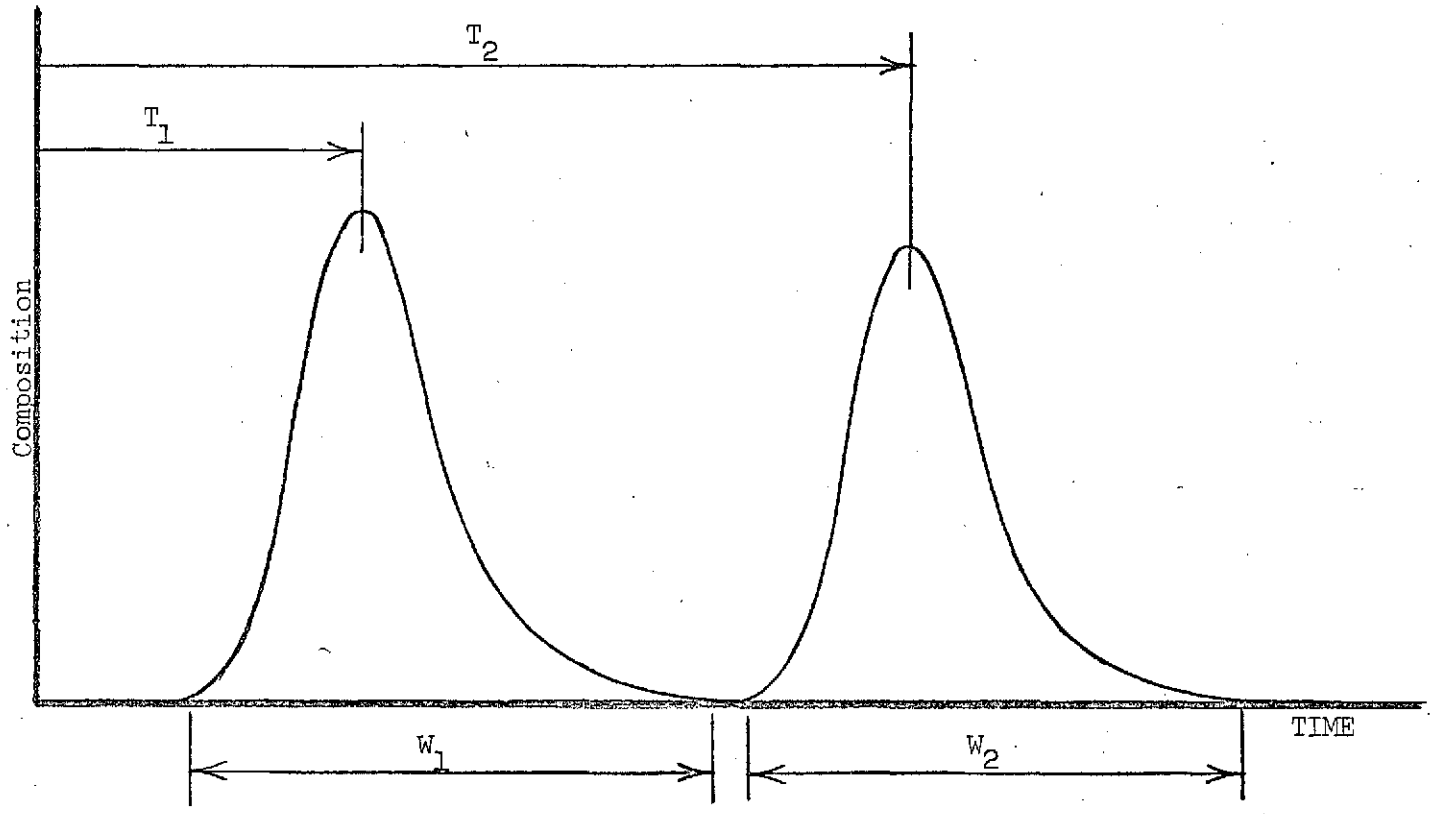

Fig. 54. Representation of Chromatograms by Peak Times and Base Widths

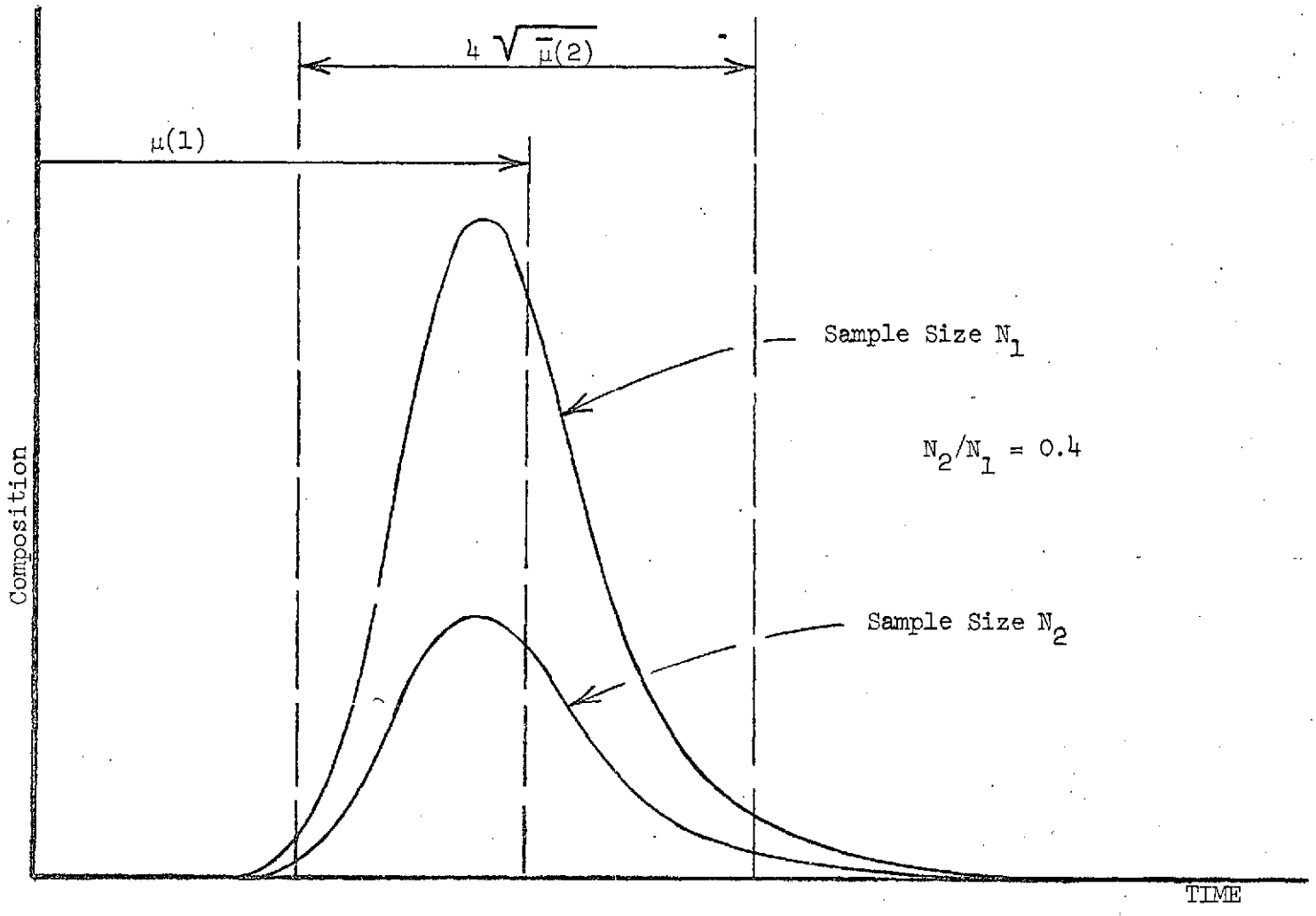

Fig. 55. Effect of Sample Size on Chromatogram

different sample sizes. The two chromatograms of the binary system shown in Fig. 56 have the same set of moments and hence the resolutions are identical. In the upper figure, the peaks are relatively distinct. However, in the lower figure the peak of the second component is not distinct because of its small sample size and intuitively a small resolution should be assigned the separation. Thus another definition of resolution, sensitive to sample size is required.

In a chromatograph, the output signal is the sum of composition contributions of all components. The resolution definition now being considered is based on these contributions:

$$R_i = A_i/A$$

where

R_i = resolution of component i for the peak where the component predominates.

A_i = contribution of component i to the area under the peak where the component predominates

A = total area under the peak of interest.

In the initial studies, the areas will be computed over the finite peak base W as given by the second moment or variance approximately, Fig. 55. This resolution which is the effective composition of the component within the peak, will range from unity for complete separation to zero for essentially no separation; i.e. the sample is small compared to amounts of other interferring chemicals. Thus each component is assigned a resolution indicative of its separation from the other components.

Present efforts involve development of a computer procedure for simulating a chromatograph model forced with an arbitrary sample injection expressed by data and using numerical convolution. The procedure is limited to a binary system and uses the equilibrium adsorption model, Ref. 18, in these initial studies. Output information will include plots of the input pulse, the resulting chromatogram, and the output curves corresponding to the two pure components. Resolution as defined above is also determined. Verification of the suitability of this resolution will follow using chemical systems previously studied experimentally. If this concept of resolution proves satisfactory, a systematic study of the effect of design parameters will be begun. These parameters include:

1. Characteristics of the chemical system (the thermodynamic parameter mR_0)
2. Carrier gas flow rate
3. Column dimensions
4. Packing dimensions
5. Injection pulse characteristics

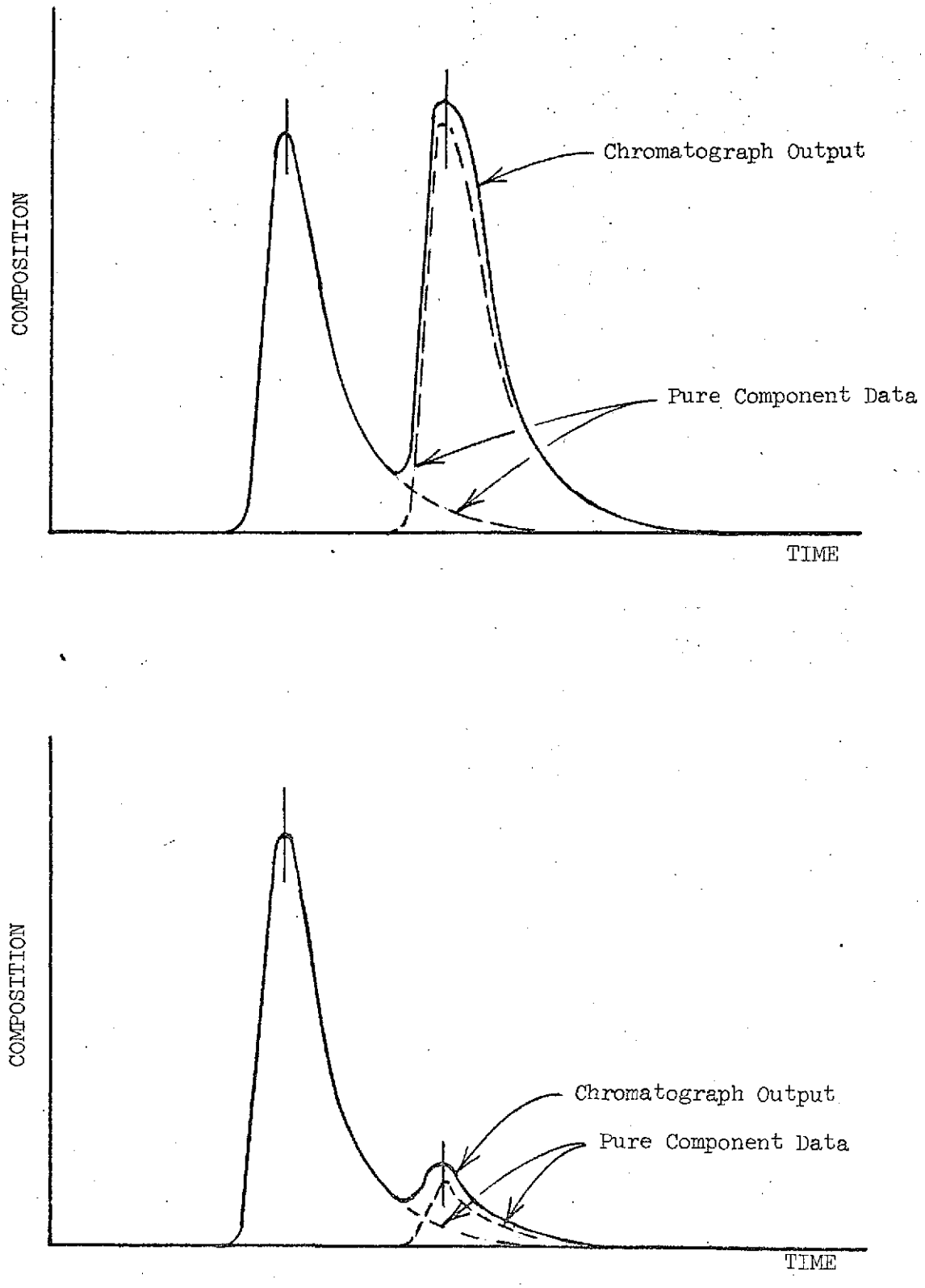

Fig. 56. Effect of Sample Size on Output for Binary System

D.2. Chromatograph Simulation Development

D.2.a. Multicomponent Chromatography - R. C. Lavoie
Faculty Advisor: Prof. P. K. Lashmet

Prior efforts have shown that representation of binary chromatograms by superposition of pure component data is a first-order approximation and in certain cases leads to large discrepancies, Ref. 16 and 19. This subtask has as its objective the generation of additional binary data and analysis of the observed nonlinear effects.

Toward the goal of producing more accurate and useful data, modification of the chromatograph equipment was first undertaken. The equipment consists of a gas chromatograph column with thermistor probes positioned to produce electrical signals proportional to the input and output compositions of the test samples, Ref. 20. The signals are detected in a DC bridge before being recorded by an oscillograph. Recording accuracy was improved by replacing a discrete, multiposition voltage divider in the bridge with a potentiometer to allow continuous attenuation of the thermistor signal. This attenuated signal, the input to the oscillograph, could be precisely adjusted to give full scale recordings. Relative error in reading the graphical output was reduced in some cases by a factor of 3 or 4.

It was noted that injection of liquid samples produced a dispersed pulse at the column inlet. For maximum resolution, the sample input to the column should be a sharp, narrow pulse, so modifications to the injection block were undertaken. The liquid sample injection block consists of cylindrical chamber containing an electrical heater. Samples are injected into the chamber by syringe where they are vaporized by the heater and carried into the column by an inert gas stream which passes through the block. A cylindrical sleeve, designed to reduce dead volume was fitted into the chamber and the power to the block heater was increased to hasten sample vaporization. As seen in Fig. 57, the input pulse was markedly improved by the changes.

To improve data reduction and to obtain more useful information, some of the computer programs were changed. First, second, and third moments of input and output pulses, which are important in model analysis, are now computed in both dimensionless and real time. Gas compositions are reported as actual sample mole fractions rather than as normalized data points, merely proportional to composition. This information is important in checking some of the assumptions used in the model derivation.

In the experimental program, new data were collected to supplement previous data and to explain deviations from predicted results. Major deviations were encountered in using the Carle minivalve to input gas samples such as ethylene, and in running binary samples on the Chromosorb-102 column. In the ethylene system, a sharp, narrow input produced a low, flat output pulse with excessive tailing, whereas the model predicted a relatively sharp, high output

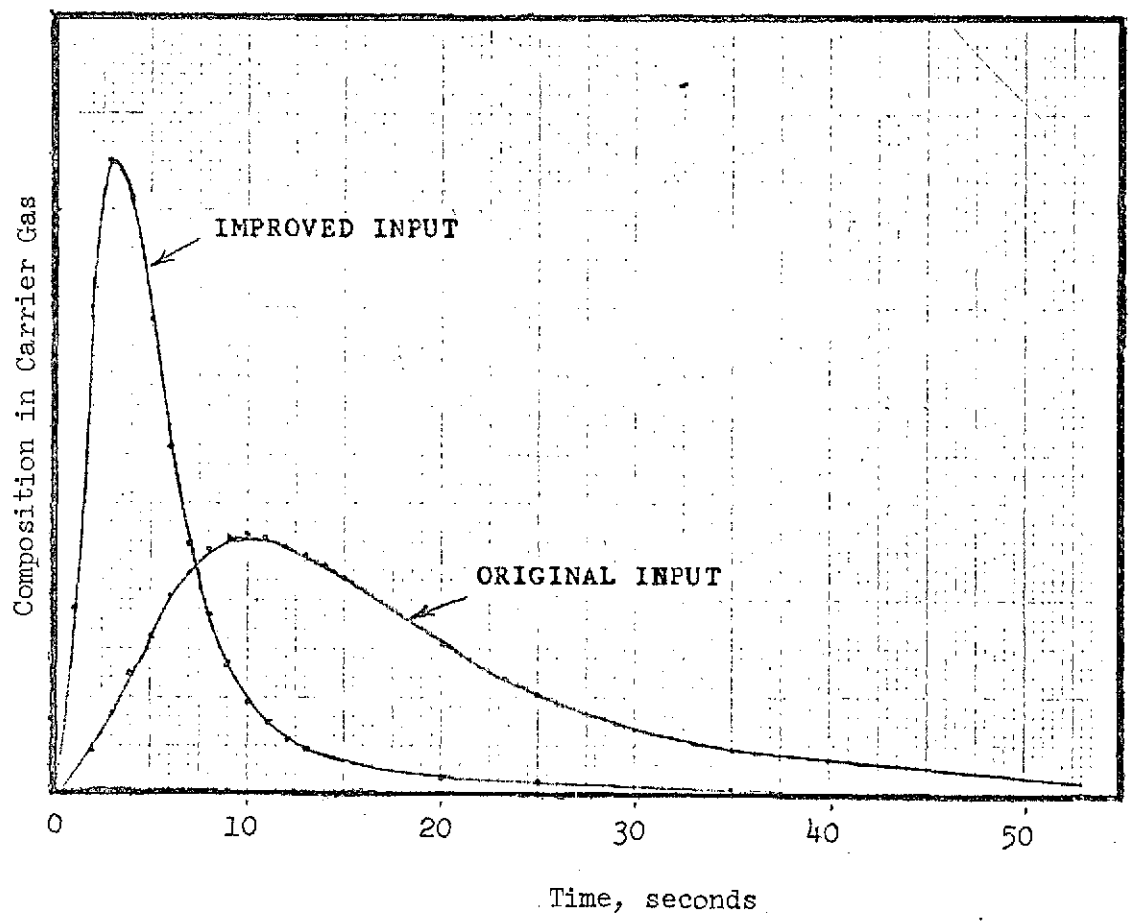

Fig. 57. Input Pulses to Column for Liquid Samples

peak. It was noted that the porous Chromosorb-102 column might be poorly represented by the model which assumes no porosity. However, similar behavior resulted when using a Carbowax-1500 column which is believed to be nonporous. It is now thought that deviations from the model are due to nonlinearities introduced by the high concentrations ($\sim$30%) present in the input pulse of the minivalve. This will be further investigated.

Model predictions of binary sample separation are based on linear superposition of pure component data. Pentane-heptane samples on Chromosorb-102 were shown to deviate markedly from this model, Ref. 19. Attempts to separate these components on the non-porous Carbowax-1500 column to determine if porosity was a factor were not successful. A new non-porous column composed of di-2-ethylhexyl sebacate (DES) on an inert substrate and described in Table II was purchased and tested.

Data from this column were especially well modeled by the simple equilibrium adsorption model, Ref. 18. Pentane and heptane samples were run at temperatures of 50 to 125° C, and adsorption activation energies of 4.0 and 6.6 kcal/mole respectively were derived from temperature behavior of the thermodynamic parameter mR_0, Fig. 58. Sample sizes ranging from 0.2 to 3.0 microliter gave no significant differences in values of mR_0. Binary samples were used, and linear superposition of pure component data predicted the binary results well. Comparison of the simulation with experimental data, shown typically in Fig. 59 indicated a slight non-linear effect in the heptane data. However, considering the error in determining the parameter mR_0 from pure component data as shown in Table III, the simulation and experimental results were essentially the same.

Future work includes using a mercury porosimeter to compare porosities of the various columns, further analysis of the Chromosorb-102 column data to determine the reasons for deviations from linear superposition, and proposing a new model to handle nonlinearities encountered in experimental work.

D.2.b. Chromatograph Model Improvement - P. T. Woodrow
Faculty Advisor: Prof. P. K. Lashmet

The objective of this task is the development and verification of a mathematical model that adequately predicts the component behavior of a sample injected into a gas chromatograph. At this time, a comprehensive model, in the form of a set of coupled, partial differential equations, has been developed and studied using the techniques of moment analysis. This model includes the following transport mechanisms: axial diffusion, axial convection, mass transfer between the interparticle and intraparticle regions, intraparticle diffusion and a finite rate of adsorption within the particle. Moment analysis of this model has shown it to be more capable of predicting characteristics of actual data than the simpler models previously studied, Ref. 16. The development and moment analysis of this model are documented in a recently issued technical report, Ref. 21.

The recent technical report, Ref. 21, also considered aspects of

TABLE II

DES COLUMN CHARACTERISTICS

Length	100 cm
Outside diameter	0.635 cm
Inside diameter	0.555 cm
Particle size	60/80 mesh (0.0250/0.0177 cm)
Coating	di-2-ethylhexyl sebacate (DES) 20% by weight
Substrate	Chromosorb P (firebrick)
Temperature range	room to 125° C
Application	separation of hydrocarbons, C_4 and heavier

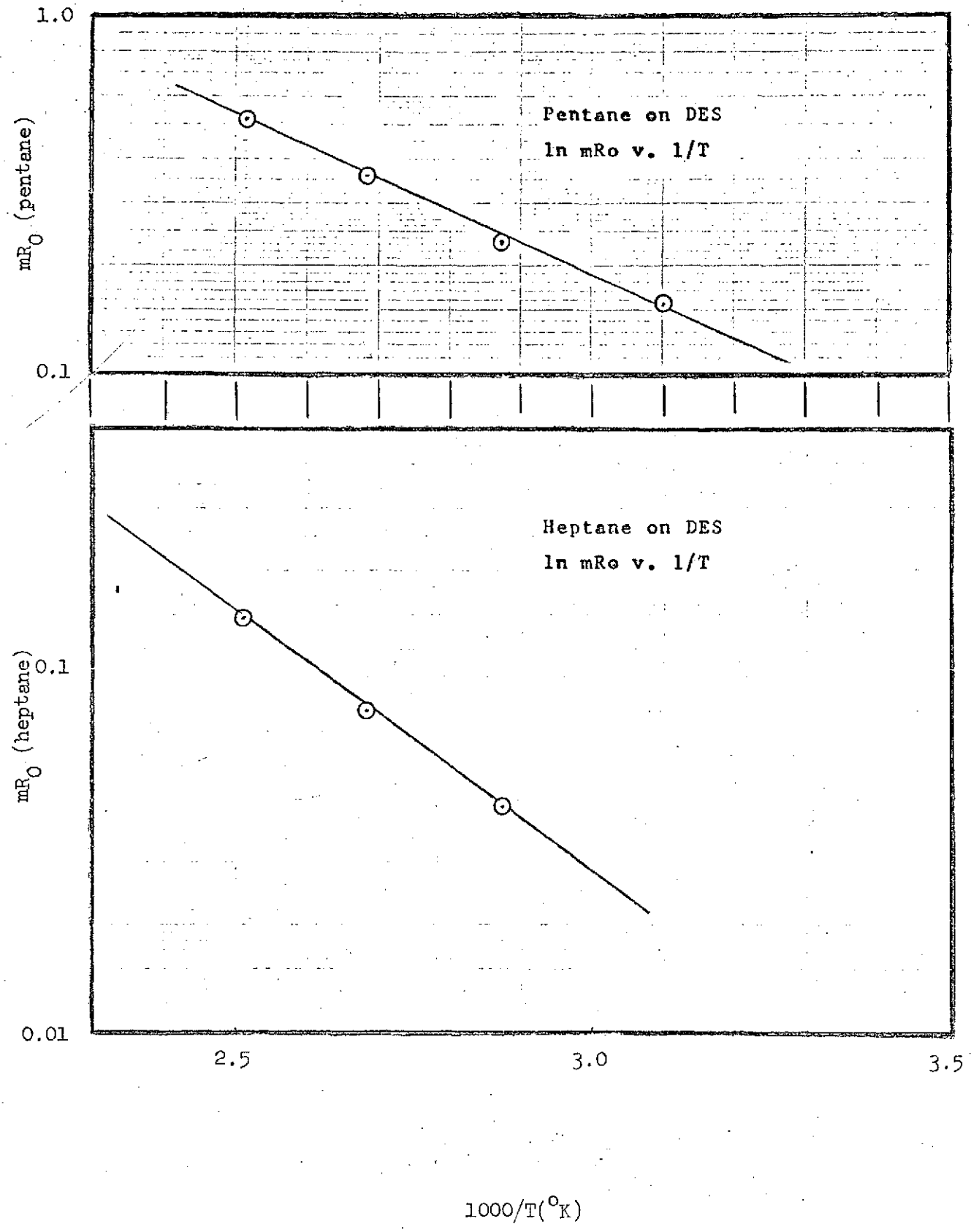

Fig. 58. Effect of Temperature Upon Thermodynamic Parameter mR_O for Pentane/Heptane System on DES Column

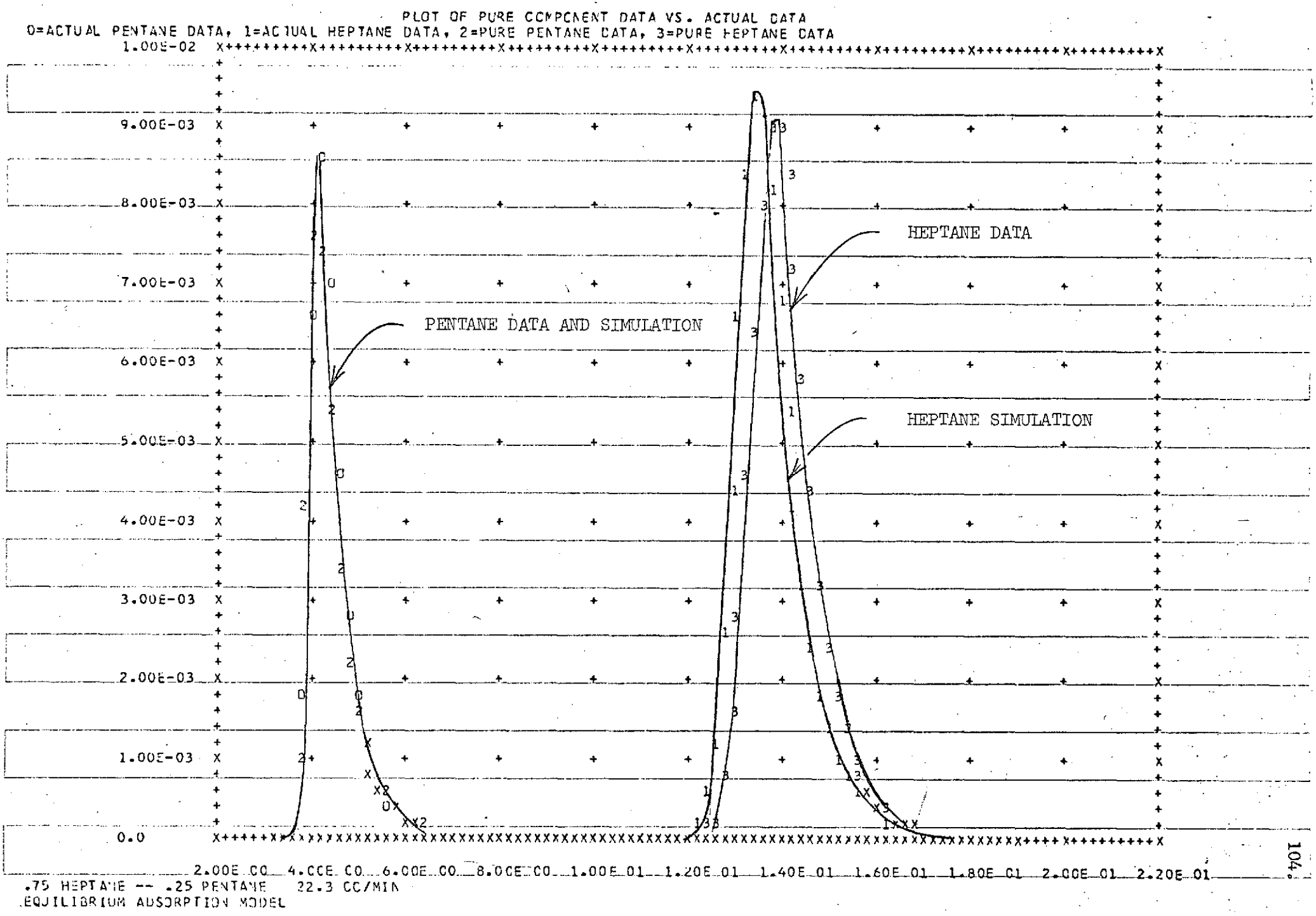

Fig. 59. Pentane/Heptane on DES Column at 100°C

TABLE III

DETERMINATION OF mR_o FOR HEPTANE ON DES COLUMN

Pure sample at 100° C

Sample size, micromoles	mR_o
1.36	0.0806
3.41	0.0751
3.41	0.0823
6.81	0.0801
6.81	0.0799
20.5	0.0795

Binary sample with pentane at 100° C

Composition, wgt. fraction	mR_o
0.01	0.0827
0.10	0.0824
0.25	0.0819
0.50	0.0822
0.75	0.0829
0.90	0.0830
0.99	0.0830

numerical analysis for the proposed model. Because of the complexity of the model, analytical techniques were not feasible and a study of applicable numerical techniques was made. The technique of orthogonal collocation, Ref. 22, is being studied and applied to several systems of equations to determine if it can be used routinely for numerical solutions and hence verification of the complicated chromatograph model. The systems of equations presently being analyzed are given in Fig. 60. Appropriate boundary and initial value conditions have been presented earlier, Ref. 21. The study of this sequence of systems is motivated by the knowledge that systems 1 and 2 of Fig. 60 have known, exact, analytical solutions, and simulations using orthogonal collocation can be evaluated directly. In addition, this sequence provides an opportunity to appraise the technique of orthogonal collocation in its ability to solve systems of one, two, and three coupled, partial differential equations.

Preliminary analysis of orthogonal collocation was recently documented, Ref. 21. Since that time, the simple model, system 1 of Fig. 60, has been studied using unit rectangular pulses and actual data as forcing functions for high and low values of the Peclet number Pe. Figure 61 shows a seventh order collocation solution using actual data as a forcing function. Figure 62 shows a fifteenth order simulation, and Fig. 63 shows the exact response. Comparison of the figures indicate that the collocation solution is very good within the region of the non-zero response. However, small oscillations are present where the response should be essentially zero. This behavior seems to be inherent in the method. Increasing the order of the collocation approximation reduces the magnitude of the oscillations so that they become unimportant when compared to the magnitude of the simulated response. Computer time rapidly increases though.

At present, collocation simulations are being made for the system 2 of Fig. 60. Subsequent to this, system 3 of Fig. 60 will be studied. The results of these studies should establish the utility of orthogonal collocation as a numerical technique for the solution of complex chromatograph models and thus give a technique wherein the importance of different transport phenomena in the chromatographic process may be assessed.

1. Simple, diffusion-convection model:

$$\left(\frac{1}{Pe\ z_0^2}\right) \cdot \frac{\partial^2 y}{\partial z^2} - \left(\frac{1}{z_0}\right) \cdot \frac{\partial y}{\partial z} = \frac{\partial y}{\partial \theta}$$

2. Inter-intraparticle model without diffusion

$$\left(\frac{1}{Pe\ z_0^2}\right) \cdot \frac{\partial^2 y}{\partial z^2} - \left(\frac{1}{z_0}\right) \cdot \frac{\partial y}{\partial z} - N_{RU}\ (y-y^*) = \frac{\partial y}{\partial \theta}$$

$$\left(\frac{1}{R_I}\right) \cdot \frac{\partial x}{\partial \theta} = N_{RU}\ (y-y^*)$$

$$y^* = m\ x$$

3. Inter-intraparticle model with diffusion

$$\left(\frac{1}{Pe\ z_0^2}\right) \cdot \frac{\partial^2 y}{\partial z^2} - \left(\frac{1}{z_0}\right) \frac{\partial y}{\partial z} - \frac{3(1-\epsilon)\beta}{\epsilon} \left(\frac{L}{R}\right)^2 \left(\frac{1}{Pe_A}\right) \frac{\partial y_i}{\partial r}\bigg|_{r=1} = \frac{\partial y}{\partial \theta}$$

$$\left(\frac{L}{R}\right)^2 \left(\frac{1}{Pe_A}\right) \left[\frac{\partial^2 y_i}{\partial r^2} + \left(\frac{2}{r}\right) \frac{\partial y_i}{\partial r}\right] - N_{RU}\ (y_i - y_i^*) = \frac{\partial y_i}{\partial \theta}$$

$$\left(\frac{1}{R_I}\right) \frac{\partial x}{\partial \theta} = N_{RU}\ (y_i - y_i^*)$$

$$y_i^* = m\ x$$

Fig. 60. Equations Being Studied by Orthogonal Collocation

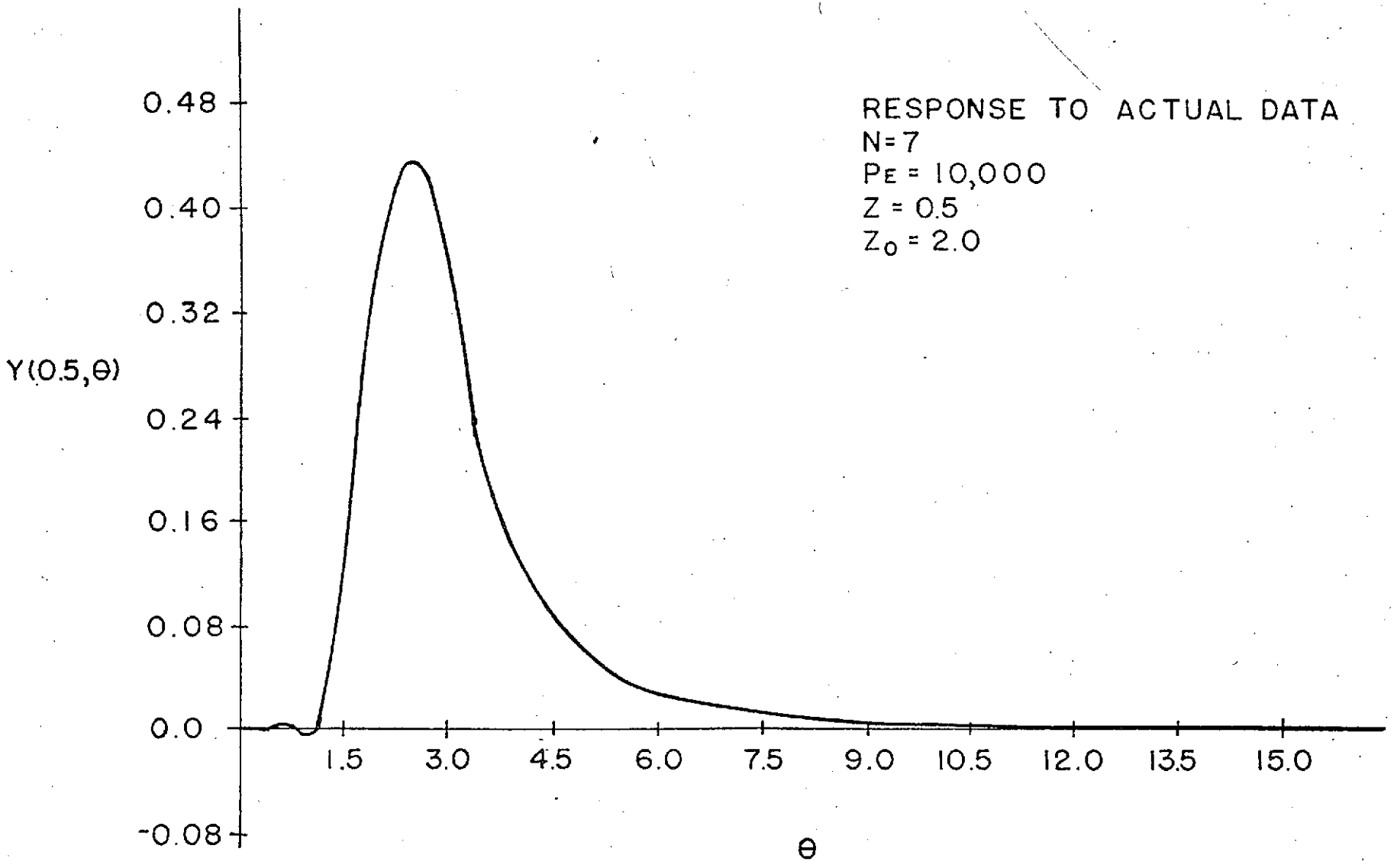

Fig. 61. Simulation of Simple Model Using 7 Collocation Points

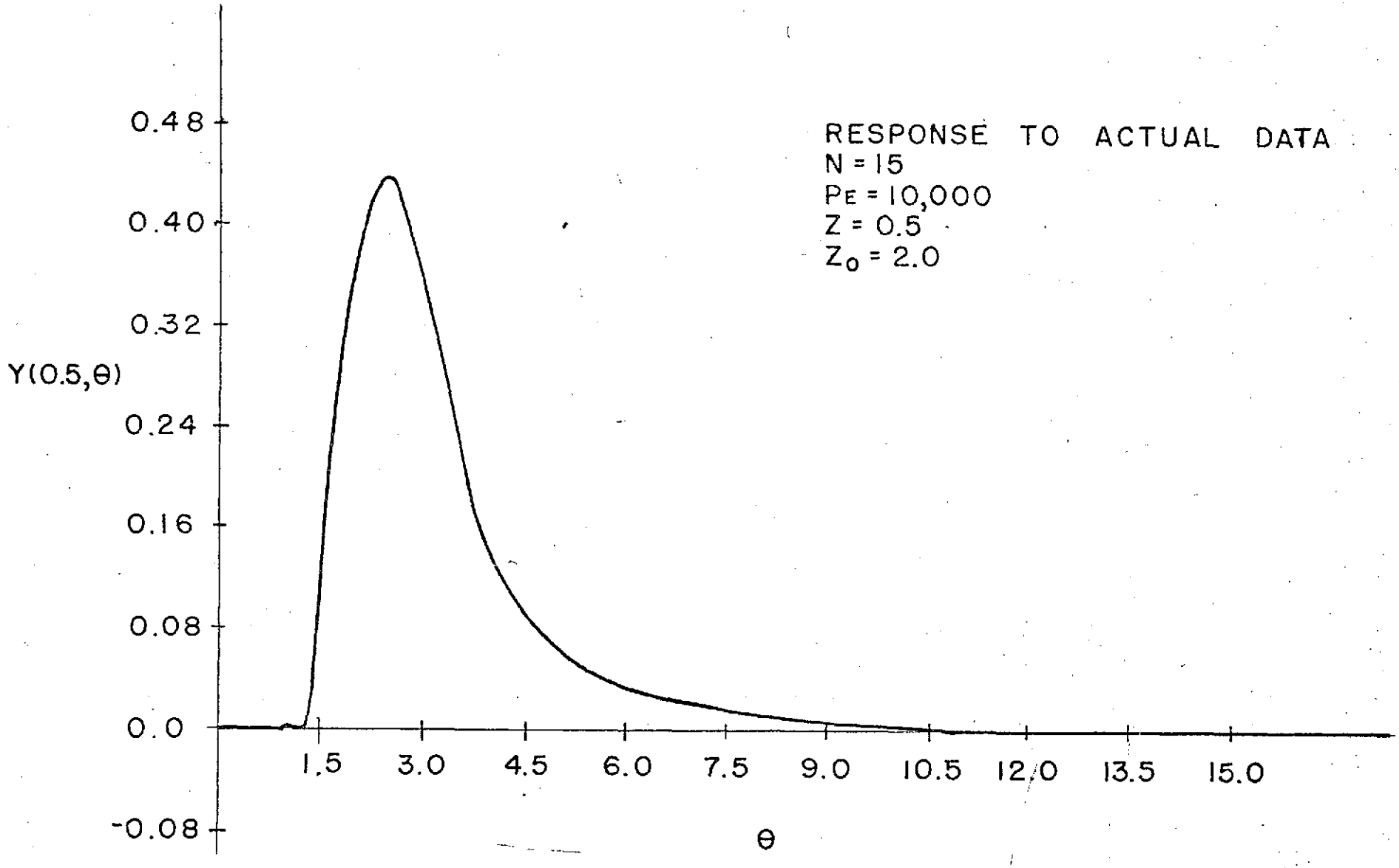

Fig. 62. Simulation of Simple Model Using 15 Collocation Points

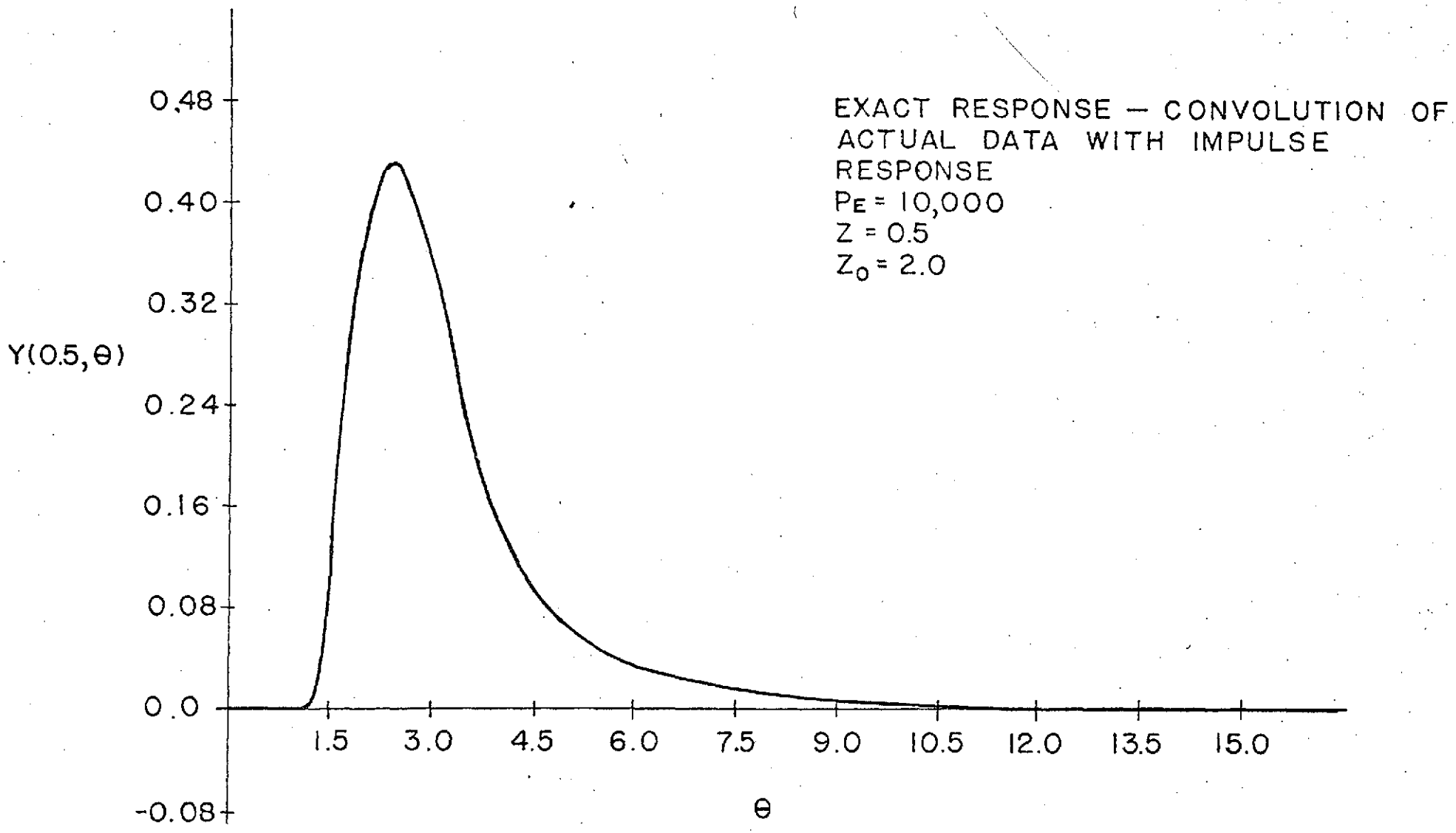

Fig. 63. Exact Response of Simple Model

REFERENCES

1. Unitrode Corporation Publications:
   a. "Thyristor New Design Ideas," No. 0373 CAT 615M, March 1973.
   b. Specification Sheet for GA-201 SCR's, No. 5-71-JC-MP, May 1971.

2. RCA Publications:
   a. "Solid State Infrared Emitting Diodes," No. OPT-1008, June 1972.
   b. Specification Sheet for 40862 (SG 2007) Laser Diode, No. 520, September 1971.

3. R. Campbell and F. Mims, Semiconductor Laser Diodes, ITT, Howard W. Sams Co., Inc., 1972.

4. Torrance, K.E. and Sparrow, E.M., Theory for Off-Specular Reflection from Roughened Surfaces," Journal of the Optical Society of America, Vol. 57, No. 9, Sept. 1967, pp. 1105-1114.

5. Christie, F.A. and DeVriendt, A.B.,"Bidirectional Reflectance from Surfaces Formed by the Ruling of Orthogonal Parallel V-grooves," 10th Aerospace Sciences Meeting, American Institute of Aeronautics and Astronautics, San Diego, California, January 17-19, 1972.

6. Zuraski, G.D., "Laser Range Measurement for a Satellite Navigation Scheme and Mid-Range Path Selection and Obstacle Avoidance," Master of Engineering Project, Rensselaer Polytechnic Institute, May 1972, pp. 26-30.

7. Motorola Application Note #AN-440, Theory and Characteristics of Photo Transistors.

8. "An Exploratory Investigation of a 1979 Mars Roving Vehicle Mission, December 1, 1970 JPL, CIT, Pasadena, California

9. Shen, C.N. and Burger, P., "Stochastic Estimates of Gradient from Laser Measurements for an Autonomous Martian Roving Vehicle," Proceedings of the 3rd IFAC Symposium, The Hague/Delft, The Netherlands, June 1973.

10. Shen, C.N. and D'Angelo, K.R., "Parameter Estimation for Martian Terrain Modeling from Gradient Data," Seventh Hawaii International Conference on System Sciences, Honolulu, Hawaii, January 1974.

11. Reed, M., Sanyal, P. and Shen, C.N., "A Practical Obstacle Detection System for the Mars Rover," accepted for presentation, Second Annual Milwaukee Symposium on Automatic Control, Milwaukee, Wisc., March 1974.

12. Newberger, A., "Characerization of Pictures by Essential Contours," M.S. Thesis, Massachusetts Institute of Technology, 1966.

13. Burger, Paul, "Stochastic Estimates of Gradient from Laser Measurements for an Autonomous Martian Roving Vehicle," Master of Engineering Project Report, Rensselaer Polytechnic Institute, May 1973.

14. McGrath, C., Patten, R. and Oey, K., "A Navigational Computer for an Unmanned Mars Roving Vehicle, MRV 72-5, Cornell University, June 1972.

15. Benoit, G.L., "Reduction of Chromatographic Data and Evaluation of a GC Model," RPI Technical Report MP-22, Rensselaer Polytechnic Institute, Troy, New York, June 1971.

16. Keba, P.S., and Woodrow, P.T., "A Comparison of Two Gas Chromatograph Models and Analysis of Binary Data," RPI Technical Report MP-27, Rensselaer Polytechnic Institute, Troy, New York, July 1972.

17. McNair, H.M., and Cooke, W.M., "Use of Statistical Moments in Chromatography," Amer. Lab., 5 (2), 12-18 (1973).

18. Voytus, W.A., "Chromatographic Systems Analysis: Moment Analysis of the Equilibrium Adsorption Model," RPI Technical Report MP-9, Rensselaer Polytechnic Institute, Troy, New York, August 1969.

19. Meisch, A.J., "Binary Chromatographic Data and Estimation of Adsorbent Porosities," RPI Technical Report MP-31, Rensselaer Polytechnic Institute, Troy, New York, May 1973.

20. Baer, S.R., and Benoit, G.L., "Chromatographic Test Facility," RPI Technical Report MP-19, Rensselaer Polytechnic Institute, Troy, New York, March 1971.

21. Woodrow, P.R., "Preliminary Numerical Analysis of Improved Gas Chromatograph Model," RPI Technical Report MP-36, Rensselaer Polytechnic Institute, Troy, New York, September 1973.

22. Finlayson, B.A., "The Method of Weighted Residuals and Variational Principles," Academic Press, New York, 1972.